NTNU

Norwegian University of
Science and Technology

Formation of Silicon Carbide in the Silicomanganese Process

Jens Erik Davidsen

Materials Science and Engineering
Submission date: June 2011
Supervisor: Merete Tangstad, IMTE
Co-supervisor: Per Anders Eidem, Eramet Norway AS

Norwegian University of Science and Technology
Department of Materials Science and Engineering

I hereby declare that this work has been carried out independently and in compliance with the examination regulations of the Norwegian University of Science and Technology, NTNU.

Jens E Davidsen
Trondheim, June 2011

Preface

This thesis describes an investigation of the formation of silicon carbide in the silicomanganese process. The work is the master thesis of the author, and a basis for evaluation of the course TMT 4905 at the Norwegian University of Science and Technology, NTNU. The work has been based on a collaboration between NTNU and Eramet Norway AS, and was part of the Resource Optimization and Recovery in the Material Industry (ROMA) project.

I would first of all give my utmost gratitude to my supervisor, Professor Merete Tangstad. Merete has not only guided me through the confusing jungle of manganese production and thermodynamics, but also given me the opportunity to visit both China and South-Africa during the final year of my masters degree

An equally large thanks goes to my co-supervisor, Dr. Per Anders Eidem at Eramet Norway AS for useful comments and ideas. Your good spirits and ability to see solutions rather than problems has been of great inspiration.

I would also like to thank Dr. Eli Ringdalen (SINTEF) for useful input and ideas, Tone Anzjøn (SINTEF) for help with the wetting experiments, Morten Raanes for the EPMA analysis, Julian Tolchard and Dr. Bjørn Eske Sørensen for help with XRD analysis and Dr. Kai Tang (SINTEF) for thermodynamic calculations. A sincere gratitude goes to everyone in the ROMA project and SiManTi group for social and technical support.

At last I would like to thank my fellow graduate students at material science, NTNU. It is amazing how fast time goes by when you're surrounded by such fantastic people. The last five years have been truly wonderful, and a time I will never forget.

Jens E Davidsen
Trondheim, June 2011

Abstract

As the silicon content in a silicomanganese alloy increase, silicon carbide becomes the stable carbon phase. Little work is published on the formation of silicon carbide in the SiMn process. This thesis examines the formation of SiC through the reaction between slag, metal and coke. The goal of the thesis has been to determine where and how SiC is formed in the silicomanganese process. Focus has been given to formation through liquid-solid reactions.

The investigation was carried out by heating metal and slag together with coke. XRD analysis of SiC formed in the process, as well as wettability testing of slag and metal toward SiC and graphite substrates were also examined. The raw materials consisted of two industrial SiMn alloys, named Metal 1 and 2 in the thesis. These had 19 and 28 wt.% Si, respectively. Two slags, Slag 1 and 2, were used in combination with the metal.

SiC was found to form on the coke particle through reaction with both slag and metal. The formation was fastest through the metal phase and the effect of increasing silicon content in the metal was evident. A temperature increase from 1600 °C to 1650 °C resulted in less SiC formed on the coke particle surface for Metal 1, but gave more SiC at the surface of the coke particle for Metal 2. The decrease in SiC on the coke particle for Metal 1 is likely to be caused by a decreased driving force, as the coexistence point of C and SiC increases with increasing temperature. For Metal 2 the relative distance is smaller, making the effect neglectable.

The formation of SiC occurs at the surface of the coke particle. The metal samples indicate that carbon diffuses through the SiC layer to react with silicon in the alloy. Formation through the slag is likely to go through the reduction of SiO_2 to Si, before reacting to form SiC.

The XRD analysis determined β-SiC to be the dominant phase formed through both slag and metal. α-SiC was found in one of the industrial

slag samples, indicating temperatures higher than 1700 °C.

The wettability testing showed both slag and metal to be non wetting toward the SiC substrate. All angles were stable with increasing temperatures.

Both slags were found to be non wetting toward graphite. The wetting angle of Slag 2 was stable with increasing temperature. Slag 1 showed decreasing wetting angle with temperature, before an abrupt change back to an angle larger than the initial angle. The sudden change is likely to be caused by a reaction product, possibly SiC, forming between the substrate and slag.

Contents

Preface iii

Abstract v

Contents vii

1 Introduction 1

2 Theory 3
- 2.1 The Si-C system . . . 3
- 2.2 Silicomanganese production . . . 5
  - 2.2.1 SiC in the SiMn process . . . 9
  - 2.2.2 Activities in SiMn system . . . 12
- 2.3 The Acheson process . . . 15
- 2.4 SiC formation and phases . . . 16
- 2.5 Wettability of SiC . . . 20
- 2.6 Growth of SiC on carbon . . . 27
- 2.7 Buoyancy of SiC . . . 27

3 Experimental 31
- 3.1 The raw materials . . . 32
- 3.2 Vertical tube furnace . . . 34
  - 3.2.1 Experimental setup . . . 34
  - 3.2.2 Sample preparation and experimental parameters . . . 35
- 3.3 Wettability testing . . . 37
  - 3.3.1 Apparatus . . . 37
  - 3.3.2 Sample preparation and experimental parameters . . . 38
- 3.4 Electron probe micro analyzer . . . 40
  - 3.4.1 Apparatus . . . 41
  - 3.4.2 Scan parameters . . . 41

3.5 X-ray diffraction 42
3.5.1 Apparatus 42
3.5.2 Sample preparation and scan parameters 43

4 Results **45**
4.1 Tube furnace results 45
4.1.1 Macro scope observations 45
4.1.2 EPMA and microscope results 52
4.2 XRD results 60
4.3 Wettability testing 62
4.3.1 Sessile drop testing 62
4.3.2 EPMA of the samples 65

5 Discussion **69**
5.1 SiC formation 69
5.2 SiC structure in the SiMn process 74
5.3 Wettability testing 74
5.4 Additional observations 79
5.4.1 Placement of SiC in the SiMn system 79
5.4.2 Cavity formation in the metal samples 81
5.4.3 Metal droplets and discharging of Slag 1 83
5.4.4 Reduction of MnO during wetting experiments 84
5.4.5 Solids on the samples during the wetting experiments 85
5.5 Industrial SiC formation 85

6 Conclusions **87**

7 Further Work **89**

Bibliography **91**

Appendix A Light microscope pictures **A**

Appendix B Wetting results **I**

Appendix C XRD patterns **Q**

Appendix D Tube furnace operation parameters **W**

Chapter 1

Introduction

Silicon carbide (SiC) is one of the hardest known substances. The hardness makes it suitable for numerous purposes, and it is used for everything from cutting disks, grinding abrasive, carbon source for clean steels to cutting of silicon wafers. SiC also has good electrical properties and is considered a candidate as semiconductor for high temperature electronics (Lindstad, 2002).

Industrially SiC is produced by the Acheson's process. Here silica, usually in the form of sand, is mixed with petroleum coke and heated giving crystalline silicon carbide. The SiC can be treated by the Lely process, where it is recrystallized to form single crystal SiC (Lindstad, 2002).

In the production of Silicon metal (Si) and ferrosilicon (FeSi), Si is reduced from quartz by solid carbon. The reduction goes through the formation of silicon monoxide gas (SiO) and SiC, which results in large amounts of SiC being formed in the furnace (Schei et al., 1998). Operation is known to become unstable as SiC builds up in the furnace (Tangstad, 2011).

In silicomanganese (SiMn) production silica (SiO_2) and manganese oxides are reduced simultaneously from a liquid slag. The resulting alloy usually has a silicon content of c. 17 - 20 wt.% Si. The alloy can be refined by adding off grade silicon metal, giving low carbon (LC) SiMn (Olsen et al., 2007). As the Si content in the alloy reaches c. 16 wt.%, SiC will become the stable carbon phase in the system. The amount of SiC formed is believed to increase with increasing Si content.

Furnace 2 at Eramet Norway Kvinesdal AS (ENK) was dug out during the spring of 2009. The furnace had been producing standard SiMn with

c. 20 wt.% Si prior to shutdown. Drill cores and loose sample from the coke bed were investigated, and a small deposit of SiC was found between two of the electrodes (Eidem, 2011). EPMA of the samples revealed that SiC was present as a separate phase in the slag, but no SiC was observed in the metal or at the coke particles (Davidsen, 2010).

As the SiC in the furnace does not react with the slag to form metal, it is a direct loss of silicon. Increasing amounts of SiC will also influence the furnace operation. It is however inevitable, so it is desired to keep the formation as low as possible. To be able to control the formation of SiC, one has to understand the basics of formation.

Little or no work has previously been published on the subject of formation of SiC in the SiMn process. The goal of this thesis will be to determine where in the SiMn process SiC is formed and to try to determine the reaction mechanism of formation. The study is limited to the formation of SiC through liquid-solid reactions, and the formation through gas phase has not been investigated in this thesis. Industrial materials have been used for the investigation in order to simulate the industrial process to as large a degree as possible.

Chapter 2

Theory

2.1 The Si-C system

Silicon carbide is one of the hardest substances in the world, with a hardness between 9 and 10 on Moh's hardness scale (Lindstad, 2002). It does not melt, but decomposes at temperatures above c. 2800 °C. SiC is insoluble in water, acids and bases, but is attacked by unsaturated metal and oxide melts. The main impurities in industrially produced SiC is free C and SiO_2 with smaller amounts of Ca, Fe, Al, Ca and N (Washington Mills, 2010).

SiC is generally divided into two different phases, α- and β-SiC. α-SiC consists of over 200 polytypes, which have hexagonal or rhombohedral structures. The different polytypes are defined by the different stacking types of the SiC layers, and the differences in thermodynamical properties are considered to be insignificant (Chase, 1998). The most common polytypes for α- and β-SiC are listed in Table 2.1.

Table 2.1: The most common polytypes of SiC and their heat of formation and entropy. "C" denote cubic crystal structure, while "H" is hexagonal and "R" is rhombohedral. Data taken from Chase (1998).

SiC type	Polytypes	$\Delta_f H^\circ$ [kJ/mol]	S°[J/Kmol]
α-SiC	4H 6H 15R	-71.546 ± 6.3	16.485 ± 0.13
β-SiC	3C	-73.220 ± 6.3	16.610 ± 0.13

β-SiC has a cubic crystal structure. According to JANAF thermochemical tables (Chase, 1998), heat of formation and equilibrium data indicate that β-SiC is the most stable phase up to c. 1700 °C. Above this the stability difference is believed to be small (Chase, 1998). As the main product of the Acheson process is α-SiC, it is likely that this structure is favored as the temperature exceeds c. 2000 °C.

The thermodynamical properties of the two SiC phases are close to equal. Heat of formation and entropy at 25 °C for the two phases are shown in Table 2.1.

The color of silicon carbide is affected by impurities, crystal structure and polytype. Pure α- and β-SiC have a white and yellow color, respectively. As the amount of impurities increase, both α- and β-SiC change toward a blue-black color (Nelson et al., 1966). Common impurities and their effect on the color of the SiC are listed in Table 2.2.

Table 2.2: Color changes in SiC caused by impurities. "H" denote hexagonal and "R" is rhombohedral crystal structure. Data is taken from Harris (1995); Lindstad (2002); Washington Mills (2010).

Impurity element	α-SiC	β-SiC
Pure	colorless	yellow
Nitrogen	green (6H) yellow-orange (4H, 8H) orange-yellow (15R)	yellow-green
Aluminum	blue-black	
Boron	brown-black	

The binary Si-C phase diagram is given in Figure 2.1. The diagram shows the work of two different researchers. High temperatures makes the determination of the system difficult. Hoel (1998) assessed the work of Scace (1959), shown with solid lines in Figure 2.1, to be the most reliable of the two. The temperature for decomposition of SiC is reported to be 2834± 40 °C in the figure, which is in good agreement with the reported temperature of 2830 °C in HSC 5.11 (Roina, 2002). SI Chemical Data (Aylward & Findlay, 2008) reports a decomposition temperature of 2986 °C. This is higher than for the two others, but supports the theory that the work of Scace is most reliable. As the maximum temperature in the SiMn process is in the area of 1600 - 1700 °C (Olsen et al., 2007), only the part of the diagram

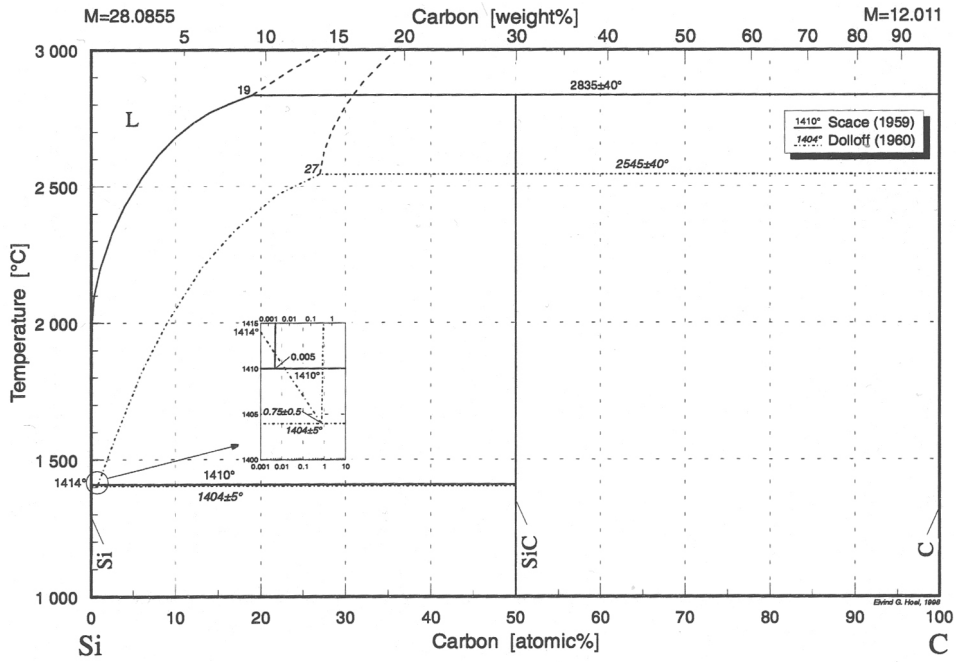

Figure 2.1: The Si-C equilibrium phase diagram. Figure is taken from Hoel (1998).

below 2000 °C will be considered here.

The diagram is a simple peritectic system with SiC as the only intermediate compound. SiC has a stoichiometric composition of 50 at.% Si and 50 at.% C. The solubility of carbon in silicon is very low. Up to 50 at.% C the system will mainly consist of Si, either solid or liquid, and solid SiC. Above 50 at.% carbon the system will consist of solid SiC and graphite.

2.2 Silicomanganese production

Carbothermic reduction of SiMn is done in submerged arc furnaces (SAF). Here carbon is used as a reducing agent while the heat is supplied by electricity (Olsen et al., 2007). An electric current is sent through the charge, and heat is created according to $P = R \cdot I^2$, where P is the effect i.e the heat created, R is the charge resistance and I is the current density. The furnaces used for SiMn production are usually in the size range of 15-40 MVA which gives a production of c. 80-220 t/day (Olsen, 2001).

The raw materials used in SiMn production mainly consists of high carbon ferromanganese (HC FeMn) slag, quartzite, coke, manganese ores and fluxes. Ferrosilicon or silicon remelts and off grade products may also be used to increase Si content in the final product. Many of the impurities found in the ore are reduced into the metal in the HC FeMn process, making the slag a relatively pure source of Mn (Olsen, 2001).

The reduction of Si and Mn in SiMn is done by a series of different reduction steps (Ding & Olsen, 1996a).

$$(SiO_2) + 2C' = \underline{Si} + 2CO(g) \tag{2.1}$$
$$(SiO_2) + 2SiC = 3\underline{Si} + 2CO(g) \tag{2.2}$$
$$(MnO) + C' = \underline{Mn} + CO(g) \tag{2.3}$$
$$(SiO_2) + 2\underline{Mn} = \underline{Si} + 2(MnO) \tag{2.4}$$
$$(SiO_2) + \underline{Si} = 2SiO(g) \tag{2.5}$$
$$\underline{Mn} = Mn(g) \tag{2.6}$$

Brackets indicates that the species are present in the slag, while underline indicates a specie in the alloy. C' is the carbon source, which can be dissolved in the metal or solid, i.e. coke. Equation (2.1), (2.3) and (2.4) are interdependent since two of them can be combined to get the third one (Ding & Olsen, 1996b). It is therefore only necessary to look at two of these when equilibrium is regarded. Equation (2.1) is usually disregarded due to it's sluggish reaction (Ding, 1993). As SiC replaces graphite as the stable carbon phase, SiO_2 in the slag is reduced according to Equation (2.2).

The reduction of SiO_2 to Si-metal with solid carbon is not possibles at temperatures below 1811 °C at ambient pressure. The presence of Fe and Mn lowers the activity of Si in the alloy, and makes the reduction of SiO_2 with dissolved carbon possible at temperatures below 1811 °C (Tranell et al., 2007).

The effect of temperature on the Si content for a Mn-Si-C_{sat} alloy in equilibrium with a SiO_2-CaO-Al_2O_3-MnO slag with $CaO/Al_2O_3 = 4$ is shown in Figure 2.2(a). The Si content increases with increasing temperature. As seen from the figure, a slag with 45 wt.% SiO_2 will give a metal with c. 19.5 wt.% Si at 1600 °C and 25 wt.% Si at 1700 °C. After tapping the alloy can be refined by adding FeSi or off grade Si-metal to achieve the wanted SiMn grade.

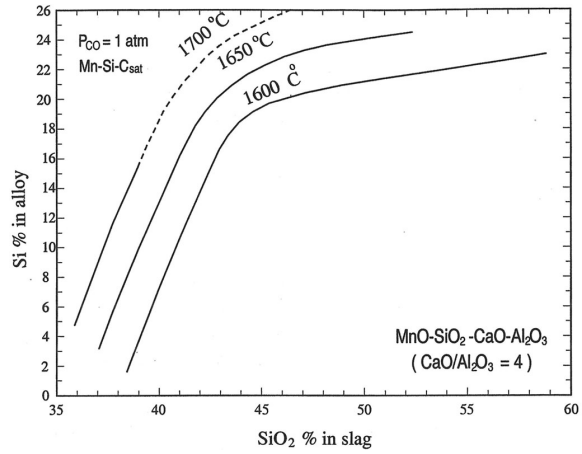

(a)

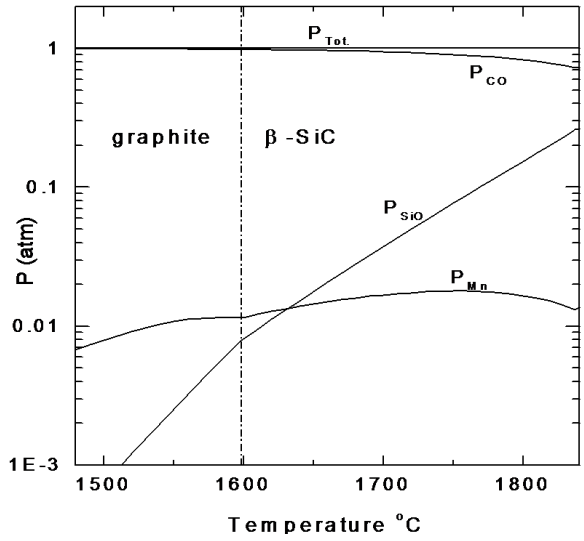

(b)

Figure 2.2: (a) The effect of temperature on Si content in an Mn-Si-C_{sat} alloy in equilibrium with a SiO_2-CaO-Al_2O_3-MnO slag with $CaO/Al_2O_3 = 4$. Figure is taken from Olsen (2001) (b) Calculated equilibrium gas pressure for a Mn-Si-C_{sat} alloy and a slag with $a_{SiO_2} = 0.2$. Figure from Tangstad (2011).

The three main gas components in the furnace are SiO(g), Mn(g) and CO(g) and total pressure in the furnace is assumed to be 1 atm. At temperatures below c. 1600 °C the partial pressures of Mn(g) and SiO(g) are low and p_{CO} is close to 1 atm (Ding & Olsen, 1996a). Figure 2.2(b) shows the calculated

equilibrium pressure of CO(g), SiO(g) and Mn(g) above a carbon saturated Mn-Si-C alloy and slag with a silica activity of 0.2. At 1600 °C, the partial pressure of SiO(g) and Mn(g) are c. 0.008 and 0.012 atm, respectively. As the temperature exceeds 1600 °C, the partial pressures will increase.

The slag can roughly be divided into reducible and "unreducible" oxides. The unreducible oxides are named so as they will not be reduced under the conditions present in the furnace. The reducible oxides in the SiMn process are mainly SiO_2, MnO and FeO and the main unreducible oxides are Al_2O_3, CaO and MgO. Iron can be reduced directly by CO(g) in the charge, before the raw materials reach the coke bed zone. At temperatures around 1600 °C practically all the iron will be present in the metal phase (Olsen et al., 2007).

The unreducible oxides are introduced through the raw materials and added for fluxing purposes. These oxides do not take part in the chemical reactions, but still affect the thermodynamical and physical properties of the slag (Olsen, 2001).

Manganese bearing slags are often described by slag basicity. The basicity describes the ratio between the basic and acid slag constituents, given by Equation (2.7). This ratio is often used to design slags for FeMn production, as the basicity will determine the physical properties of the slag as well as the composition of the tapped metal and slag.

$$B = \frac{MnO + CaO + MgO}{Al_2O_3 + SiO_2} \tag{2.7}$$

In SiMn production both MnO and SiO_2 are reduced out from the slag. Another expression is therefore used, containing only the unreducible oxides. This ratio, called the R-ratio, is given by Equation (2.8). The ratio will stay constant through the whole process as neither CaO, MgO or Al_2O_3 are reduced.

$$R = \frac{CaO + MgO}{Al_2O_3} \tag{2.8}$$

The slag also contains minor amounts of other oxides such as BaO, K_2O, Na_2O, FeO, TiO_2 and P_2O_5. The total amount of these is usually low, around 6 wt.%, and they are usually neglected for thermodynamical calculations (Swinbourne et al., 1993).

2.2.1 SiC in the SiMn process

As the reduction of SiMn is done with coke, the produced alloy will be saturated with carbon. With increasing amounts of Si, the solubility of C decreases significantly. Where a saturated Mn-Fe-C_{sat} alloy will contain about 7-8 wt.% C, a Mn-Fe-Si-C_{sat} alloy with c. 20 wt.% Si will have less than 2 wt.% C at c. 1600 °C (Olsen, 2001). The carbon solubility of SiMn as a function of Si-content is shown in Figure 2.3.

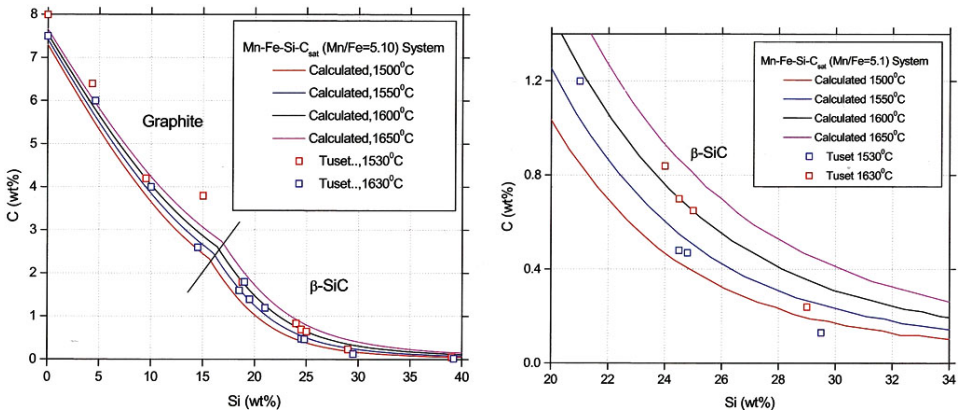

Figure 2.3: Calculated carbon solubility as a function of Si content in a Mn-Fe-Si-C_{sat} alloy with Mn/Fe = 5.1 between 1500 ° C and 1650 ° C. The graph on the right side show a close up of the high Si area. Figure is taken from Olsen et al. (2007).

At the coexisting point, shown by a line in Figure 2.3, dissolved carbon in the melt is in equilibrium with SiC. Here SiC replaces graphite as the stable carbon phase. At 1600 °C this is at c. 17 wt.% Si, while at 1650 °C it has increased to c. 17.5 wt.%. The dissolved carbon reacts with the Si in the melt to form SiC according to Equation (2.9). If the slag has a high silica content, SiC may form through the slag phase according to Equation (2.10).

$$\underline{Si} + C' = SiC(s) \tag{2.9}$$

$$(SiO_2) + 3C' = SiC(s) + 2CO(g) \tag{2.10}$$

The reaction presented in Equation (2.10) can again be dived into two stages. First the reduction of Si from the slag followed by a reaction between Si and C to form SiC, Equation (2.1) and (2.9), respectively.

The point of coexistence between C and SiC will vary with composition of the melt and temperature. The Si content at the coexistence point will increase with increasing temperature and decrease with increasing Mn/Fe-ratio in the alloy (Ding, 1993).

Below the coexisting point carbon activity will be at unity as long as the alloy is saturated on C. The activity of the SiC will therefore be a function of the Si activity in the alloy and temperature, Equation (2.11) (Ding & Olsen, 1996a). The activity of Si in the alloy is therefore of importance for the formation of SiC.

$$a_{SiC} = K(T) \cdot a_{Si} \tag{2.11}$$

Little research seems to be done on the structure of the SiC found in SiMn production. Several sources (Ding & Olsen, 1996a; Hoel, 1998; Olsen et al., 2007) describes β-SiC as the product of the reaction between Si and carbon dissolved in the alloy, Equation (2.9).

Hoel (1998) claims that during solidification SiC crystallizes into a cubic modification, β-SiC, and that α-SiC only can be obtained through a gas phase.

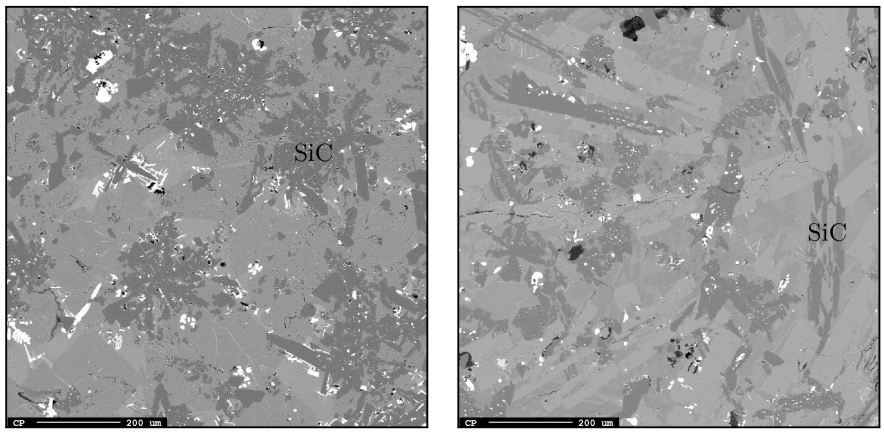

(a) V1 4500 (b) B5-62

Figure 2.4: SiC in solidified standard SiMn slag. Dark gray phase in the pictures are SiC, marked in both pictures. Taken from Davidsen (2010).

Investigation of samples from an excavation of an industrial SiMn SAF was done by the author during the autumn 2010 (Davidsen, 2010). SiC was here only found in the slag, and not observed in the metal or on the coke

particles. Two of the slag samples containing SiC are shown in Figure 2.4.

Figure 2.5 shows the calculated vertical section of a Mn-Si-Fe-C phase diagram for a typical std. and LC SiMn alloy.

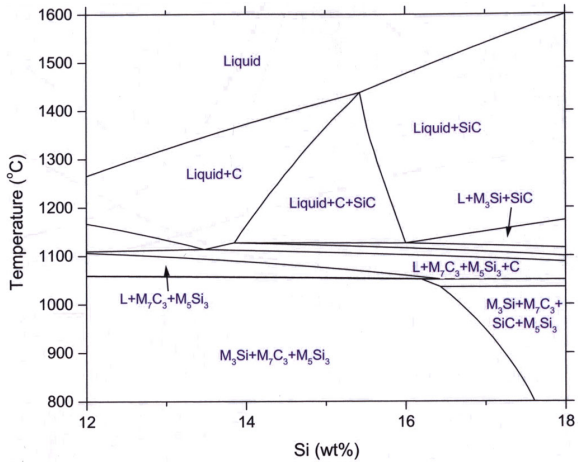

(a) Std. SiMn

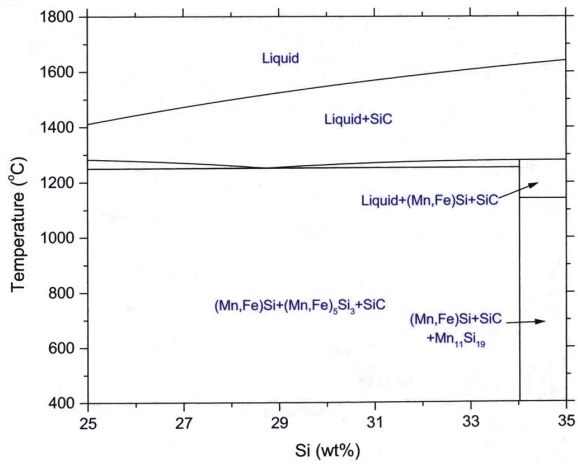

(b) LC SiMn

Figure 2.5: Vertical section of the Mn-Si-Fe-C phase diagram: (a) For a typical std. SiMn alloy with 2 wt.% C and 12 wt.% Fe (b) For a typical LC SiMn alloy with 0.2 wt.% C and 8 wt.% Fe. Figures are taken from Olsen et al. (2007).

From the figures it can be seen that a rapidly cooled alloy with 18 wt.% Si will result in $(Mn,Fe)_3Si$, $(Mn,Fe)_5Si_3$, $(Mn,Fe)_7C$ and SiC. For an alloy

with 30 wt.% Si the result will be (Mn,Fe)Si, $(Mn,Fe)_5Si_3$ and SiC. The binary Si-Mn phase diagram determines Mn_3Si, Mn_5Si_3 and MnSi to hold c. 14 wt.%, 23 wt.% and 34 wt.% Si, respectively (Hoel, 1998).

2.2.2 Activities in SiMn system

Figure 2.6 and 2.7 shows the calculated activities of Mn and Si for Metal 1 and 2 in equilibrium with carbon as a function of temperature. Figure 2.8 and 2.9 shows the calculated MnO and SiO_2 activities as a function of temperature for Slag 1 and 2. The composition of the alloys and slags used in the calculations are shown in Table 2.3. The activities were calculated using FactSage software with the FTOxide FactOxide database.

Table 2.3: The alloys and slags used for the activity calculations, based on the alloys and slags used as raw material. All numbers in wt.%.

Alloy	Si	Mn	Fe	C
Metal 1	20.9	69.0	10.0	1.0
Metal 2	28.7	62.4	8.9	0.03

Slag	SiO_2	MnO	Al_2O_3	CaO	MgO
Slag 1	43	9	16	23	9
Slag 2	44	4	16	28	8

The Si content in Metal 2 is higher than for Metal 1, resulting in a higher silicon activity. The increased Si content will result in less manganese and a lower Mn activity.

Slag 1 has about twice as much MnO as Slag 2, giving a higher MnO activity. Slag 2 has more SiO_2 than Slag 1, but the amount of CaO is also higher. This gives a lower silica activity than for Slag 1. The activity of SiO_2 is between 0.30 and 0.31 for both slags in the temperature range of 1600 to 1650 °C.

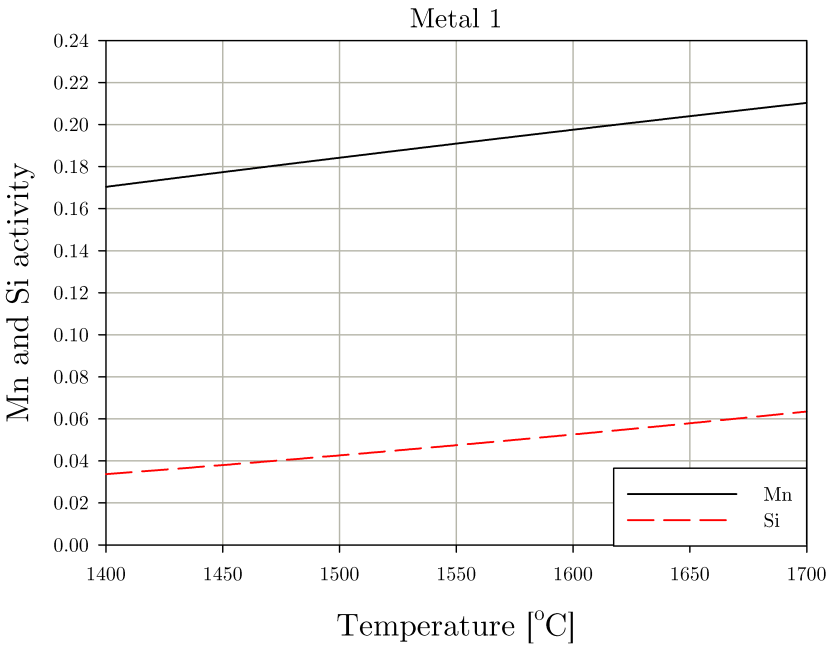

Figure 2.6: The Mn and Si activities for Metal 1.

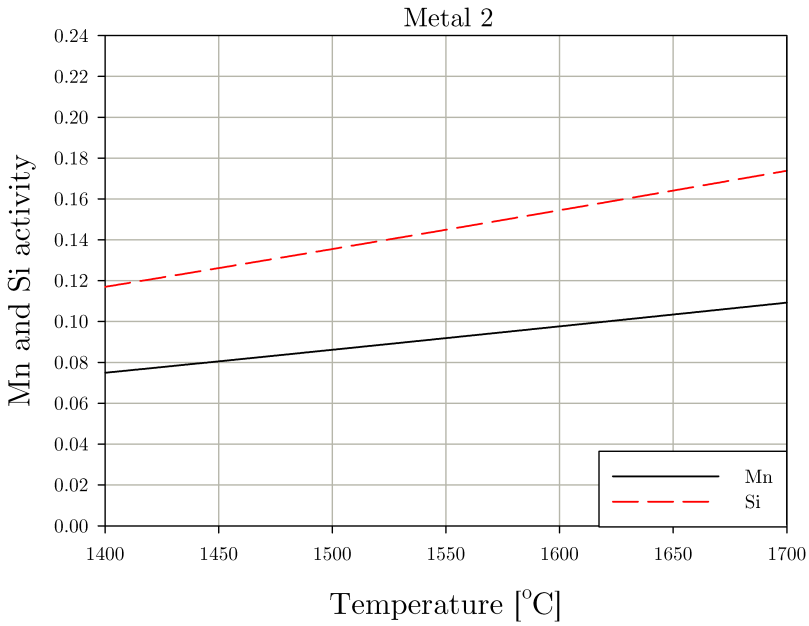

Figure 2.7: The Mn and Si activities for Metal 2.

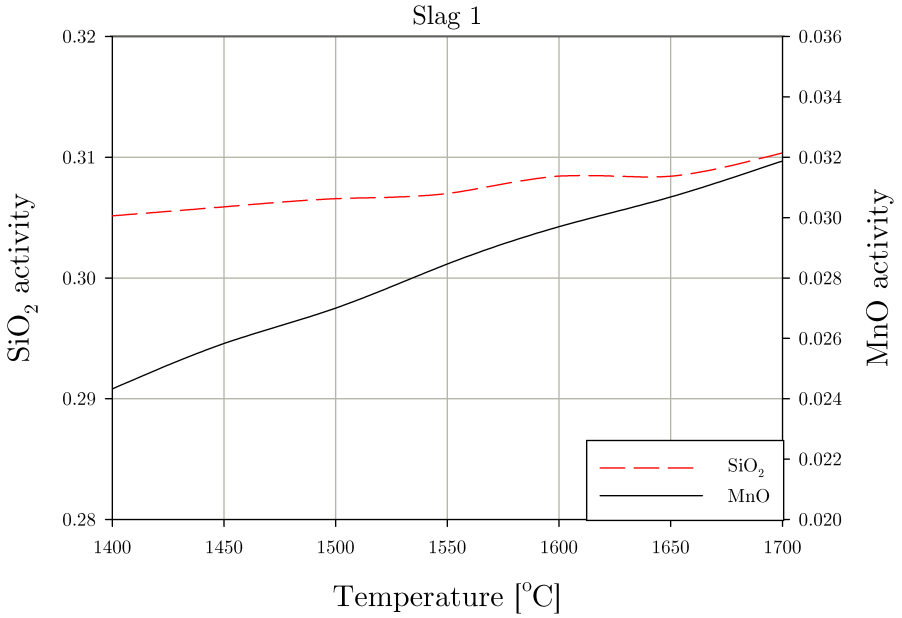

Figure 2.8: The SiO_2 and MnO activities for Slag 1.

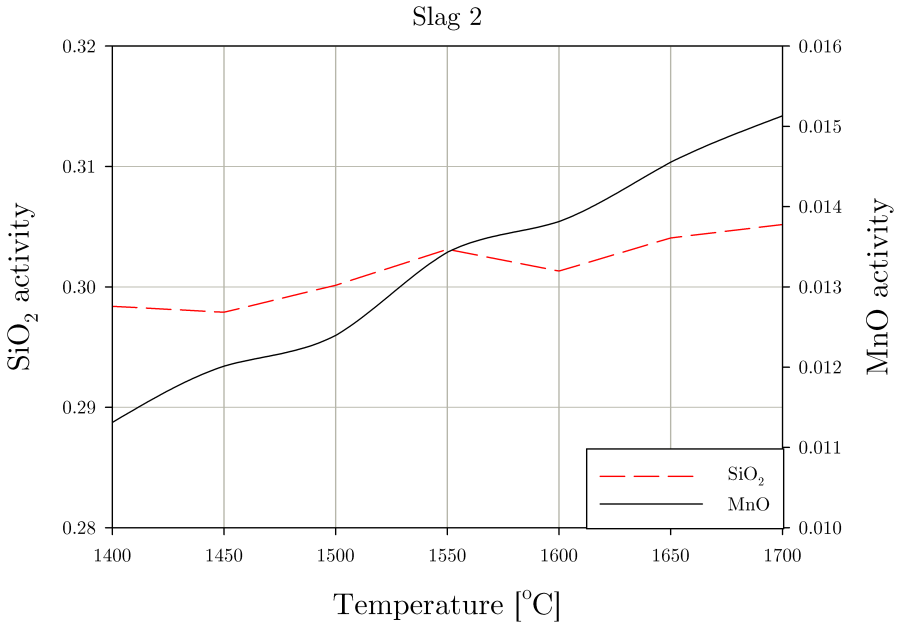

Figure 2.9: The SiO_2 and MnO activities for Slag 2.

2.3 The Acheson process

There is not much work done on formation of SiC in the SiMn process. About 95 % of all SiC made today is made by the Acheson process. It is thus revied in order to get an understanding on how SiC is formed in this process.

The process was developed in the late 19^{th} century by Dr. Edward G. Acheson, and the principles for the process today is essentially the same as for the original process (Neerland, 1986). The Acheson process is a batch process and does not achieve more than 10-15 % conversion of the raw materials into SiC.

A sketch of a typical Acheson furnace is shown in Figure 2.10. The design is relatively simple, consisting of a refractory frame with carbon electrodes going through the end walls. The sides can be removed so the furnace can be excavated after firing. The size of the furnace varies with lengths up to 40 meter and width up to 5 meters (Lindstad, 2002). The furnace is fueled by electricity, and heat is produced from the resistance in the graphite core as current passes through it.

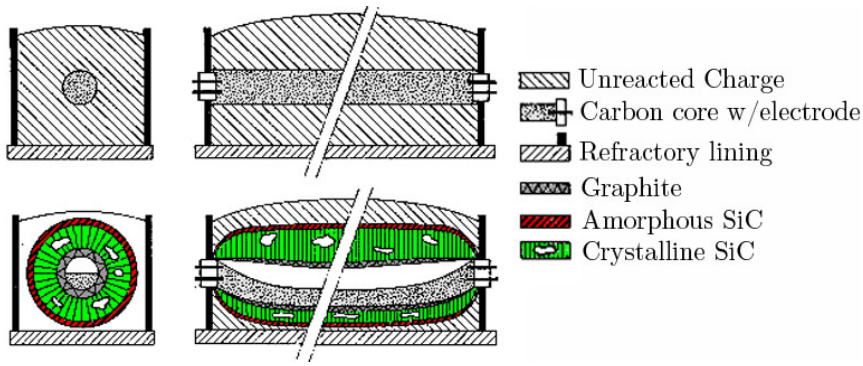

Figure 2.10: Sketch of the Acheson furnace before and after firing, from the side with cross section. Figure is taken from Kordina (1994).

The charge usually consists of silica, finely ground petroleum coke and sawdust. The silica is normally added in the form of sand. The sawdust is added to create porosity, which is needed for the SiC crystals to grow (Dhanaraj et al., 2010; Gupta et al., 2001; Lindstad, 2002). The furnace is fired for 24-48 hours, and reach temperatures up to 2700 °C. When the furnace has cooled down the walls are removed and the furnace is excavated.

Equation (2.12) shows the overall reaction in the Acheson process. The silica is either a solid or liquid, depending on the temperature at the time of reaction. As the temperature exceeds the melting point of silica, c. 1700 °C, SiO_2 melts, becoming glassy and highly viscous.

$$SiO_2(s,l) + 3C(s) = SiC(s) + 2CO(g) \tag{2.12}$$

The reaction becomes thermodynamically favorable above c. 1500 °C. As long as the temperature is below c. 1700 °C the main product from this reaction will be β-SiC. As the temperature increases α-SiC may also form (Lindstad, 2002; Neerland, 1986).

After a certain amount of time the maximum temperature, up to 2700 °C, is reached. At temperatures as high as this more reactions become active. Closest to the core decomposition, sublimation and volatilization of produced SiC occurs according to Equation (2.13), (2.14) and (2.15), respectively. Equation (2.15) is not a reaction, but rather indicates the possible products from sublimation of SiC.

$$SiC(s) \rightarrow C(s) + Si(l) \tag{2.13}$$

$$SiC + SiO(g) \rightarrow 2Si(g) + CO(g) \tag{2.14}$$

$$SiC(s) \rightarrow C(s) + Si(g) + Si_2C(g) + SiC_2(g) \tag{2.15}$$

Further out in the furnace, where the temperatures are lower, the gases are recrystallized back to SiC. This happens according to the reversed form of Equation (2.14) and (2.15). The SiC produced through the gas phase reactions is believed to be primarily α-SiC. The transformation from β- to α-SiC was found by Lindstad (2002) to be irreversible.

According to Moe (2011) the SiC produced at Washington Mills AS in Orkanger, Norway, consists of α-SiC with c. 90 wt.% 6H and 5 wt.% of 4H and 15R, respectively. The maximum production temperatures for the plant lies between 2400 and 2500 °C.

2.4 SiC formation and phases

Nelson et al. (1966) reported the product to be β-SiC when crystals were grown from a carbon saturated silicon melt at 1500 °C.

Zhou & Singh (1995) investigated the growth of SiC particles in a Si-Mo melt with up to 10 wt.% Mo in the temperature range of 1430-1510 °C. They found the product from the Si-C reaction to be primary β-SiC.

Ivantsov & Dmitriev (1998) examined the solubility of SiC in transition metals (TM) and their high Si alloys. The SiC crystals were grown by heating the Si alloy in a graphite crucible. The temperature ranged from 1700 to 1950 °C with silicon concentrations varying from 40 to 80 at.%. The phase of the precipitated SiC crystals were found to vary with the depth of the melt. Crystals at the surface of the melt were found to be mainly α-SiC, type 6H. From the mid section of the crucible the crystals showed a wider range of α polytypes, including 6H, 15R and 21R. At the bottom of the crucible β-SiC was found, but with smaller amounts of α, type 6H.

Krishnarao & Subrahmanyam (1995) looked at formation of SiC from a mixture of rice husk silica and carbon black. The experiments were done both with and without a Co catalyst in the temperature range of 1300 to 1600 °C. β-SiC was reported to form above 1550 °C for the samples without catalyst and above 1400 °C for the samples with the Co catalyst.

Li et al. (2009) investigated the formation of SiC nanowires from SiO(g). The carbon source used was pyrolyzed bamboo slices, and process temperature was set to 1300 °C. The product from the reaction is reported as random β-SiC nanowires.

In production of Si-metal, large amounts of SiC are formed. As the production of Si goes through the formation of SiC and SiO(g), both of these compounds are present in large quantities. SiO(g) is produced in the lower part of the furnace, where the temperatures exceeds 2000 °C. It will ascend the furnace, and react with the charge further up.

SiC can in this way, in addition to precipitation from liquid metal, form by reaction between SiO(g) and carbon or CO(g) according to Equation (2.16) and (2.17) (Schei et al., 1998).

$$SiO(g) + 2C(s) = SiC(s) + CO(g) \tag{2.16}$$

$$3SiO(g) + CO(g) = 2SiO_2(s) + SiC(s) \tag{2.17}$$

Excavation data from industrial Si furnaces (Ciftja, 2011a,b) shows that SiC from the Si process consists of both α- (2H, 4H, 6H, 15R) and β-SiC (3C). There were no direct pattern regarding where the different phases were found, but α-SiC had a tendency to dominate the areas where condensation was observed. The samples taken from the areas close to the bottom showed larger amounts of β-SiC.

From the information found in the articles cited above, the following assumptions can be presumed:

- ▷ α- and β-SiC can be formed through both gas phase and precipitation in melt as well as through reaction between SiO_2 and carbon
- ▷ Temperature is an important factor, β-SiC seems to be dominant at lower temperatures, i.e. below c. 1700 °C, which corresponds with the theory stated in JANAF thermochemical tables (Chase, 1998).

The various experiments and their outcome are summarized in Table 2.4.

Table 2.4: Summary of the different SiC types and how they were produced.

System	Medium	Temp [°C]	Phase	Polytypes	Source	Comment
SiO+C	gas	1300	β	3C	Li et al. (2009)	
SiO_2+C	solid/gas	1300-1600	β	3C	Krishnarao & Subrahmanyam (1995)	$CoCl_2$ as catalyst
Si+Mo+C	liquid	1430-1510	β	3C	Zhou & Singh (1995)	
Si+C	liquid	1500	β	3C	Nelson et al. (1966)	
Si+TM+C	liquid	1700-1950	α, β	6H, 15R, 21R, 3C	Ivantsov & Dmitriev (1998)	TM=transition metals
Si+O+C	gas/liquid	up to 2100	α, β	2H, 4H, 6H, 15R, 3C	Ciftja (2011a,b)	Si-metal production
SiO_2+C	solid/gas	up to 2500	α	4H, 6H, 15R	Moe (2011)	Acheson process

2.5 Wettability of SiC

The wettability of SiC on metal and slag is important for several aspects. It can help explaining both if reaction between the two species is possible and in which phase SiC can be expected.

The degree of wetting between two substances is a way of measuring how well these interact with each other. Wettability between a solid and a liquid can be expressed by the wetting angle, θ. This angle is the result of a balance between the gravitational forces acting on the liquid phase and surface tension between the phases involved (Safarian, 2007).

For the case of a liquid completely wetting a solid substrate θ is 0°, while for the case of a completely non-wetting liquid θ is 180°. The transition between a wetting and non-wetting slag is set at 90°. An angle smaller than 90° is considered as wetting, while larger than 90° is non-wetting. This is illustrated in Figure 2.11.

For the case of a liquid metal or slag on a solid substrate the angle is determined by the interfacial tensions between liquid-solid, liquid-gas and gas-solid. These are connected through the Young's equation, given by Equation (2.18) (Seetharaman, 2005). The subscripts l,g and s denotes liquid, gas and solid, respectively.

$$\gamma_{l,g} \cos\theta = (\gamma_{s,g} - \gamma_{s,l}) \tag{2.18}$$

The wetting angle is dependent on the surface tension of the liquid and solid toward the gas phase. This causes the angle to change with changing atmosphere.

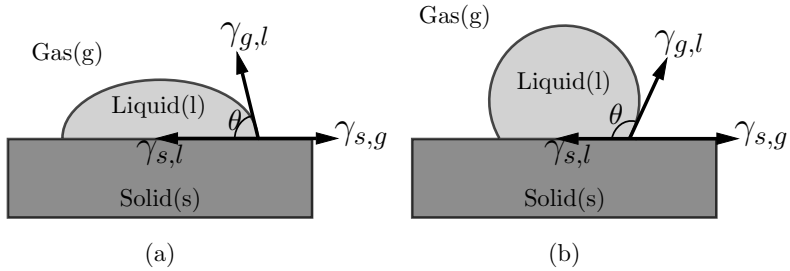

Figure 2.11: Illustrative wetting angles for (a) a wetting liquid and (b) a non-wetting liquid.

If chemical reaction occurs at the interface, the wetting may be enhanced. In this case the Young's equation, Equation (2.18), has to be corrected. The

smallest possible contact angle for the system is then defined by Equation (2.19) (Safarian & Tangstad, 2009).

$$\cos\theta_{min} = \cos\theta_0 - \frac{\Delta\gamma_r}{\gamma_{l,g}} - \frac{\Delta G_r}{\gamma_{l,g}} \tag{2.19}$$

where θ_0 is the wetting angle in absence of reaction, $\Delta\gamma_r$ is the changes in interfacial energy caused by the reaction and ΔG_r is the change in free energy per unit area released by the reaction.

The wetting angle can also be measured by capillary rise in a vertical tube. If the liquid wets the tube material, the liquid phase will rise up the capillary walls. The other case, a non wetting liquid, will give capillary depression, shown in Figure 2.12.

The static height, h, the liquid will be pulled up in the tube is found by a balance between the capillary forces, $2\pi r\gamma_{l,g}\cos\theta$, and the drag of gravity, $\pi r^2 h\rho g$ (von Bahr, 2003). Here r is the tube radius, ρ is the liquid density and g is the acceleration of gravity. An expression for h, given by Equation 2.20, is found when the two competing forces are balanced.

$$h = \frac{2\gamma_{l,g}\cos\theta}{\rho g r} \tag{2.20}$$

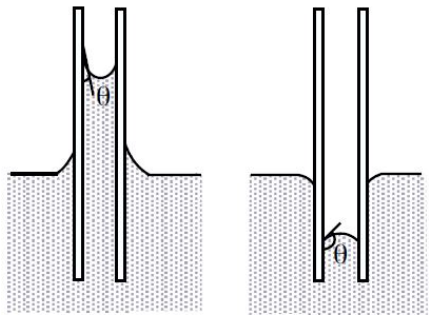

Figure 2.12: Capillary rise for a wetting liquid (left) and capillary depression for a non wetting liquid (right). Figure is taken from von Bahr (2003).

The wetting angle can be measured experimentally by several methods. In this report the sessile drop method has been used, and the apparatus is explained in Section 3.3. With the sessile drop method the sample is filmed while heated, and θ can be approximated from the pictures.

The wetting between SiC and CaO-SiO_2 slags were investigated by Safarian & Tangstad (2009). They investigated CaO-SiO_2 slags containing 47, 50,

55 and 60 wt.% SiO_2 in a vertical tube furnace. The slags were heated on a SiC substrate up to 1600 °C in CO(g) and Ar(g) atmospheres. The samples with 50 and 60 wt.% SiO_2 were tested on a substrate made of sintered SiC powder. The wettability of the slag on the substrate was so good that the liquid slag was sucked down into the substrate after melting. Crystalline SiC was therefore used for the remainding experiments. Gas evlolution was observed, indicating that the system is a reactive system. As no metal was found it was concluded that the gas was likely to be SiC and SiO_2 which reacted to form CO(g) and SiO(g).

The wetting angle was found to be relatively stable with changing temperature and heating rates. Gas phase and slag composition were found to be the two main factors affecting the wetting angle. The contact angle increased with increasing SiO_2 concentration. Wettability was better in Ar(g) than in CO(g). The wetting angles found in the experiments varied from 20 to 73° in Ar(g) atmosphere and 58 to 87° in CO(g) atmosphere for the slags with 47 and 60 wt.% SiO_2, respectively. A picture of the slag/SiC interface is shown in Figure 2.13.

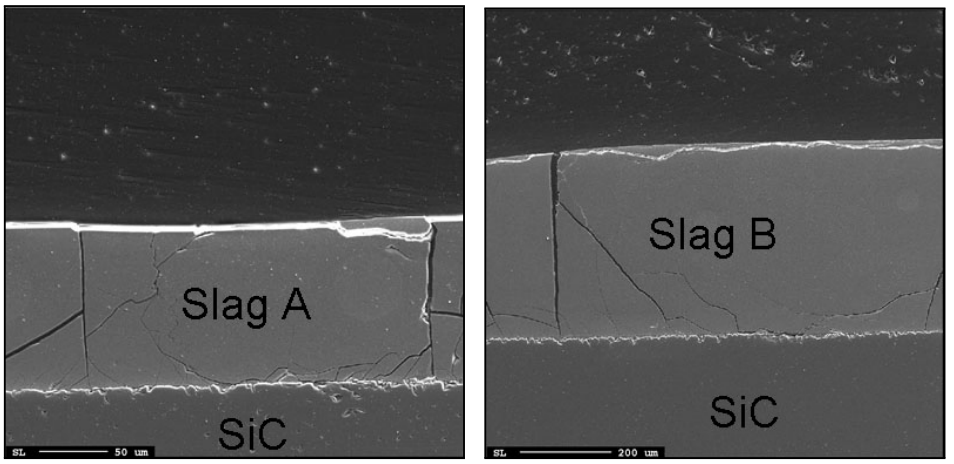

(a) (b)

Figure 2.13: The slag-SiC interface for the two slags A and B, taken from Safarian & Tangstad (2009).

Park et al. (2010b) investigated the dissolution of a SiC particle in a CaO-SiO_2-MnO slag in a confocal scanning laser microscope. They looked at two different slags with 10 wt.% MnO, CaO/SiO_2=1, and 20 wt.% MnO,

CaO/SiO_2=0.5. A SiC particle was placed on top of the molten slag and filmed as it dissolved at 1600 °C.

They found that the slag with 10 wt.% MnO and the highest CaO/SiO_2 ratio, completely wet the particle after 12 minutes. The slag with the lower CaO/SiO_2 ratio did not fully wet the SiC particle throughout the whole experiment. The dissolution of the particle was also faster in the more basic slag. Bubble formation was observed at the interface between SiC and slag, indicating a reactive system. They assumed the gas formation was a product of the reaction between MnO in the slag and SiC.

Mailliart et al. (2009) investigated the wetting between SiC and glass. They used a slag with 23 wt.% CaO, 15 wt.% Al_2O_3 and 62 wt.% SiO_2 which were studied in air at temperatures between 1100 and 1590 °C with the sessile drop technique. The sustrate used for the experiments were sintered α-SiC. They found the wetting to be good, with minimum angle, θ, of 20±4° at 1400 °C. The angle increased with temperature and was measured to c. 50° at 1590 °C.

Gas formation was observed during the experiments. However, no reaction products were found when the samples were investigated by SEM. They also estimated the reaction between SiC and oxides in the melt to be thermodynamically unfavorable. As the experiments were carried out in air, they concluded that the bubble formation was due to oxygen dissolved in the melt which reacted with SiC at the interface.

Ciftja (2009) looked at the wetting between Si-metal and a substrate made from compressed SiC powder. The metal wet the substrate well, and final wetting angle was measured to 18.7° at 1450 °C. This angle is assumed to be somewhat lower than for a solid substrate as the metal infiltrated the substrate. Microscopy pictures reveals that the substrate was dissolved by the liquid metal, shown in Figure 2.14. Ciftja (2009) also tested the wettability of Si-metal on graphite substrates with different roughness. The wetting angle was found to change with the roughness of the substrate, increasing with increasing roughness.

Park et al. (2010a) investigated the carbide capacity of $CaO\text{-}SiO_2\text{-}MnO$ slags. They looked slags with MnO content ranging from 0 to 50 wt.%. The slags were heated to 1500 °C and held for 15 hours. The carbide capacity was found to be strongly affected by slag composition and increase with increasing basicity. The experiments showed that a CaO/SiO_2 ratio of c. 0.8 gave the highest dissolution of carbon in the slag system. For a silica

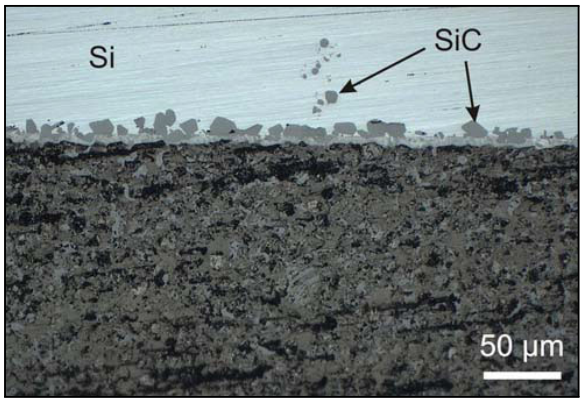

Figure 2.14: The interface between the SiC substrate and Si-metal. Figure is taken from Ciftja (2009).

saturated slag the carbide capacity was found to decrease with increasing MnO content up till c. 35 wt.%.

The wetting properties of a slag can change when an electric potential is introduced. Kazakov et al. (1993) investigated the effect of electrical potential on slag impregnation of porous refractories. They applied electrical potential to a slag with 46 wt.% CaO, 5 wt.% SiO_2, 38 wt.% Al_2O_3 and 11 wt.% FeO at 1520 °C. They measured the cappilary rise in a cylindrical tube as a potential was applied in the range of +2 V to -10 V at the slag interface. The height of impregnation, given by Figure 2.15(a), varied as the potential was varied and had a pronounced drop between 0 and -2 V. At lower potential the height increased.

The change in wetting properties by applying electrical potential to a molten slag was also confirmed by Mills (2011), shown in Figure 2.15(b). As can be seen in the figure, the wettability of the slag decreases with increasing negative potential.

Table 2.5 summarizes the wetting properties toward SiC for the different systems. The slag basicity, B, has been calculated according to Equation 2.7.

For the slags investigated by Safarian & Tangstad (2009) and Park et al. (2010a), which have the composition closest to that used in SiMn production, the trend is an increase in wetting as the basicity increases. Safarian & Tangstad (2009) found the wetting angle under CO(g) atmosphere to decrease with 29° when the basicity was changed from 0.67 to 1.13.

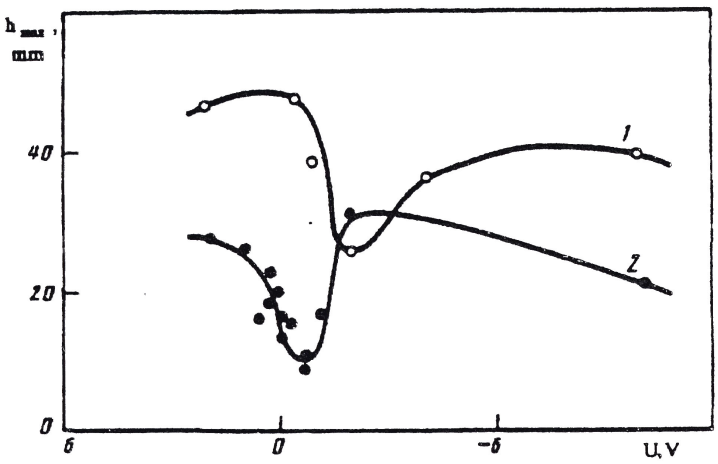

(a)

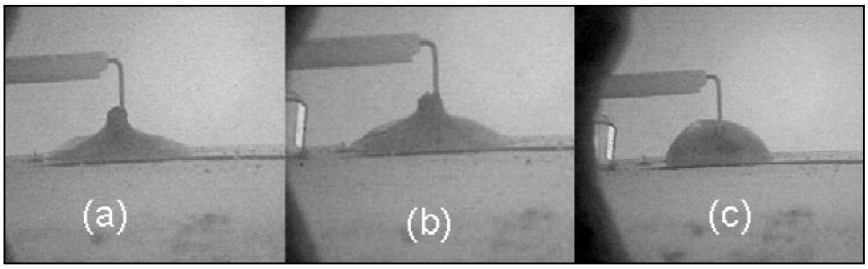

(b)

Figure 2.15: (a) Capillary rise as a function of applied potential. Open circles are for tubes with 7 mm diameter, while solid circles are for tubes with 4 mm diameter (b) Changes in the wetting of a molten slag as an electrical potential is applied at (*a*) 0 V (*b*) -1 V and (*c*) -2 V. Figure is taken from Mills (2011).

Table 2.5: Wetting properties for the different systems and basicities.

System	Slag basicity	Temp [°C]	SiC type	Gas	Wetting	Source
CaO-SiO_2-Al_2O_3	0.30	1100-1590	sintered SiC	Air	20° at 1400 °C 50° at 1590 °C	Mailliart et al. (2009)
CaO-SiO_2	0.67-1.13	up to 1600	sintered and crystalline SiC	Ar(g) CO(g)	73-20° 87-58°	Safarian & Tangstad (2009)
CaO-SiO_2-MnO	0.88-1.22	1600	fused SiC	Ar(g)	low B < high B	Park et al. (2010b)
Si-metal	-	1450	pressed SiC powder	Ar(g)	18.7°	Ciftja (2009)

2.6 Growth of SiC on carbon

SiC will form on a carbon particle either through the reaction with Si from the metal phase, $\underline{Si}$, or SiO_2 from the slag phase, (SiO_2), according to Equation (2.9) and (2.10), respectively. The case of reaction between metal and carbon will be discussed here.

The thickness of the SiC layer will depend on the speed the reactants are transported to the reaction interface. For the simplified growth model of SiC on a carbon particle, the following steps will be of main importance:

1. Transport of Si in the bulk alloy to the carbon surface.
2. Transport of Si from the metal phase through a SiC layer.
3. Transport of C from the carbon particle through the SiC layer.
4. Chemical reaction between Si and C at the carbon particle surface.

Before a product layer is formed, the transport of Si and C, step 2 and 3, can be neglected. However, as soon as a layer of SiC is formed, the reactants needs to be transported through this layer before it can grow thicker. The rate of chemical reactions at high temperatures is fast, and can be considered not to be rate determining. The growth rate is then determined by solid state diffusion of the slowest specie.

Hon & Davis (1980) investigated the self-diffusion of Si in crystalline β-SiC at temperatures between 2010 and 2274 °C and concluded that the diffusion of C in SiC is about two orders of magnitude larger than for Si.

The rate of formation can be described be Equation (2.21) (Ghosh, 2001).

$$r = Ak\,(U_1 - U_2) \tag{2.21}$$

where r is the rate of reaction, A is the area of the reaction interface, k is the reaction constant and $U_1 - U_2$ is the driving force for the reaction. For U_2 the amount at equilibrium for the reactant is often used. As the rate of reaction is dependent on the area, it is also dependent on the surface tension, i.e. wettability, between the reactants.

2.7 Buoyancy of SiC

As mentioned in Section 2.2.1, SiC has previously been observed as a separate phase in SiMn slag when industrial samples were investigated. If the

SiC is formed in the metal phase, the density difference may explain why the SiC is transported into the slag.

When the removal of a solid particle in a liquid system is regarded, there are several factors that has to be taken into consideration. These are the density difference between the particle and the liquid medium, viscosities and movement of the particle and system, respectively (Sandvik et al., 1999).

If the density of the particle is lower than that of the bulk fluid, it will rise. The speed of the particle is determined by forces working on the particle. If the flow is assumed laminar, the main forces are the buoyancy caused by difference in density, and downward drag caused by gravity, shown schematically in Figure 2.16(a). Friction from melt flowing downward will contribute to the downward drag.

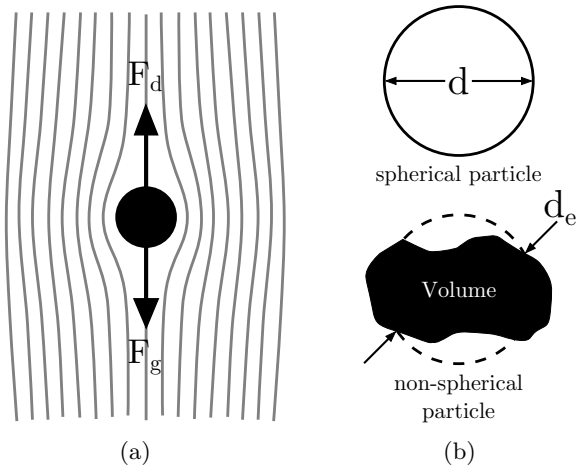

Figure 2.16: (a) Sketch of the forces working on a particle suspended in a liquid with laminar flow and (b) the equivalent diameter, d_e of a particle with the volume V. After Sandvik et al. (1999).

Sandvik et al. (1999) describes the buoyancy for a small particle. The simplest case is a particle rising in a gravity field. The resultant forces acting on the particle, F_R, is a function of particle size, gravity and the difference in densities. F_R can then be described by Equation (2.22):

$$F_R = \frac{\pi d^3}{6} (\rho_f - \rho_s) g \tag{2.22}$$

Where d is the particle diameter [m], ρ_s is the particle density [kg/m^3], ρ_f

is the fluid density [kg/m^3] and g is the acceleration of gravity [9.81 m/s^2].

At a certain point, there will be a balance between the outer forces working on the particle and the frictional forces. At this point the particle will obtain a constant velocity, referred to as terminal velocity. For laminar flow this will be given by Stoke's Equation, Equation (2.23):

$$F_{sphere} = \frac{1}{8} \cdot \frac{24}{Re} \cdot \pi \rho_f \nu^2 d^2 = 3\pi d \nu \mu \tag{2.23}$$

Where Re is the Reynold's number [-], ν is the velocity [m/s] and μ is the viscosity of the fluid [kg/ms]. By combining Equation (2.22) and (2.23) an expression for the terminal velocity of the particle is obtained, Equation (2.24):

$$\nu_{stokes} = \frac{d^2 g \left(\rho_f - \rho_s\right)}{18\mu} \tag{2.24}$$

For particle sizes under c. 100 μm the equation can also be used for non-spherical particles. The equivalent diameter of the particle, d_e, can then be calculated based on the particle volume according to Equation (2.25):

$$d_e = \sqrt[3]{\frac{6V}{\pi}} \tag{2.25}$$

Where V is the particle volume, illustrated in Figure 2.16(b). For this case, Equation (2.24) is then modified to Equation (2.26):

$$\nu_{stokes_2} = \frac{d_e^2 g \left(\rho_f - \rho_s\right)}{30\mu} \tag{2.26}$$

The density of a liquid slag is only slightly dependent on structure, making a reasonable approximation relatively simple (Mills, 2011). The density can be approximated through the molar volume of the slag, V_{slag}, which can be calculated according to Equation (2.27).

$$V_{slag} = \sum \left(X_1 V_1\right) + \left(X_2 V_2\right) + \left(X_3 V_3\right) + ... + \left(X_n V_n\right) \tag{2.27}$$

where X is the molar fraction and the subscripts detonate the different species in the slag. When the molar volume is known, the density of the slag, ρ_{slag}, can be calculated by Equation (2.28). M_{slag} is the molecular weight of the slag.

$$\rho_{slag} = \frac{M_{slag}}{V_{slag}} \tag{2.28}$$

Table 2.6: Densities for the main species in SiMn alloys and slags. All data for the liquid phase, data is taken from FactSage 5.0 and Aylward & Findlay (2008).

Specie	Density [kg/dm^3]	Molecular weight [g/mol]	Molar volume [dm^3/mol]
SiC	3.22	40.10	0.012
Si	2.33	28.09	0.012
Mn	7.20	54.94	0.008
Fe	7.86	55.85	0.007
C	2.27	12.01	0.005
SiO_2	2.34	60.09	0.026
MnO	5.45	70.94	0.013
Al_2O_3	3.99	101.96	0.026
CaO	3.45	56.08	0.016
MgO	3.58	40.31	0.011

The same approach can also be used for the alloys (Seetharaman, 2005). Density data for the main species in SiMn alloys and slags are listed in Table 2.6.

Table 2.7 shows the molar volume, molecular weight and calculated density for the alloys and slags. Molar volume and density were calculated using Equation (2.27) and (2.28), respectively as well as data from Table 2.6. The alloys and slags from Table 2.3 were used for the calculations.

Table 2.7: Calculated metal and slag densities.

	V [dm^3/mol]	M [g/mol]	ρ [g/dm^3]
Metal 1	0.0090	44.60	4980
Metal 2	0.0095	43.13	4520
Slag 1	0.0203	61.24	3010
Slag 2	0.0206	60.85	2950

If the Metal 1 and Slag 1 in Table 2.3 is used as an example, the viscosity, μ, for the slag at 1600 °C is c. 0.279 Pa $\cdot$ s and decreases to 0.215 Pa $\cdot$ s at 1650 °C (Tang, 2011). For the metal the viscosity at 1600 °C can be calculated to c. 0.014 Pa $\cdot$ s (Battezzati & Greer, 1989).

Chapter 3

Experimental

To determine where and how SiC is formed in the SiMn process, several experiments were carried out. Slag and metal were heated in graphite crucibles together with a coke particle to see if SiC was formed. The wettability toward SiC was also tested to find out how the different species interacted.

The main focus were given to melting experiments in a vertical tube furnace. Slag and metal were heated together with a coke particle to form SiC. HC FeMn and pure Si were also mixed together to precipitate SiC from carbon dissolved in the alloy.

SiC from the industrial SiMn process was investigated with X-ray diffraction (XRD) to find out which SiC phase is present in this system.

Wetting experiments were done with metal and slag on a crystalline SiC substrate. This will show how good slag and metal wet SiC, and will be helpful when determining the origin of the SiC, as well as explaining the results from the tube furnace.

3.1 The raw materials

Two industrial grade SiMn alloys with c. 19 and 29 wt.% Si have been used for the experiments. These will be called "Metal 1" and "Metal 2" for the rest of the thesis. Two slags were also provided, one for each metal. These will be called "Slag 1" and "Slag 2" and used in combination with Metal 1 and 2, respectively. The origin of the slags will not be discussed due to confidentiality. Composition for the slags and alloys are listed in Table 3.1 and 3.2.

In addition to the metal and slag, the raw materials consisted of HC FeMn and Polish coke. All the material was provided by Eramet Norway AS.

Table 3.1: Chemical composition in wt.% for the slags. Analysis done by Eramet Norway Kvinesdal AS.

	SiO_2	MnO	Al_2O_3	CaO	MgO	K_2O	FeO
Slag 1	42.4	9.1	15.2	22.5	7.5	0.76	0.65
Slag 2	43.4	3.9	15.3	27.8	6.9	0.72	0.20

	TiO_2	BaO	Na_2O	S	B	Total
	0.26	0.71	0.36	0.47	0.68	100.59
	0.13	0.74	0.36	0.48	0.66	100.59

Table 3.2: Chemical composition in wt.% for the alloys. Analysis done by Eramet Norway Kvinesdal AS and Eramet Norway Porsgrunn AS.

Alloy	Si	Mn	Fe	C	P	Ca	S	Sum
HC FeMn	0.06	77.5	15.0	6.9	0.17	n/a	n/a	99.7
Metal 1	19.2	68.9	10.0	0.88	0.16	0.004	0.017	99.5
Metal 2	28.8	62.1	8.3	0.03	0.07	0.004	0.005	99.7
Si	99.9	n/a	0.04	n/a	0.00	n/a	0.014	100.0

The raw material was crushed down to a size of -5 mm, and split with a splitter into 4 different batches. Batch one was used for the experiments at 1600 °C, while batch 3 was used for the 1650 °C experiments.

The composition of the industrial SiC is listed in Table 3.3. This is crude SiC from the Acheson process and consists of α-SiC with c. 90 wt.% 6H,

5 wt.% 4H and 5 wt.% 15R (Moe, 2011). "Free Si" and "Free C" are carbon and silicon which are present as a seperate phase in the SiC crystals.

Table 3.3: Chemical composition of crude SiC from Washington Mills in wt.%. Data from Moe (2011).

SiC	Free C	Free Si	SiO_2	Fe	Al	Ca
98.55	0.5	0.5	0.5	0.075	0.02	0.02

The analysis of the coke is shown in Table 3.4.

Table 3.4: Chemical analysis for the coke. All numbers in wt.%.

H_2O	Ash	Volatiles	Fixed C
3.9	10.1	1.1	88.9

The coke particles were ground into balls with c. 20 mm diameter, and dried at 50 °C for 48 hours before they were used. Figure 3.1 gives the diameter of the coke particle measured in three different directions. The closer the three values are, the rounder the coke particle.

The roundness of the particles can be measured by a shape coefficient. An often used and simple measure is the minimum diameter divided by the maximum diameter, d_{min}/d_{max} (Sandvik et al., 1999). This coefficient will be 1 for a sphere, and decrease as the roundness decreases. The coke particles had a shape coefficient ranging from 0.85 to 0.96, shown on the right y-axis in Figure 3.1.

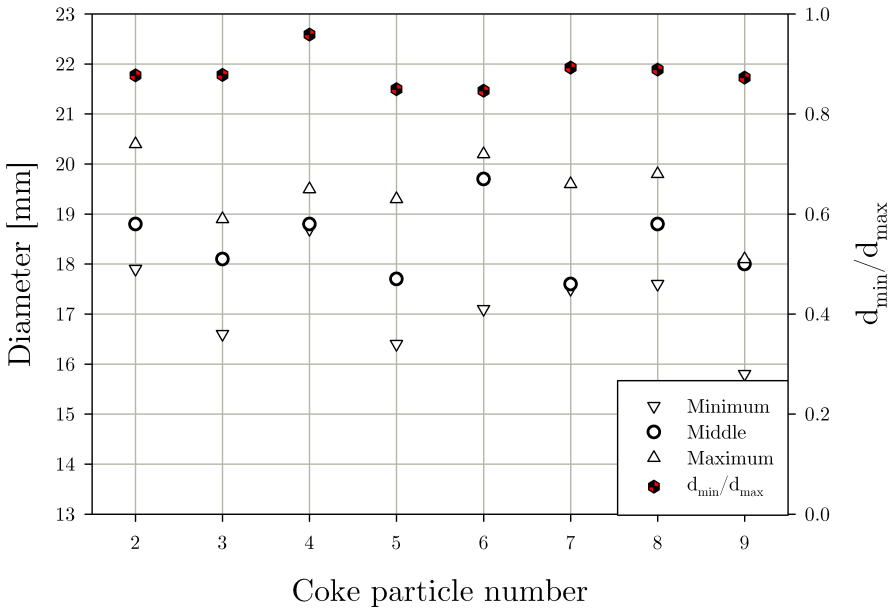

Figure 3.1: Diameter of the coke particles, ranging from the shortest to the longest side, as well as the shape coefficient. The "coke particle number" corresponds to the experiment in which they were used, see Table 3.5. Experiment 1 was carried out without a coke particle.

3.2 Vertical tube furnace

The vertical tube furnace makes it possible to heat the samples in an inert gas atmosphere. The heat is supplied by a resistance graphite element and the furnace can hold samples at temperatures up to c. 1700 °C.

3.2.1 Experimental setup

Figure 3.2 shows a picture of the furnace used for the experiments. A cross sectional sketch and operation procedure for the furnace can be found in Appendix D.

A sketch of the crucible used for the experiments is shown in Figure 3.3(a). To ensure that the coke particle is submerged into the liquid, a graphite tap is suspended from the lid. Three holes were also drilled to ensure free gas flow in and out of the crucible.

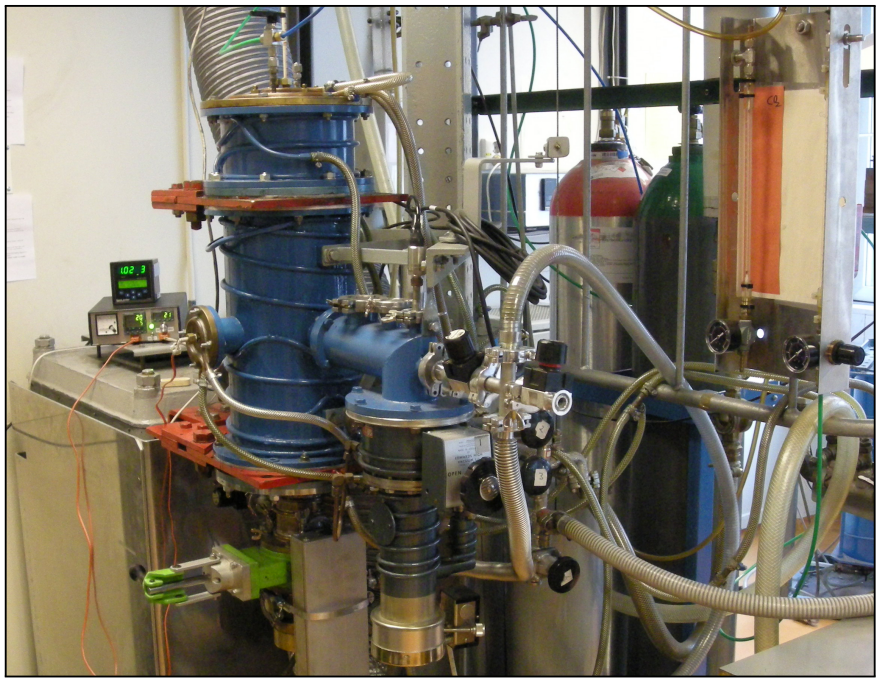

Figure 3.2: The vertical tube furnace. The controller is shown to the far left.

3.2.2 Sample preparation and experimental parameters

The crucible was filled with crushed metal and slag according to experiment type, summarized in Table 3.5. The crucibles were all filled up to c. 6 mm below the top, and the amount present is therefore variating from experiment to experiment. With the exception of the HC FeMn & Si experiment, a rounded coke particle was added under the tap of each crucible, as illustrated in Figure 3.3(b).

The samples were heated to holding temperature and held for one hour, with the exception of the HC FeMn & Si experiment which was held for 90 minutes. All experiments were run under argon atmosphere, with a gas flow of c. 2.5 dm^3/min. The gas was Argon 4.0, which has a purity of minimum 99.99 % Ar (Yara Praxair, 2011). Detailed data for the heating program is shown in Table D.2 in Appendix D.

The Slag 1 sample at 1650 °C crept out of the crucible. The experiment with Slag 2 at 1650 °C were therefore not carried out in order to prevent damaging the heating element or other furnace components.

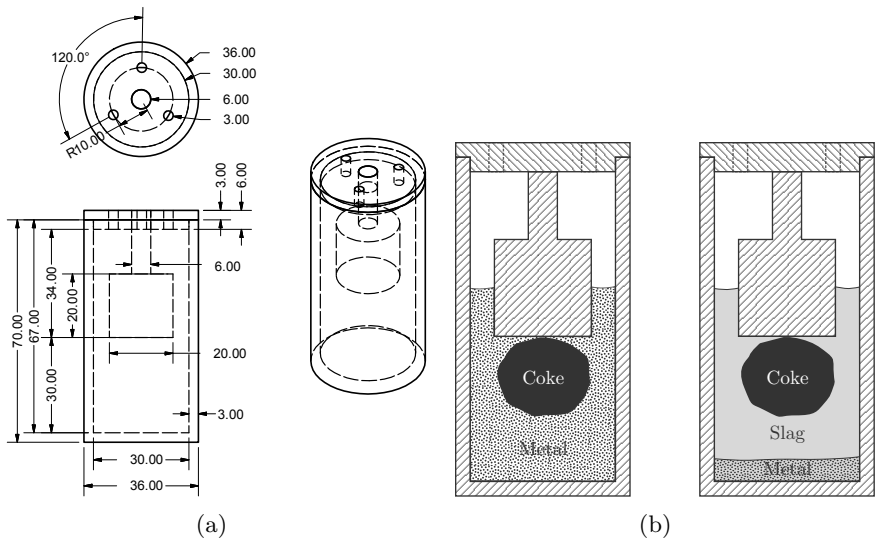

Figure 3.3: The crucible used for the experiments (a) Technical sketch with crucible dimensions (b) Illustrative drawing of the filled crucible for the metal and slag experiments, respectively.

For the HC FeMn & Si sample, some of the top layer of the sample was removed before the crucible was filled with epoxy. This was crushed and analyzed by XRD in order to determine which SiC phases had formed.

The cooled crucibles were filled with Struers Epofix epoxy to prevent change in the sample during cutting. When the epoxy had hardened, the crucibles were cut lengthwise in two in a Struers Discotom with a diamond cutting blade.

A section of the cut crucible was selected from the cross section for investigation by EPMA. The samples were selected form the coke/metal and coke/slag transitions. This was done to find out if there had been any SiC formed on the coke particle.

The EPMA samples were cast in 25 mm forms with Struers Clarocit epoxy. Grinding was done with Struers #1000, #1200, #2400 and #4000 grid size SiC paper and polished with 1 μm polishing cloth. No coarser SiC paper than #1000 was used to prevent damage on the sample surface. All samples were dried at 50 °C for c. 2 hours to remove moisture after grinding. In addition the samples were put in a drying cabinet at 75 °C over night before investigated in the EPMA.

The samples selected for EPMA were also pictured using a Leica MEF4M

Table 3.5: List over the experiment types and amount of metal and slag used. Experiment #9, with Slag 2 at 1650 °C, was not carried out.

#	Experiment	m_{metal} [g]	m_{slag} [g]	m_{coke} [g]	T_{max} [°C]	t_{hold} [min]
1	HC FeMn & Si	43.87+25			1600	90
2	Metal 1	112.04		3.07	1600	60
3	Metal 1	109.69		3.14	1650	60
4	Metal 2	97.64		3.81	1600	60
5	Metal 2	110.62		3.31	1650	60
6	Slag 1	10.11	56.44	3.65	1600	60
7	Slag 1	10.09	51.72	2.60	1650	60
8	Slag 2	10.14	50.21	4.26	1600	60
9	Slag 2	10.07	52.15	2.06	1650	60

light microscope with 2.5x magnification. These pictures were put together with Adobe Photoshop CS4 software to form an overview of the whole coke particle boundary.

3.3 Wettability testing

The wettability testing give a real time observation of how a sample behaves when melted on a substrate.

3.3.1 Apparatus

The wetting experiments were done in a horizontal tube furnace, shown schematically in Figure 3.4.

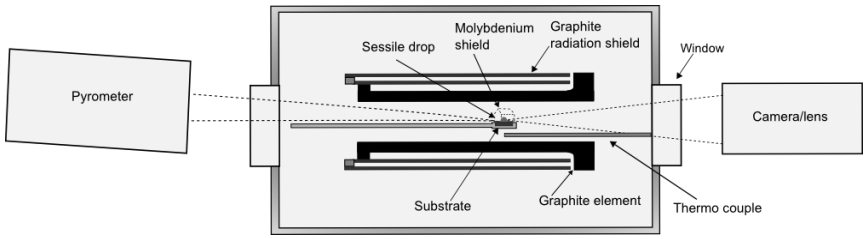

Figure 3.4: The furnace used for the wetting experiments. Modified after Safarian & Tangstad (2009).

The element and heat shield in the furnace are both constructed of graphite, which allows fast heating and cooling rates (Safarian & Tangstad, 2009). The sample is placed on a substrate in the holder at the center of the furnace. A molybdenum heat-shield is placed over the sample, marked "sessile drop" in Figure 3.4, to protect it from heat radiation from the graphite element.

The temperature is controlled by a type C thermocouple, and checked by a Keller PZ20 pyrometer, which is focused on the substrate in front of the sample. A firewire camera with a telecentric lens is placed at the side of the furnace and focused on the sample. The camera records up to 15 frames per second at a maximum resolution of 1392×1040 pixels.

The setup can be run with Ar- or CO-gas. Heating rate ranges from 5 to 300 °C/min, which gives the possibility of reaching target temperature in a short time. The substrate where the sample is placed is small with a diameter of 10 mm. This limits the amount of sample for each test to a couple of grams at most. The wetting angle between substrate and sample can be measured based on the pictures recorded during heating.

3.3.2 Sample preparation and experimental parameters

Six different wetting experiments were done, two for the alloys on SiC, two for the slags on SiC and two for the slags on graphite. The experiments on SiC substrate was done under CO(g) atmosphere, while the ones on graphite were done under Ar(g) atmosphere. The latter ones were done under Ar(g) in order to compare these results with the ones from the tube furnace. Furnace operation for the sessile drop experiments were assisted by Tone Anzjøn, SINTEF.

For the samples, c. 0.01 g was cut out from the raw material. The samples were taken close to the center of the bulk material.

The SiC substrate was made from a large crystal of crude SiC from Washington Mills AS, Orkanger. The chemical analysis of the SiC is shown in Table 3.3. Single crystals were broken off from the larger piece and polished with a diamond grinding disk down to c. 0.5 mm thick plates. The sample was placed on top of the SiC plate which again was placed on a graphite substrate, shown in Figure 3.5.

An overview of all samples with heating rates are shown in Table 3.6. The experiments were stopped when the sample was fully melted, and no more

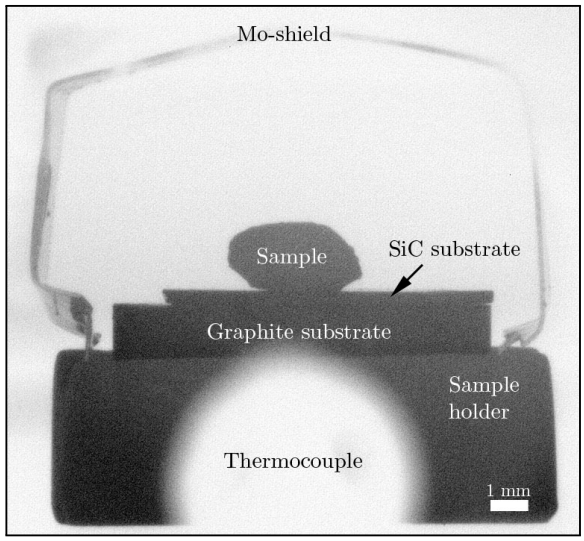

Figure 3.5: The sample as placed inside the furnace, colors are inverted from original picture.

change was observed. Due to problems with the first Metal 2 sample, Metal 1 and 2 were tested twice.

The temperatures were measured by both a thermocouple and a pyrometer. The thermocouple was placed inside the furnace, and may obtain an error as it wears down. The temperatures measured by the pyrometer will be used for the rest of the thesis.

The wetting angles, θ, were calculated using ImageJ software with the DropSnake plugin (`http://rsbweb.nih.gov/ij/`). A sphere was fitted to the particle, shown in Figure 3.6, and the contact angle was calculated by the software.

For the EPMA analysis the samples were ground with Struers MD Piano disks with grid size #220, #600 and #1200, respectively. The Piano disks were used as the SiC substrate is too hard for the standard SiC paper. Fine grinding was done with Struers #2400 SiC paper before the samples were polished with Struers 1 μm polishing cloth. The samples were put in a drying cabinet at 70 °C the night before they were analyzed. The Slag 2 and Metal 2 samples fell off the substrate during cooling and the EPMA analysis were done without substrate.

Table 3.6: List over the experiments with heating rates. Stop temperature are the temperature measured by pyrometer at the time the furnace was turned off.

#	Sample	Heating rates	T_{Stop} [°C]
1	Metal 1	300 °C/min to 900 °C 20 °C/min to stop °C	1642
2	Metal 2	Same as Metal 1	1627
3	Slag 1	300 °C/min to 900 °C 20 °C/min to 1300 °C 10 °C/min to stop	1727
4	Slag 1 on graphite	Same as Metal 1	1717
5	Slag 2	Same as Slag 1	1620
6	Slag 2 on graphite	Same as Metal 1	1691

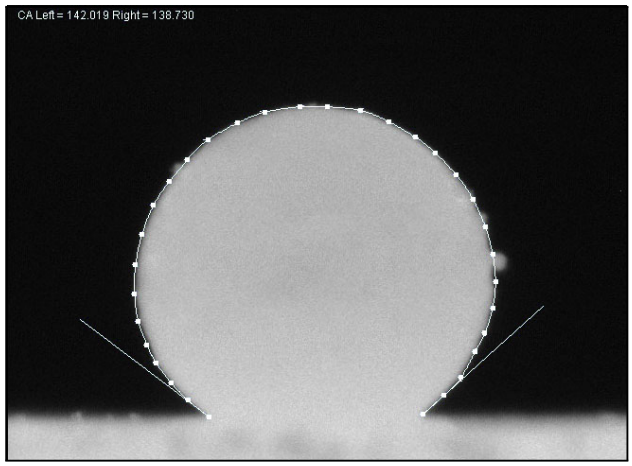

Figure 3.6: The Slag 1 droplet on the SiC substrate at 1360 °C, with fitted circle.

3.4 Electron probe micro analyzer

The Electron Probe Micro Analyzer (EPMA) combines the high resolution advantages of a scanning electron microscope (SEM) with high quality chemical analysis. The EPMA is therefore an invaluable tool when investigating the coke boundary of the coke particle.

3.4.1 Apparatus

JEOL JXA-8500F EPMA was used for analyzing the wetting and tube furnace samples.

The EPMA is basically a SEM equipped with wavelength dispersive X-ray spectrometer (WDS). As the electrons from the field emission gun hit the sample surface, X-rays are generated. Each element send out a X-ray which is unique and characteristic for this particular element.

The WDS has a crystal which is placed between the sample and detector, shown in Figure 3.7. Both the lattice distance, d, and the angle, θ, are known for the system. This can be used to calculate the wavelength, λ, according to Bragg's law, Equation (3.1). The calculated wavelength is compared to recorded data for pure substance and the elements can be determined.

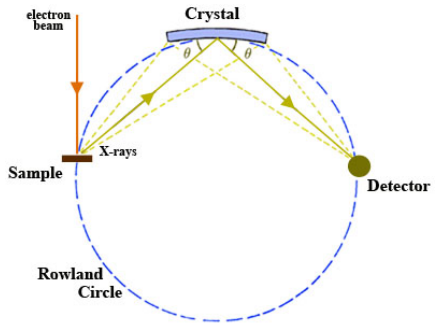

Figure 3.7: A sketch of the WDS setup. Figure is taken from Goodge (2009).

Particles down to 1 μm in diameter can be investigated. As one crystal only can analyze a certain range of waves several WDS units are needed to cover the element range of interest (Goodge, 2009). The JEOL JXA-8500F has 5 WDS units and is able to detect elements in the range of beryllium to uranium (JEOL AB, 2008).

3.4.2 Scan parameters

Before the samples were ground and polished, they were cast into 25 mm diameter forms with Struers Epofix. The grinding parameters for the wetting- and tube furnace samples are described in Section 3.3.2 and 3.2.2, respectively.

Three analysis were taken of each phase in order to exclude outlaying values. The numbers shown in the results are an average of the analysis taken for each phase. The EPMA analysis were done with assistance from Morten Raanes, NTNU.

The microprobe was set to look for the following elements:
Slag: Mn, Si, Al, Fe, Ti, Ca, Mg, K, Ba, Na, S
Metal: Mn, Si, Fe, C, S, P

As the software is not programmed to search for carbides, the detection of SiC will only be qualitative when investigated by the EPMA. When analyzed as metal, SiC will show up as a mix of c. 62-70 wt.% Si and c. 24 wt.% C, with some other minor constituents. This corresponds to a mole ratio of c. 53-56 mol% Si and 44-47 mol% C.

The samples are cast in epoxy before investigation in the EPMA. Together with residue hydrocarbons from the preparation, this causes some contamination in the vacuum chamber. A carbon layer is added to the sample surface to prevent the electrons from building up. These factors combined create an error in the carbon analysis of up to c. 4 wt.% (Raanes, 2011).

3.5 X-ray diffraction

X-ray diffraction determines the crystal structure of the samples and is used to determine whether it is α- or β-SiC that is present in the sample.

3.5.1 Apparatus

The X-ray diffraction analysis were done with a Bruker AXS D8 Focus. Slag samples containing SiC from an industrial SiMn furnace, and the top layer of the HC FeMn and Si samples were analyzed with XRD to determine the SiC phase present.

A crystalline material has a crystal structure with unique parameters for that specific compound or element. These parameters are defined by a unit cell with cell lengths a, b, c which are connected by three angles α, β, γ. The lattice plane spacing, d, is detected by the XRD.

In the machine, X-rays with a wavelength λ are projected onto the sample at an angle θ, illustrated in Figure 3.8. Diffraction occurs when rays that

have traveled a complete number, n, of wavelengths hit the sample surface (PANalytical B.V, 2010).

Bragg's law, Equation (3.1), gives the relationship between d and λ. θ is varied by rotating the sample and this will give conditions where the Bragg's law are satisfied for the different d-spacings (PANalytical B.V, 2010).

$$n\lambda = 2d\sin\theta \tag{3.1}$$

The results are recorded by the detector and plotted as intensity against angular position. Each crystalline element produces a signature pattern, and by comparing to a database the phases in the sample can be identified.

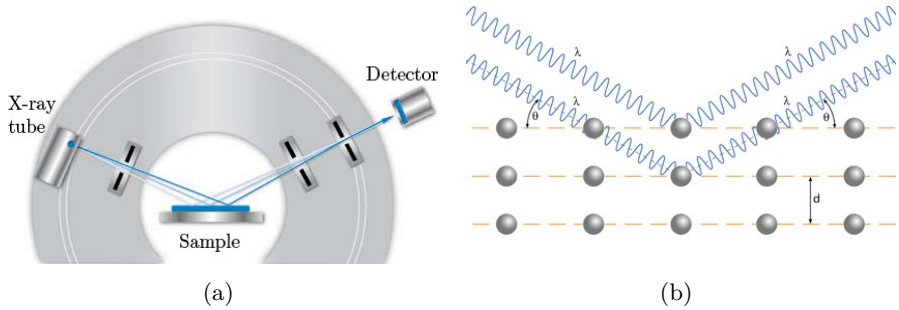

Figure 3.8: (a) Sketch of the XRD setup (b) Sketch of the atom layers and X-rays. Figures are taken from Bruker AXS (2011); PANalytical B.V (2010)

3.5.2 Sample preparation and scan parameters

To investigate the SiC formed in the SiMn process, three slag samples from the coke bed of Furnace 2, Eramet Norway Kvinesdal AS were investigated. The HC FeMn & Si sample was tested to compare the SiC formed in the metal to the SiC found in the furnace.

For each analysis about 5 g of finely crushed sample is needed. The material was crushed in a Siebtechnik TS100 vibratory disk mill with a steel disk for 90 seconds. The target was a powder with a particle size smaller than 40 μm. The ground powder was then spread evenly onto the specimen holder. A glass plate was used to compress the powder, make the surface leveled with the sample holder and remove the excess powder.

The samples were then put into the sample changer and a quick scan was done of one sample to find the main peaks. A slower scan was then performed over the area of interest. Scan parameters for the scans are listed in Table 3.7.

The SiC was to hard for the steel mill to crush finely, which caused background noise in the scans. The final scans were therefore assisted by Bjørn Eske Sørensen, NTNU.

Table 3.7: Scan parameters for the metal and slag.

Start angle [°]	End angle [°]	Step size [°]	Step time [sec]
3	80	0.009	174

Chapter 4

Results

The results from the tube furnace- and wetting experiments and the XRD analysis are shown in this chapter. Extensive material from the analysis is given in the appendices.

4.1 Tube furnace results

The tube furnace results show where and how much SiC that was formed on the coke particle. SiC was formed both through the slag and the metal, with the metal samples giving the most SiC.

4.1.1 Macro scope observations

Figure 4.1 to 4.8 show the crucibles after they were cooled and cut lengthwise. The section selected for EPMA is marked on the crucible, and the polished sample is shown to the right.

With the exception of the HC FeMn & Si sample, all the experiments indicated good wetting toward the crucible, and both metal and slag were pulled up along the graphite.

The experiment with HC FeMn & Si, 1600 °C, Figure 4.1, was done to form SiC from the carbon dissolved in the HC FeMn alloy. As can be seen in Figure 4.1(a), the solidified metal inside the crucible consisted of porous and well mixed metal phase. No separate top layer was observed. The

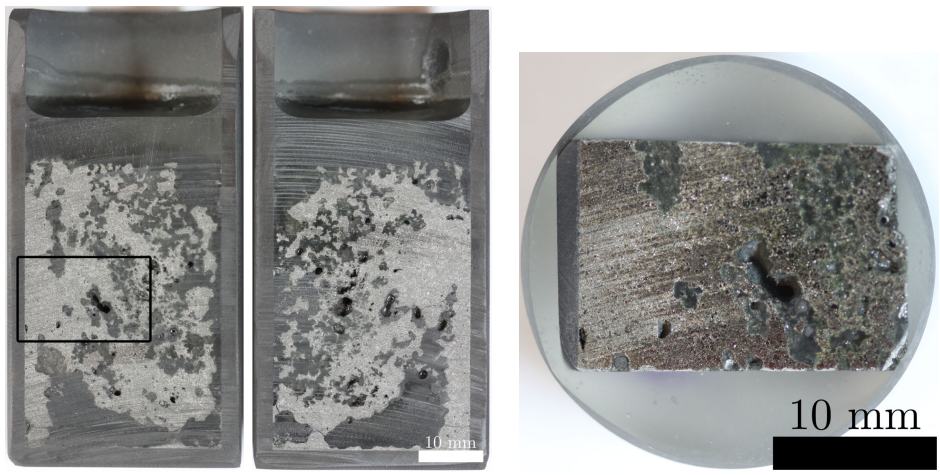

(a) (b)

Figure 4.1: The HC FeMn and Si sample (a) Right after cutting, the gray phase is metal while the rest is epoxy (b) Section chosen for EPMA.

pores may have been caused by gas formation during the holding time. The section chosen for EPMA, shown in Figure 4.1(b), was taken from the mid section of the sample.

The Metal 1 samples are shown in Figure 4.2 and 4.3 for 1600 °C and 1650 °C, respectively. The coke particle had risen to the top of the metal, as was expected from the density difference. Both samples had a cavity beneath the coke particle, at the center of the crucible. The 1650 °C sample had a larger cavity, which reached almost the full height of the coke particle.

The samples selected for EPMA are shown in Figure 4.2(b) and 4.3(b). Both of the samples shows the lower half of the coke particle in contact with the metal. There is no visible trace of a reaction product on the coke/metal interface. For both samples the metal has shrunk during solidification, creating a gap between the coke and metal. The gap is larger for the 1600 °C sample.

The Metal 2 experiments are shown in Figure 4.4 and 4.5 for 1600 °C and 1650 °C, respectively. The cross sections is close to equal for both experiments. A cavity was observed stretching from c. 10 mm below the coke

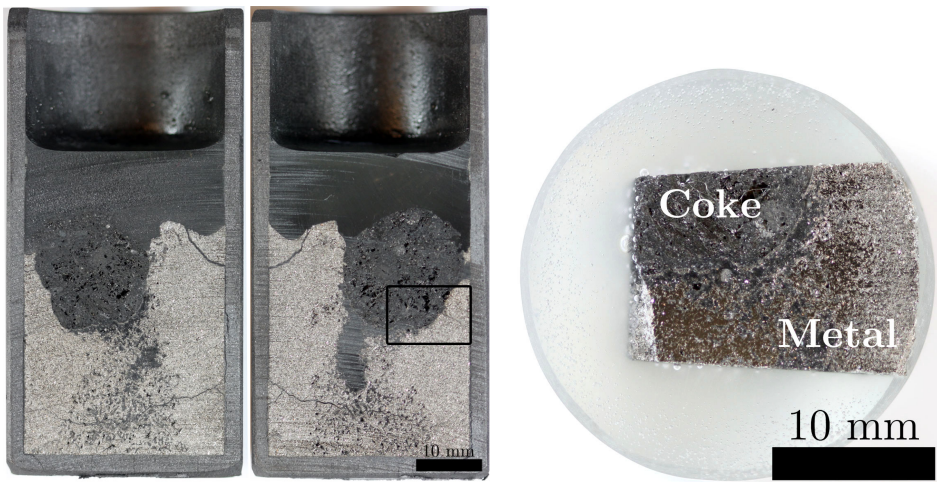

(a) (b)

Figure 4.2: The Metal 1, 1600 °C sample (a) Coke particle surrounded by gray metal (b) Section chosen for EPMA.

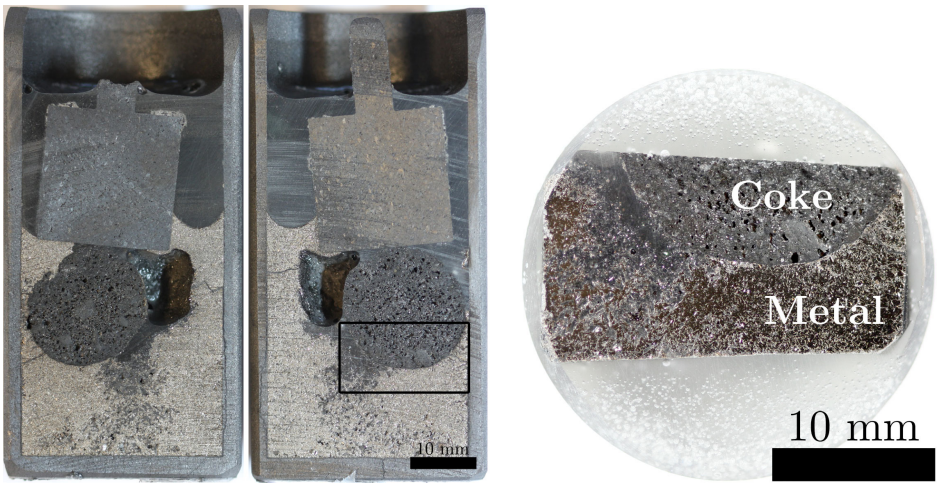

(a) (b)

Figure 4.3: The Metal 1, 1650 °C sample (a) Coke particle submerged into the metal (gray) with a cavity going alongside the coke particle (b) The section chosen for EPMA, coke particle at the top.

particle and all the way to the top of the crucible. The cavities are similar to those observed in the Metal 1 samples, only larger and deeper.

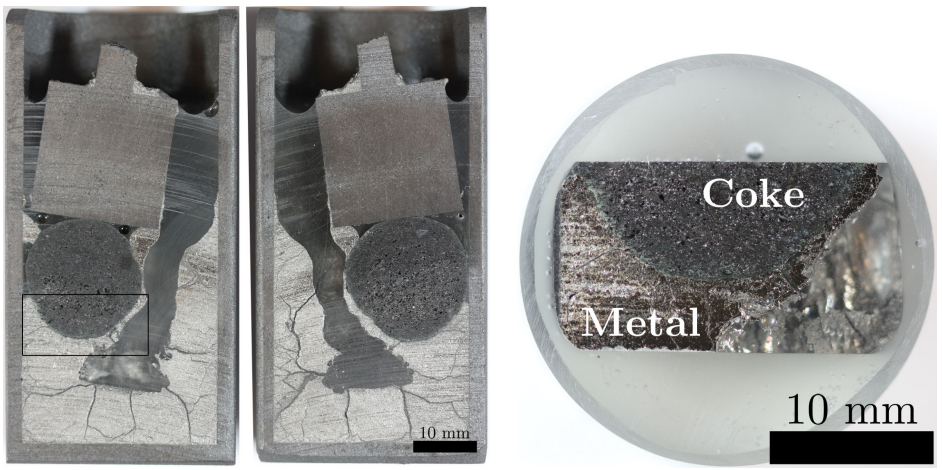

(a) (b)

Figure 4.4: The Metal 2, 1600 °C sample (a) Coke particle submerged in metal (gray) (b) The sample chosen for EPMA, coke on top, cavity to the right.

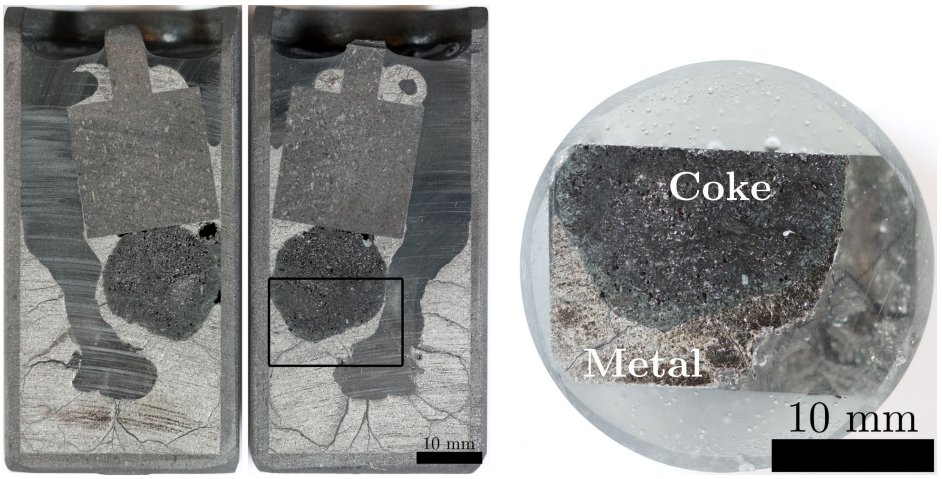

(a) (b)

Figure 4.5: The Metal 2, 1650 °C sample (a) Coke particle (black) submerged in metal (gray) (b) The sample chosen for EPMA, coke on top, cavity to the right.

Both samples had a large amount of cracks in the metal, likely to be caused by shrinkage during solidification. Some metal was also observed at the top of the graphite tap. This may be metal that was charged and did not descended down in the crucible when melting.

The samples chosen for EPMA are shown for in Figure 4.4(b) and 4.5(b) for the 1600 °C and 1650 °C samples, respectively. A gray-green layer had formed on both samples at the coke/metal interface. The layer was thicker for the 1650 °C sample.

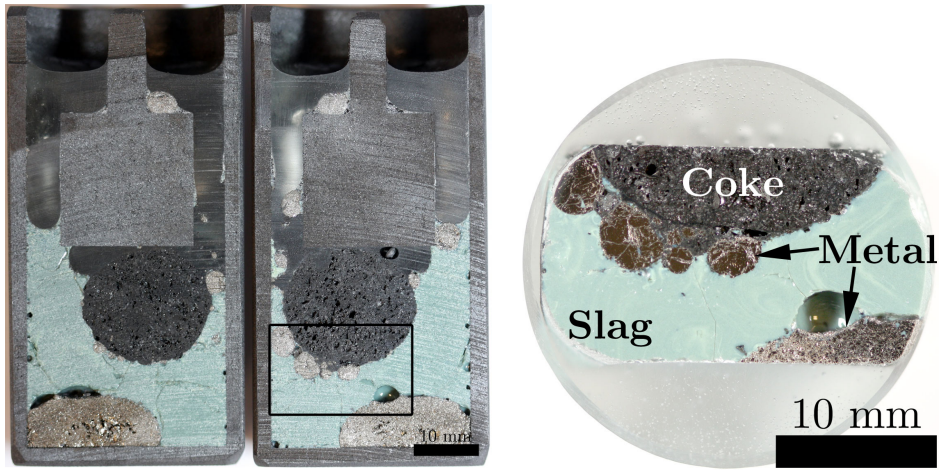

(a) (b)

Figure 4.6: The Slag 1, 1600 °C sample (a) Coke particle submerged in slag (green), surrounded by metal droplets (b) The sample chosen for EPMA, coke particle on top with metal droplets attached, slag (green) and original metal at the bottom right.

Figure 4.6 and 4.7 shows the experiments with Slag 1 at 1600 °C and 1650 °C, respectively. For Slag 1 at 1600 °C, several metal droplets were found around the coke particle. Metal was also observed at the graphite tap. During charging of the sample the metal was added first, and therefore placed at the bottom of the crucible. The metal is denser than the slag, and was expected to stay at the bottom of the crucible.

As can be seen in Figure 4.7(a), almost all the slag in the crucible is gone for the 1650 °C sample. The inside of the crucible was covered with a thin layer of solidified slag, both on the crucible walls and on the tap suspended from the lid.

The areas selected for EPMA were chosen so that both the coke particle, slag and the original metal was included. The EPMA samples for Slag 1 at 1600 °C and 1650 °C are shown in Figure 4.6(b) and 4.7(b), respectively. For the 1650 °C sample, some slag was found in the gap between the coke

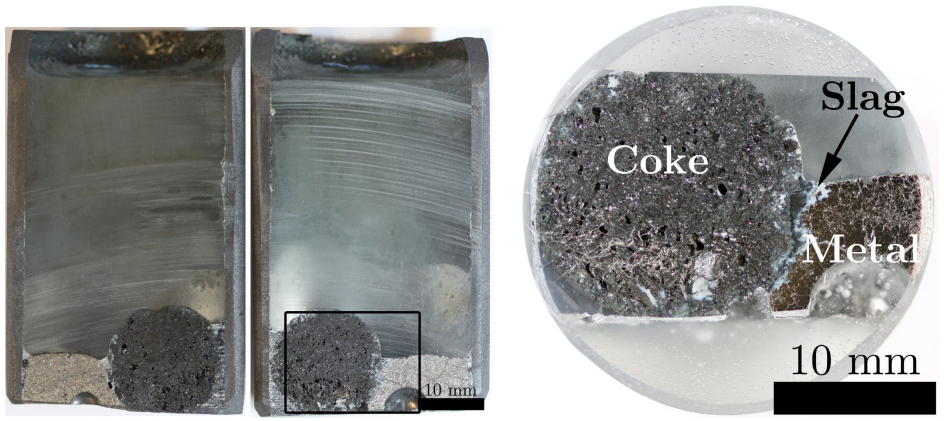

(a) (b)

Figure 4.7: The Slag 1, 1650 °C sample (a) Coke particle (black) and metal (gray) at the bottom of the crucible (b) The sample chosen for EPMA, coke to the left, some slag in the middle and metal at the right.

particle and the metal.

Figure 4.8 shows the Slag 2, 1600 °C sample. The slag was more compact than Slag 1. The added metal was located at the bottom of the crucible. No metal was seen higher up in the crucible. Slag had crept up the crucible walls almost all the way to the top, indicating good wetting between the slag and graphite.

The part chosen for EPMA is shown in Figure 4.8(b). The slag was very brittle, and cracks formed during solidification, sawing and grinding. Some light green spots was seen where slag had penetrated into the coke close to the slag/coke boundary.

Figure 4.9 shows the holder with crucible right after Slag 1, 1650 °C was taken out of the furnace. Traces of slag was observed all the way from the holes in the lid to the bottom of the sample holder. The escaped slag had gathered at the bottom seal.

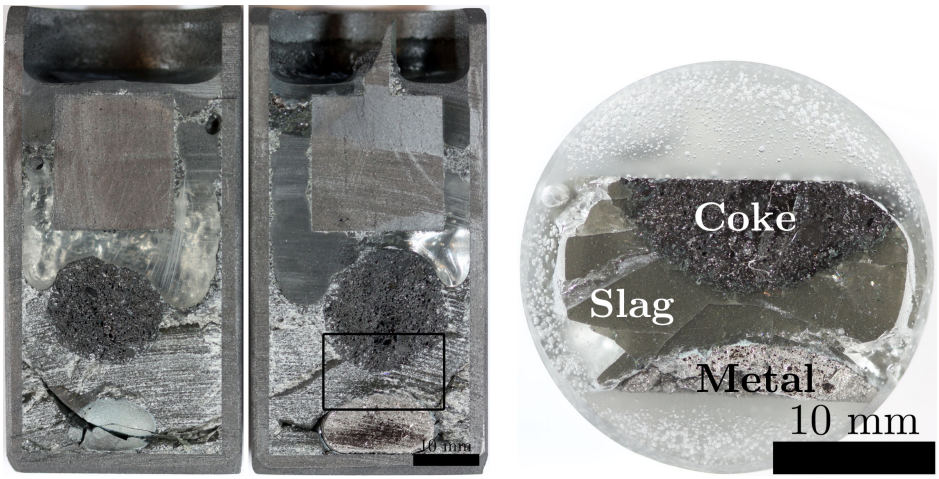

(a) (b)

Figure 4.8: The Slag 2, 1600 °C sample (a) Coke particle (black) on top of the slag (b) Sample selected for EPMA, coke particle at the top (black), slag in the middle (green) and metal at the bottom (gray).

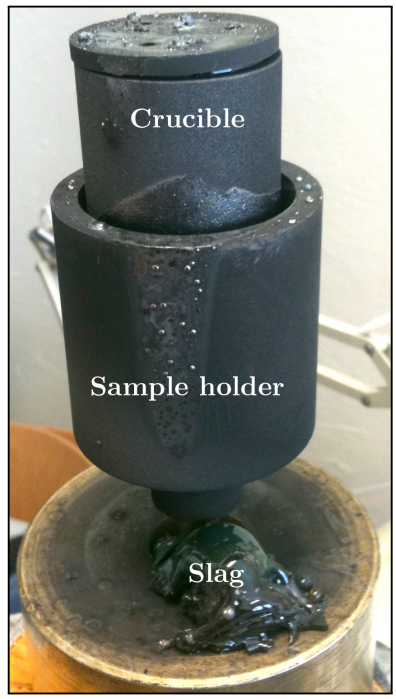

Figure 4.9: The sample holder with crucible after the Slag 1, 1650 °C experiment. The sample holder is in the lowered position.

4.1.2 EPMA and microscope results

Sections of the eight samples from the tube furnace were analyzed by EPMA. The metal and slag phases were analyzed and, with the exception of Metal 1, the slag/coke and metal/coke boundaries were mapped. The analysis from the EPMA give a detailed overview of the coke particle boundary, as well as where and how much SiC that had formed.

The general result was that the metal samples gave the most SiC, and the amount increases with increasing Si content. SiC was found on the slag samples, but to a smaller extent.

The analysis from the EPMA are listed in Table 4.1 and Table 4.2 for the slag and metal analysis, respectively.

Table 4.1: The slag analysis from EPMA of the tube furnace samples. All values in wt.%.

Sample	Phase	SiO_2	MnO	Al_2O_3	CaO	MgO	K_2O	FeO	TiO_2	BaO	SO_3	Total
Slag 1, 1600 °C	gray	40.8	2.2	20.1	22.41	9.7	0.78	0.01	0.07	0.71	1.52	98.5
Slag 1, 1650 °C	dark gray	30.9	0.4	24.9	28.2	10.8	0.02	0.02	0.06	0.85	1.79	97.9
	dendrites	29.4	0.4	24.1	36.2	5.5	0.03	0.02	0.01	0.44	1.82	97.9
	gray	33.4	0.2	27.1	14.9	20.3	0.05	0.01	0.11	1.50	2.01	99.7
Slag 2, 1600 °C	gray	41.4	1.5	17.5	27.49	6.7	0.44	0.037	0.069	0.945	1.229	97.37

Both Slag 1 and 2 gave a homogeneous phase after solidification from 1600 °C. Compared to the original slag composition, shown in Table 3.1, the SiO_2, MnO and FeO content were lower with a decrease of 1.6 and 2.0 wt.%, 6.9 and 2.4 wt.% and 0.64 and 0.16 wt.%, for Slag 1 and 2, respectively. The other elements in the slag had a relative increase.

Slag 1 at 1650 °C was not homogeneous, which made it difficult to compare total composition to the original slag. However, the SiO_2, MnO and FeO content for these three phases are much lower than the original slag. The phase with the most SiO_2 had only 33.4 wt.%.

The metal analysis are shown in Table 4.2. All samples solidified into two separate phases. The phases had c. 9 and 23 wt.% Si for Metal 1 and c. 23 and 33 wt.% Si for Metal 2. SiC mainly consisted of Si and C, with small amounts of impurities.

The analysis from the HC FeMn & Si experiment showed that the metal had a high Si content, confirming a successful attempt to increase the silicon content in the alloy. Large amounts of SiC were observed in the sample.

The analysis for the Slag 1, 1600 °C sample showed that the metal droplets had about the same composition as the original metal. The iron content was lower, but the overall composition was about the same. The slag used for the experiment had 0.65 wt.% FeO. It is unlikely that a metal with 8.5 wt.% Fe is produced during the experiment.

All metal samples had a high carbon content, in most phase measured to c. 2-3 wt.%.

Figure 4.10 to 4.13 show pictures taken of the samples by EPMA. Light microscopy pictures, showing an overview over the whole coke boundary, can be found in Appendix A for all the samples except the HC FeMn & Si sample.

Figure 4.10(a) show a picture taken of the HC FeMn & Si sample. SiC was found in the metal and not as a separate phase at the top, which was expected from the density difference. The rest of the sample had a similar distribution of SiC.

A section of the Metal 1, 1600 °C sample is presented in Figure 4.10(b). A layer of SiC is found at the edge of the coke particle. No SiC was observed in the metal phase further out.

A section of the coke/metal interface of the Metal 1, 1650 °C sample is shown in Figure 4.10(c). This sample had less SiC than the 1600 °C sample, and only a few clusters of SiC were observed along the edge of the coke particle.

Table 4.2: The metal analysis from EPMA of the tube furnace samples. All values in wt.%.

Sample	Phase	Si	Mn	Fe	C	P	S	Total	Comment
HC FeMn and Si,	dark gray	61.9	0.3	0.0	23.3	0.02	0.01	85.6	SiC
1600 °C	light gray	23.4	67.1	9.4	2.3	0.01	0.01	102.2	
	gray	34.1	54.5	12.6	2.7	0.01	0.01	103.9	
Metal 1,	light gray	9.4	75.1	11.3	2.9	0.02	0.01	98.8	
1600 °C	gray	22.6	65.6	11.0	2.2	0.01	0.00	101.7	
	dark gray	67.5	1.3	0.2	23.4	0.01	0.00	92.5	SiC
Metal 1,	dark gray	67.8	0.4	0.1	24.4	0.02	0.00	92.7	SiC
1650 °C	light gray	9.4	75.9	11.0	3.2	0.00	0.00	99.6	
	gray	22.0	65.6	10.6	2.6	0.00	0.01	101.1	
Metal 2,	light gray	23.2	69.1	7.2	1.8	0.00	0.01	102.1	
1600 °C	gray	33.3	57.2	10.1	2.1	0.00	0.00	102.7	
Metal 2,	light gray	22.7	68.2	7.3	2.3	0.00	0.00	101.1	
1650 °C	gray	33.3	57.0	9.9	2.6	0.00	0.00	102.8	
Slag 1,	light gray	9.5	77.1	10.1	2.8	0.00	0.00	99.6	org. Metal
1600 °C	gray	22.6	66.6	9.8	2.0	0.00	0.00	101.1	org. Metal
	light gray	9.9	78.4	8.6	2.7	0.01	0.00	99.7	“new” metal
	gray	23.0	68.3	8.5	1.9	0.01	0.01	102.0	“new” metal
Slag 1,	light gray	9.4	77.0	10.2	2.7	0.00	0.01	99.3	
1650 °C	gray	22.3	67.2	9.5	2.0	0.00	0.00	101.3	
Slag 2,	light gray	22.7	68.6	6.9	2.5	0.00	0.00	101.6	
1600 °C	gray	32.5	57.3	9.8	2.8	0.01	0.00	102.5	

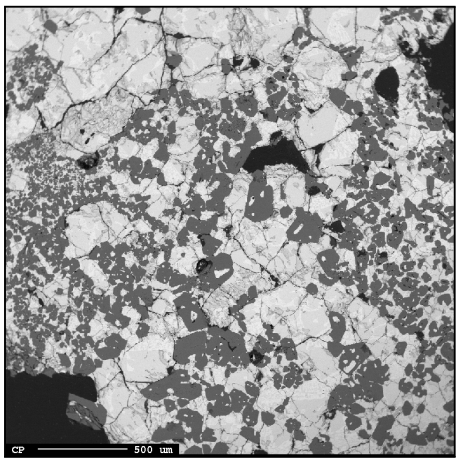

(a) HC FeMn and Si

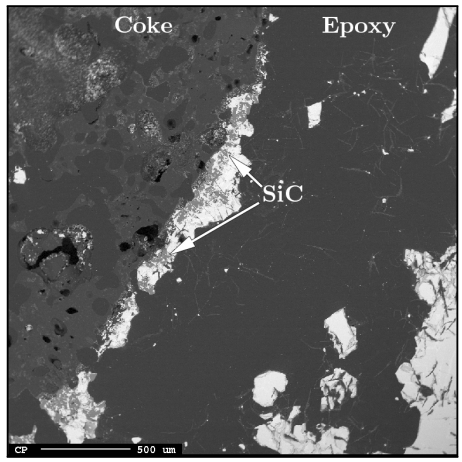

(b) Metal 1, 1600 °C

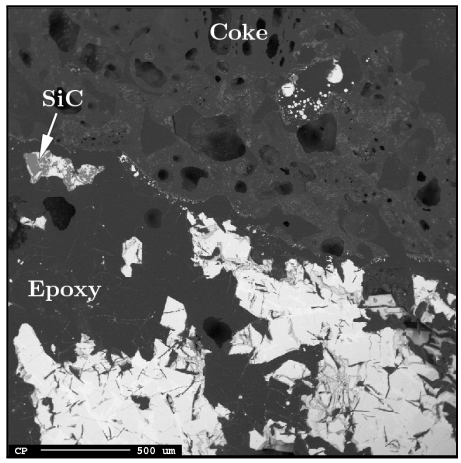

(c) Metal 1, 1650 °C

Figure 4.10: (a) The HC FeMn & Si sample, the gray phase is metal while dark gray phase is SiC (b) The Metal 1, 1600 °C sample (c) The Metal 1, 1650 °C sample. The gray phase in the two latter figures is metal.

The mapping of Metal 2 at 1600 °C and 1650 °C is shown in Figure 4.11(a) and 4.11(b), respectively. To the left is a backscatter image of the sample, while the mapping is to the right. Carbon, SiC and Si are marked in green, yellow and red, respectively.

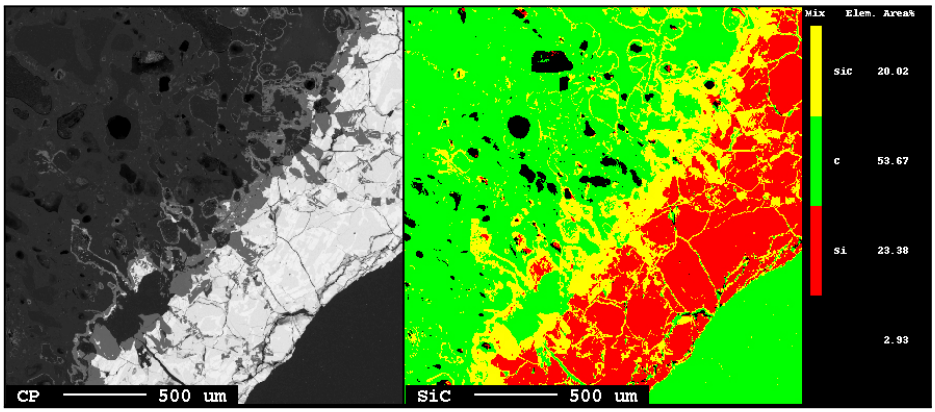

(a) Metal 2, 1600 °C

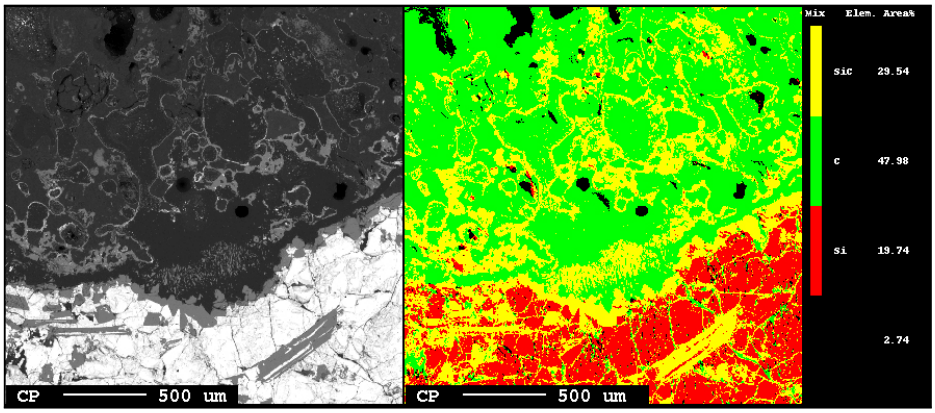

(b) Metal 2, 1650 °C

Figure 4.11: (a) Map of the Metal 2, 1600 °C sample. (b) Map of the Metal 2, 1650 °C sample. In both images, the coke particle is to the upper left in black-gray and the metal to the lower right in light gray. SiC (gray) is shown in between. The right image is a map for C, Si and SiC marked with green, red and yellow, respectively. The black areas are cavities in the coke particle.

Metal 2 had substantially more SiC than Metal 1 at the coke particle boundary. A layer of SiC was observed along the edge of the coke particle at both 1600 and 1650 °C. Several places SiC was also observed further away from

the coke/metal boundary.

As can be seen in Figure 4.11, SiC penetrated deeper into the coke particle for Metal 2 at 1650 °C. No mapping was done of the Metal 1 samples, making it impossible to compare the depth of penetration for the two alloys. Based on the amount of SiC present, and the amount of Si in the alloys, it can be assumed that the layer is thickest for Metal 2.

Mapping for Slag 1, 1600 °C and 1650 °C is given in Figure 4.12. As for the metal, the backscatter image is shown to the left and the mapping to the right.

A thin layer of SiC was observed at the edge of the coke particle, more pronounced for the 1650 °C sample. In this sample the slag seemed to penetrate deeper than for the 1600 °C sample, indicating that the slag might have been less viscous. Higher porosity in the coke particle may also affect the depth of penetration.

Mapping of Slag 2 at 1600 °C is presented in Figure 4.13. The slag had penetrated fairly deep into the coke particle. Less SiC formed at the coke particle than for Slag 1, and only a small amount of SiC was observed close to the slag. The metal drop at the bottom contained minor amounts of SiC.

An approximation of the thickness of the SiC layer and depth of penetration into the coke particle are summarized in Table 4.3. The "Amount" is an estimate of how much SiC that was present in the mapping, relative to the sample with the most SiC. The scale goes from 1-5, where 1 is the least and 5 is the most. As no mapping was carried out for Metal 1 it is hard to determine the amount and depth of penetration. The thickness of the SiC layer is, however, estimated. Metal 1, 1650 °C is not included as there were only found clusters of SiC.

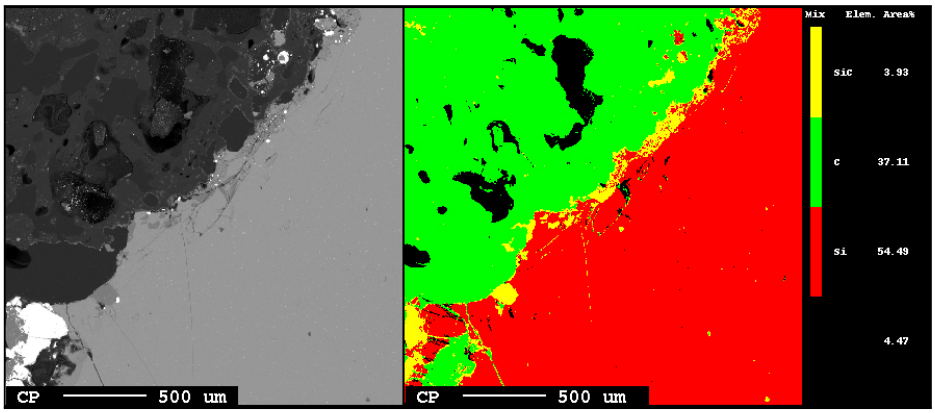

(a) Slag 1, 1600 °C

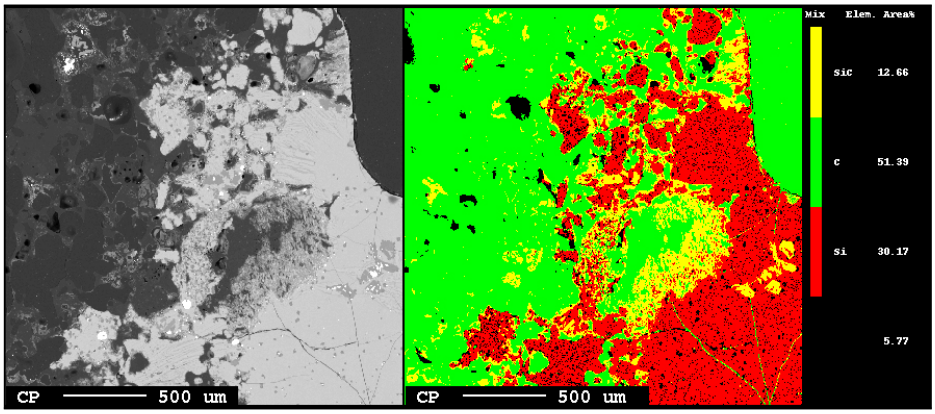

(b) Slag 1, 1650 °C

Figure 4.12: (a) The Slag 1, 1600 °C sample (b) The Slag 1, 1650 °C sample. In both images, a backscatter image with the coke particle (black-gray) and the slag (gray) is shown on the left side. Some metal droplets (white) can be seen in both slags. The right image is a mapping for C, Si and SiC represented by green, red and yellow, respectively.

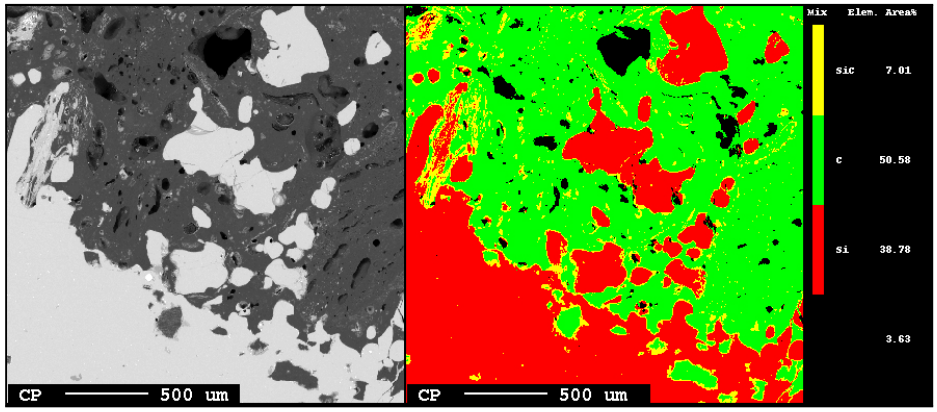

Figure 4.13: The Slag 2, 1600 °C sample. A backscatter image with the coke particle (dark gray) and the slag (gray) is shown on the left side. A few metal droplets (white) can also be seen. The right image is a mapping for C, Si and SiC represented by green, red and yellow, respectively. The black spots are cavities.

Table 4.3: Estimation of thickness, depth and amount of SiC from the mapping of the samples. The amount is ranged relatively, where the sample with the most SiC is 5, and the one with the least SiC is 1.

Sample	SiC layer [μm]		Penetration depth	Amount
	Min	Max	[μm]	
Metal 1, 1600 °C	70	150	n/a	-
Metal 2, 1600 °C	100	300	1850	4
Metal 2, 1650 °C	90	400	1900	5
Slag 1, 1600 °C	40	130	1470	2
Slag 1, 1650 °C	40	230	1400	3
Slag 2, 1600 °C	20	180	2100	1

4.2 XRD results

Three samples containing SiC taken from Furnace 2, ENK were investigated by XRD. SiC from the HC FeMn & Si sample was also analyzed. This was done to determine the phase of the SiC formed in the industrial SiMn process.

The XRD patterns for HC FeMn & Si sample and the three industrial slag samples are given in Figure 4.14. The peaks for β-SiC (3C) and α-SiC (6H) are marked where found. The full scans with additional patterns are shown in Appendix C.

β-SiC was found in all four samples. In one of the slag samples, B5-61, 6H α-SiC was found in small quantities. The sample was taken from the coke bed, just beneath the tip of an electrode. This is the hottest zone in the furnace, and the formation of α-SiC indicate that the temperature has been higher than 1700 °C.

In the HC FeMn & Si sample β-SiC, MnSi and Mn_5Si_3 were found. This is expected when cooling the alloy, if the alloy obtained a Si content between 25 and 30 wt.% as the silicon was dissolved.

The slag samples were complex, and a large amount of peaks were found. The same metal phases as in the HC FeMn & Si sample were observed in several of the slag samples, indicating that there had been metal in the slag when crushing. Graphite was also present in all of the slag samples, likely to be residue from coke particles.

Due to the complexity of the system, the slag was difficult to analyze. The slag phase present is likely to be Augite ($Ca(Mg, Fe^{3+}, Al)(Si, Al)_2O_6$). The peaks are displaced relative to the XRD pattern. This is likely to be caused by the solubility of, among other, Al which increases with increasing temperature. As the slag contains very small amounts of FeO, Fe^{3+} may be replaced by Mn^{3+}, affecting the pattern (Sørensen, 2011).

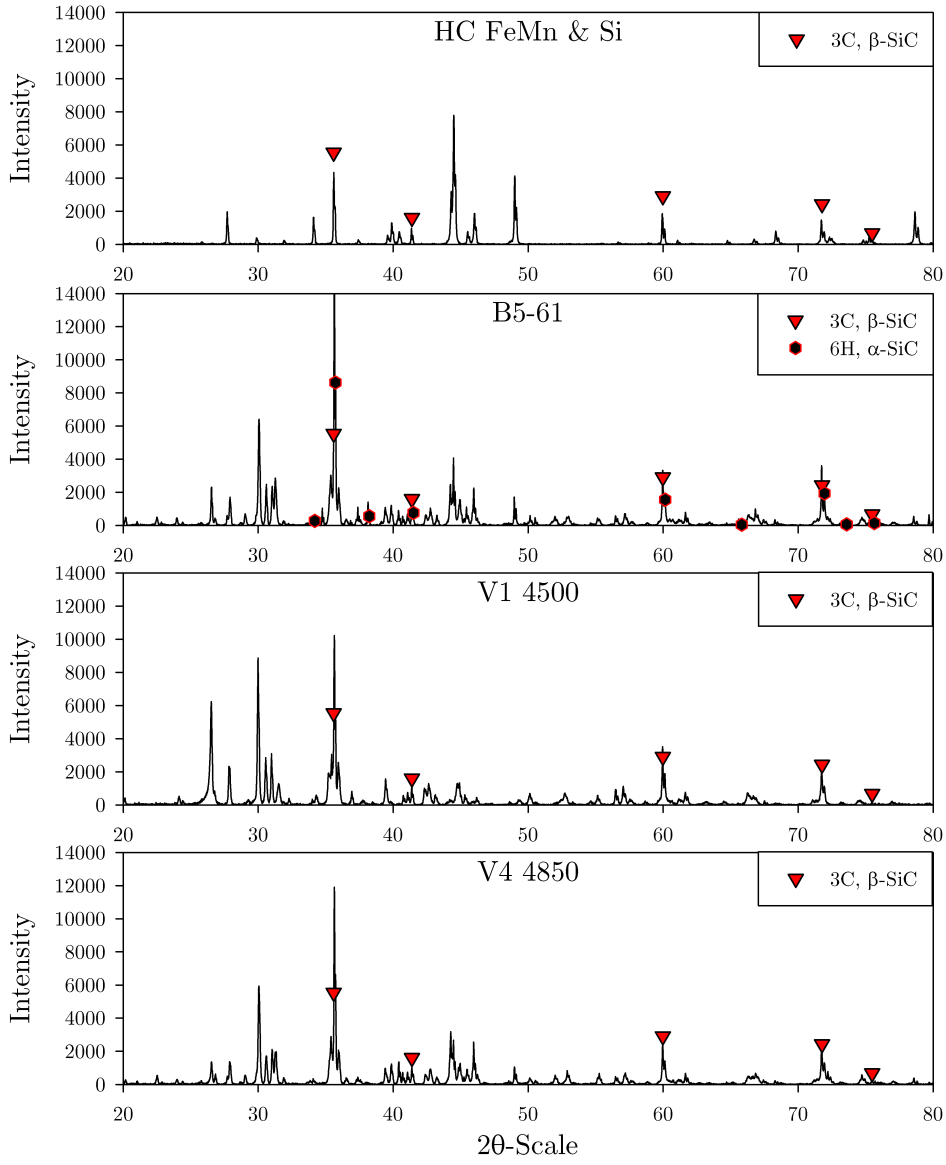

Figure 4.14: The XRD pattern for the three slag samples and the metal sample. The scans are normalized. The additional peaks are explained in Appendix C.

4.3 Wettability testing

The wettability tests were carried out to determine how good the liquid slag and metal wet a SiC substrate. These results are useful for explaining whether the SiC is likely to end up in the slag or metal phase, as well as the reactivity of SiC toward the metal and slag.

4.3.1 Sessile drop testing

Both the metal and slag samples were non wetting toward the SiC substrate. None of the angles changed with increasing temperature. On graphite, Slag 2 was non wetting and the angles were stable with temperature. Slag 1 started as non wetting and the wetting angle slowly decreased down to below 90°, before increasing with further temperature increase.

The measured wetting angles are summarized in Table 4.4. θ is measured from a picture taken right after the sample was fully melted. Both sides of the drop were measured. The difference between the two sides give an estimation of the accuracy of the measurements. The Metal 2 sample did not fully melt, and an accurate angle was not obtainable. A summary of softening and melting temperature for the different experiments can be found in Table 4.5.

Table 4.4: Measured wetting angles for slag and metal. For Metal 1 on SiC and Slag 1 on graphite both the lowest and largest angles are included.

Sample	Substrate	θ_{left} [°]	θ_{right} [°]
Metal 1	SiC	101/151	96/149
Metal 2	SiC	> 90	> 90
Slag 1	SiC	142	139
Slag 1	Graphite	90/157	88/159
Slag 2	SiC	111	135
Slag 2	Graphite	144	146

Figure 4.15 show how Slag 1 changed with increasing temperature. After the sample was fully melted gas evolution was observed, as well as solid particles moving on the sample surface. The other slag samples showed

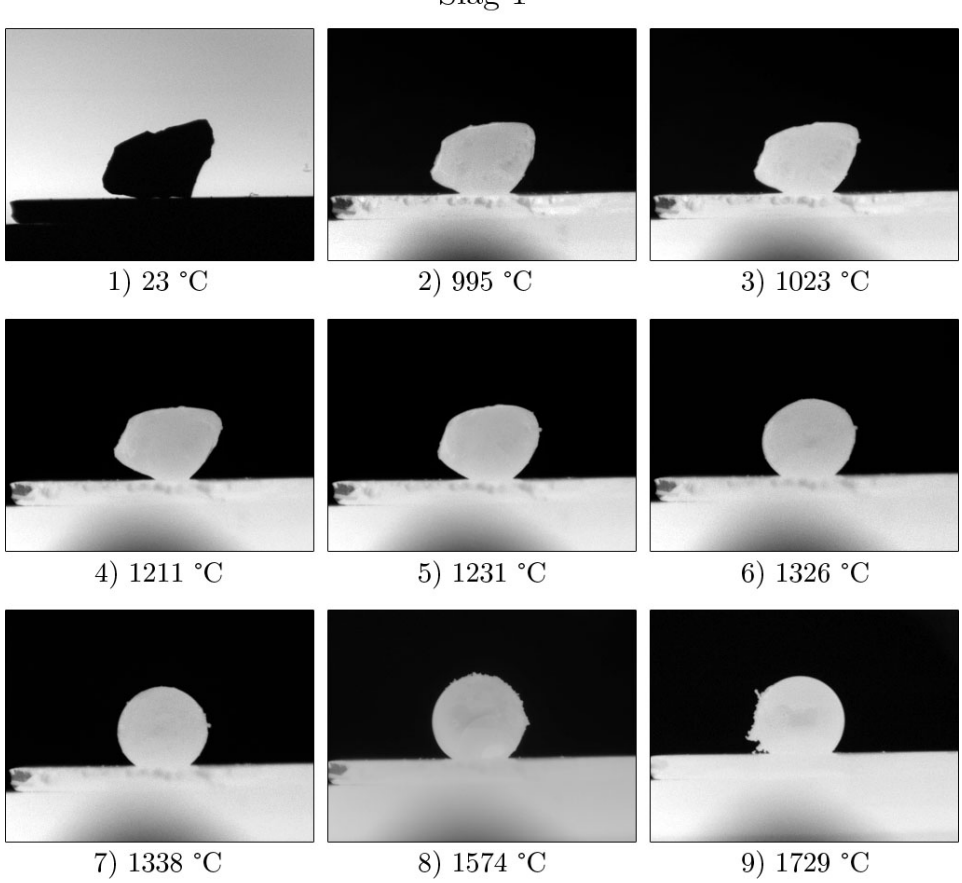

Figure 4.15: Changes in Slag 1 on SiC substrate with increasing temperature.

a similar behavior. Overview of the rest of the samples can be found in Appendix B.

Slag 1 on graphite substrate was the only sample that changed angles with increasing temperature. The measured angles as a function of temperature are shown in Figure 4.16. The sample was fully melted at c. 1220 °C, and formed a sphere with a low wetting angle, $150° \pm 1°$. The angle decreased steadily until gas formation started at c. 1500 °C. At this point the sample started to move on the substrate and the wetting angle continued to decrease. At 1612 °C the sample had the best wetting with an angle of $89° \pm 1°$, before it increased to $158° \pm 1°$ at the end of the experiment.

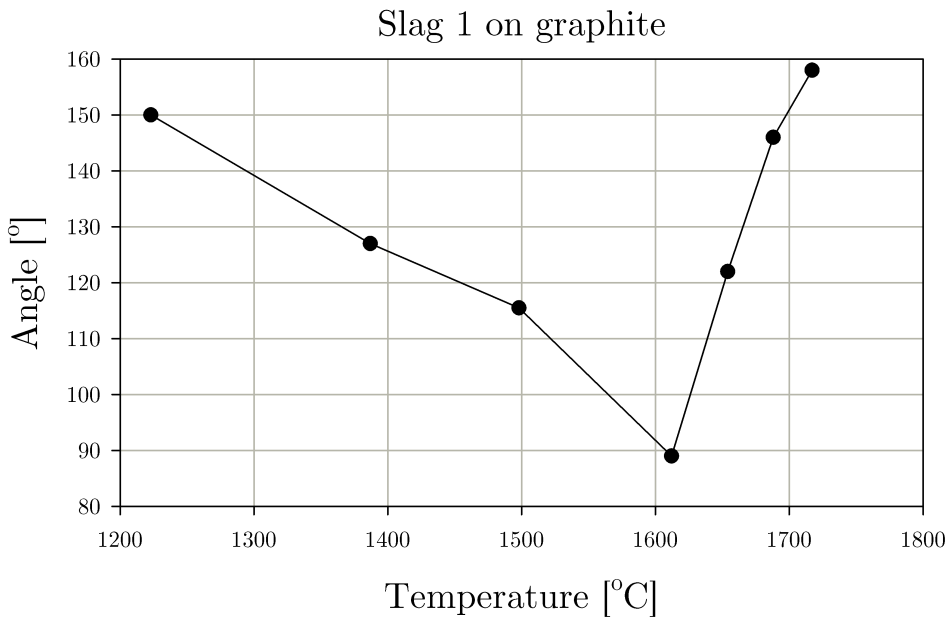

Figure 4.16: Change in wetting angle for Slag 1 on graphite as a function of temperature.

The wetting angle for the rest of the samples did not change noticeably with increasing temperature, illustrated by image number 7 - 9 in Figure 4.15 for Slag 1 on SiC substrate.

Table 4.5: Overview over the different wetting samples, with the temperature for softening, fully melted sample and stopping temperature.

#	Sample	Substrate	$T_{softening}$ [°C]	T_{melted} [°C]	T_{stop} [°C]
1	Metal 1	SiC	1200	1531	1642
2	Metal 2	SiC	1240	n/a	1627
3	Slag 1	SiC	994	1332	1727
4	Slag 1	Graphite	945	1220	1717
5	Slag 2	SiC	946	1305	1620
6	Slag 2	Graphite	937	1214	1691

The slag samples all softened between 900 and 1000 °C. The samples were completely melted above c. 1200 °C for Slag 2, and above 1300 °C for Slag 1. The difference in melting point for the Slag 2 samples were only 6 °C compared to 27 °C for Slag 1. The difference was small and it can

be assumed that the two samples had close to equal composition for both slags.

The metal samples softened above 1200 °C, and the Metal 1 was completely melted at c. 1531 °C. None of the metal samples reacted with with the substrate.

Metal 1 showed similar behavior during heating for both samples, but the wetting angles changed from the first to the second run. The first sample stabilized at $98.5° \pm 2.5°$ while the second at $150° \pm 1°$. The large difference suggest that these experiments should be taken as an indication toward the wetting properties, rather than as actual numbers.

The Metal 2 sample did not melt completely and had solids left when the experiment ended. The metal that melted showed a high wetting angle, likely to be close to that of the second Metal 1 sample.

4.3.2 EPMA of the samples

Samples from the wettability testing were investigated by EPMA. This was done to see if any reduction or oxidation had taken place, and to examine the interface between the substrate and sample.

Table 4.6 and 4.7 gives the slag and metal analysis from the EPMA.

Table 4.6: The slag analysis from the EPMA. Both slags were homogeneous, all values are in wt.%.

Sample	SiO_2	MnO	Al_2O_3	CaO	MgO	K_2O
Slag 1	44.2	0.54	19.5	22.8	9.1	0.00
Slag 2	42.7	0.69	17.4	28.3	6.4	0.00

	FeO	TiO_2	BaO	SO_3	Total
	0.00	0.17	0.69	0.07	97.08
	0.00	0.16	0.98	0.73	97.44

Figure 4.17 and 4.18 shows the pictures taken of the same samples.

Table 4.7: The analysis from the metal samples. The last sample, "Slag 2", is the particle found in Slag 2. All values are in wt.%.

Sample	Phase	Si	Mn	Fe	C	P	S	Total
Metal 1	light gray	9.8	73.9	11.9	3.1	0.09	0.00	99.0
	dark gray	23.3	63.8	11.0	2.5	0.00	0.00	101.1
Metal 2	light gray	23.5	65.9	9.3	1.9	0.00	0.01	101.0
	dark gray	33.9	54.3	12.4	2.2	0.01	0.00	102.9
Slag 2	particle	68.8	0.0	0.00	23.9	0.03	0.00	93.1

Both of the slag samples solidified to a homogeneous phase. The analysis from Table 4.6 shows that the MnO content decreased significantly for both slags. Almost no FeO or K_2O was left in the slag either. The other components in the slag had a minor increase, as their relative amount increases when MnO was removed.

Slag 1, Figure 4.17(a) and 4.17(b), indicate poor wetting toward the SiC substrate. The sample does not show any signs of dissolving the SiC. None of the particles on top of the slag droplet were found on the polished cross section.

A close up of Slag 2 is shown in Figure 4.17(c). A particle was found on the surface close to the top of the slag droplet and was identified as SiC. This is likely to be one of the solid particles observed on the liquid droplet surface.

The analysis from the EPMA determined the metal to consist of three different metal phases with c. 10, 23 and 34 wt.% Si, respectively. The first two phases were present in the Metal 1 samples, while the latter two were present in the Metal 2 samples.

The Metal 1 sample consisted of two separate metal phases. The EPMA pictures, Figure 4.18, shows a pit at the contact area of the metal and SiC substrate. The SiC has been eroded by the metal, and is present as a separate phase.

A closeup of the metal/SiC interface is shown in Figure 4.18(b). A larger SiC particle can be seen in the metal, c. 50 μm from the substrate. Some SiC was observed on the top of the metal droplet, Figure 4.18(a). If this SiC origins from the substrate or the metal sample is unknown.

The Metal 2 sample consisted of two metal phases with c. 23 and 34 wt.% Si, respectively. No SiC was observed in the studied cross section. As the

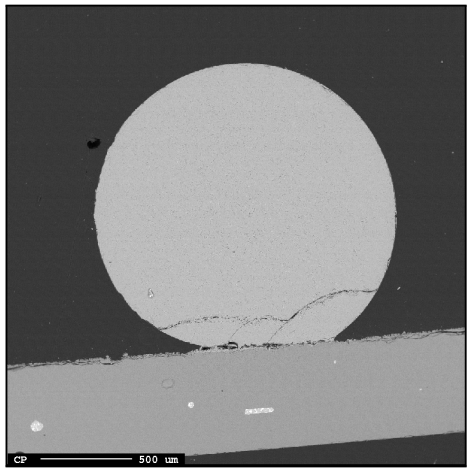

(a) Slag 1, taken at 40x

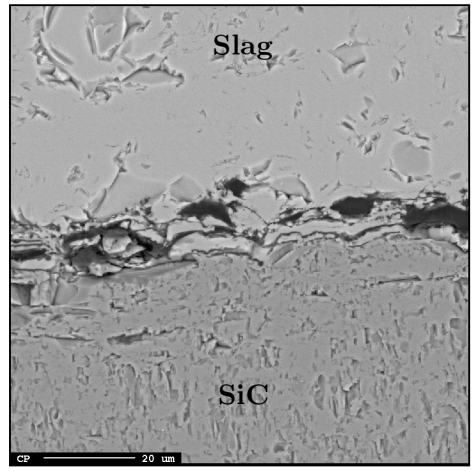

(b) Slag 1, taken at 1000x

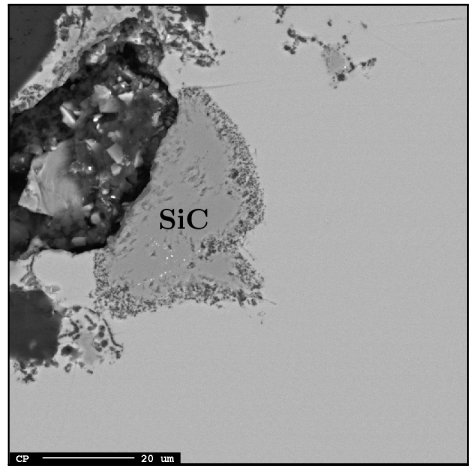

(c) Slag 2, taken at 1000x

Figure 4.17: (a) Overview of the Slag 1 on SiC substrate (b) Close up on the interface between the Slag 1 and SiC interface (c) the Slag 2 sample with a SiC particle.

sample fell of the substrate, the interface between metal and SiC was not studied.

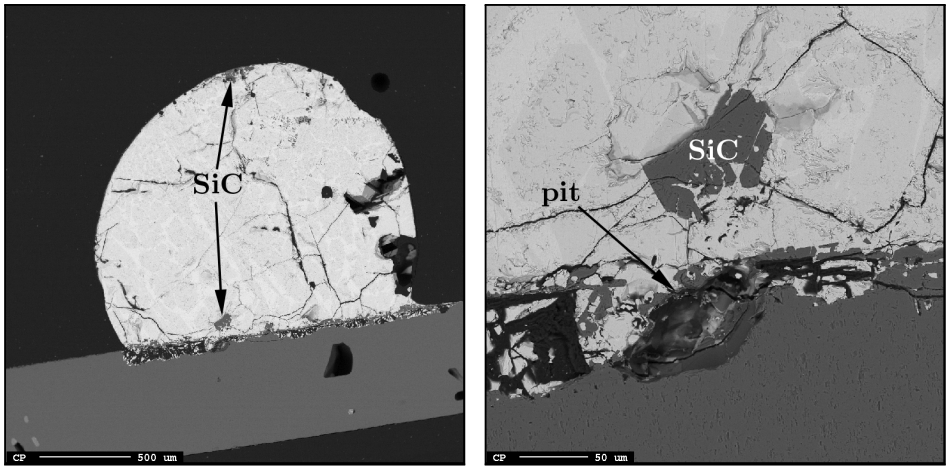

(a) Metal 1, taken at 40x (b) Metal 1, taken at 300x

Figure 4.18: The Metal 1 sample (a) overview of metal on the substrate (b) close up on SiC dissolved by the metal.

Chapter 5

Discussion

5.1 SiC formation

The results from the tube furnace showed that SiC was formed on the coke particle through both slag and metal. The metal samples had the largest amount of SiC, with a SiC layer along the coke/metal interface. For the slag samples, a thin SiC layer was observed on the slag/coke interface. The HC FeMn & Si sample resulted in large amounts of SiC, verifying formation of SiC through carbon dissolved in the metal.

If the samples were held at high temperature and equilibrium for an infinite time, the coke particles would be expected to transform into SiC until this was the only carbon phase present, or the Si content in the metal decreased to that of the point of coexistence for graphite and SiC.

The general speed of formation of SiC was found to be slow on the coke particles. The coke particles had a diameter of c. 20 mm, and the thickest SiC layer observed was in the order of 400 μm. The total conversion of carbon to SiC is, in other words, low for all the experiments.

Formation through metal

With the exception of Metal 1, 1650 °C, all the metal samples had a visible SiC layer going along the coke/metal boundary. Metal 2 had more SiC than Metal 1. This is likely to be caused by the higher Si content in the alloy. Metal 1 will at 1600 °C have a Si activity of c. 0.05, against c. 0.15 in Metal 2, i.e. three times as high. This will result in more SiC being formed,

as the formation is dependent on Si activity, Equation (2.9) and (2.11). $K(T)$ is the equilibrium constant, which is dependent on temperature, unit activity of carbon is assumed.

$$\underline{Si} + C' = SiC(s) \tag{2.9}$$

$$a_{SiC} = K(T) \cdot a_{Si} \tag{2.11}$$

The effect of increased temperature gave different results. For Metal 1, the increase from 1600 °C to 1650 °C resulted in a decrease in SiC. The effect on Metal 2 was the opposite, giving a thicker SiC layer. The cause might be a combination of decreased driving force, increased reaction rate and increased silicon activity as temperature increases.

The rate of formation of SiC can for the metal be described by Equation (5.1). Here the driving force is described by the difference in Si content in the metal, and at the point of coexistence for graphite and SiC.

$$r = Ak\left((wt.\%Si)_{metal} - (wt.\%Si)_{C/SiC}\right) \tag{5.1}$$

The point of coexistence between C and SiC will for SiMn alloys be above c. 16 wt.% Si. It will increase with temperature, decreasing the driving force. For Metal 1, with 19.22 wt.% Si, this decrease in driving force may explain the lower amount of SiC formed at 1650 °C. The increase in the C/SiC point will with a temperature increase of 50 °C, be in the order of 0.5 wt.%. This increase might not alone explain the pronounced drop in SiC on the coke boundary as the temperature was increased. The samples are porous, and the SiC layer is thinner than 50 μm. Some of the carbide may have been removed during cutting and polishing.

For Metal 2, with 28.8 wt.% Si, the difference between Si in the metal and at the point of coexistence is much larger. This makes the relative decrease in driving force smaller. The effect of increased reaction rate and activity with increasing temperature may cause the increasing amount of SiC formed.

The results from Metal 1 and 2 indicate that the effect of temperature is clear at lower Si contents, but becomes insignificant as the Si content in the alloy approaches 30 wt.%.

The HC FeMn & Si sample formed a large amount of SiC. SiC has formed as the metal melted and Si dissolved into the FeMn alloy. The HC FeMn alloy had 6.9 wt.% C, and it can be assumed that the majority of this has reacted

to form SiC. Large amounts of SiC were found in the sample, confirming the formation of SiC through carbon dissolved in the metal, Equation (5.2).

$$\underline{Si} + \underline{C} = SiC(s) \tag{5.2}$$

Formation through slag

The slag samples had less SiC than the metal samples, and Slag 1 had a slightly thicker SiC layer than Slag 2. The activity of silica is higher for Slag 1 than Slag 2. At 1600 °C, a_{SiO_2} is 0.31 for Slag 1 against 0.30 for Slag 2. Formation of SiC from the slag phase is likely to proceed according to Equation (2.10). As can be seen from Equation (5.3), increasing SiO_2 activity will result in more SiC. It is assumed that the carbon activity and partial pressure of CO(g) is the same for both slags.

$$(SiO_2) + 3C' = SiC(s) + 2CO(g) \tag{2.10}$$

$$a_{SiC} = \frac{K(T) \cdot a_C^3 \cdot a_{(SiO_2)}}{p_{CO}^2} \tag{5.3}$$

However, the difference in activity is small. The calculations are done for a simplified system, where the elements with lowest amount are neglected. With this in mind, the difference in SiO_2 activity is too small to explain the amount in formed SiC.

The porosity of the coke particle and penetration of the slag may account for some of the difference. For Slag 1 the coke particle appears denser than the one used for Slag 2. This resulted in a SiC layer that was thicker, but mainly found at the very edge of the coke particle. Slag 2 penetrated deeper into the coke particle, and the mapping revealed small clusters of SiC further away from the coke/slag boundary. The apparent difference in SiC formed on the coke particle may be caused by the fact that SiC from Slag 2 is more spread than for Slag 1.

For Slag 1 there was more SiC with increasing temperature, but the effect of temperature was modest. In the range of 1600 to 1650 °C, the activity of SiO_2 does not increase noticeably for this slag. Viscosity of the slag will increase with increasing temperature, giving a more fluid slag. This may cause deeper penetration and a larger area of reaction. The area of the coke particle which was investigated was more porous for 1650 °C than for 1600 °C. This contributes to a larger reaction area which will result in more SiC.

Slag 1, 1650 °C is not directly comparable as the slag crept out of the crucible. The EPMA showed that the slag phases remaining in the crucible had 34 wt.% Si at the most. A 10 wt.% decrease in SiO_2 will cause a significant activity drop, which again will cause decreased SiC formation. It is therefore likely that the SiC was formed before the slag crept out of the crucible. Because of this incident the effect of temperature on Slag 1 is difficult to determine. It does, however, seem moderate.

Mechanisms of formation

For both metal and slag, SiC was mainly present at the very edge of the coke particle. For the metal the SiC was found as a separate layer between the coke and the metal. The metal seemed to erode the SiC and transport it into the metal phase. In the slag samples SiC was mainly present in the slag, close to the slag/coke interface. Both cases are shown in Figure 5.1.

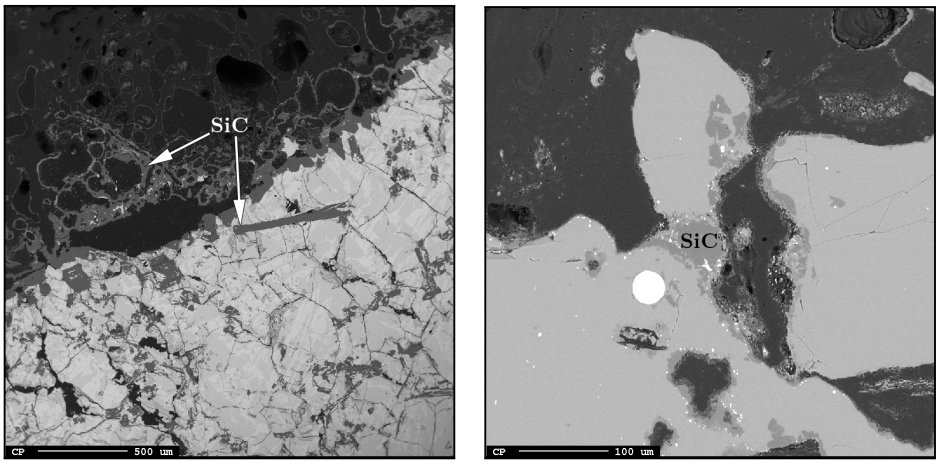

(a) Metal 2, 1650 °C (b) Slag 2, 1600 °C

Figure 5.1: (a) The Metal 2, 1650 °C sample, coke particle (black) at the top, SiC (gray) and metal (light gray). The gap between the metal and coke is likely to be a result of shrinkage during solidification. (b) Slag 2, 1600 °C sample, coke particle (dark gray) at the top with slag (light gray) and SiC (gray). Some metal droplets (white) are seen in the slag.

For the metal the SiC layer is thickest at the coke/metal interface. With increasing distance from the coke/metal boundary into the coke particle,

the thickness of the SiC layer decreases significantly. Several of the pores in the coke particle only had a thin SiC layer at the very surface. This indicates that the SiC layer grow out from the coke particle, rather than into it.

Hon & Davis (1980) found the diffusion of C in β-SiC to be c. 100 times faster than Si between 2010 and 2274 °C. At temperatures around 1600 °C it can be assumed slower, but the diffusion of C is still likely to be much faster than that of Si. The diffusion of C will then be the rate determining step. Carbon will diffuse through the SiC layer and react with Si in the metal, Equation (5.4). $[C]$ denotes carbon dissolved in the already formed SiC.

$$\underline{Si} + [C] = SiC(s) \tag{5.4}$$

For the slag samples SiC is mainly observed in the slag phase. From what can be observed in Figure 5.1(b), SiC is transported into the slag phase after it is formed. Silica in the slag is likely to be reduced by carbon on the coke particle, Equation (5.5). The Si metal then react with the solid carbon to form SiC, Equation (5.6).

$$(SiO_2) + 2C(s) = \underline{Si} + 2CO(g) \tag{5.5}$$

$$\underline{Si} + C(s) = SiC(s) \tag{5.6}$$

Metal droplets, shown in white, can be observed close to the coke particle boundary, indicating that the slag had been reduced. The coke particle close to these metal droplets has porous structure, indicating that carbon was consumed. The EPMA analysis confirmed a drop on SiO_2 and MnO content in the slag after the experiment, verifying that the slag had been reduced.

Reliability and industrial comparability

The findings above seems to be relatively consistent. The mechanical preparation of the samples may have removed some of the more fragile or brittle phases. The pick of cross section also influences the results, as the depth of the sample is not investigated.

The pictures of the Metal 1, 1600 °C sample showed very little SiC. As discussed, low Si activity and lower driving force may be contributing factors. The low amount of SiC may also be caused by a unlucky pick of the cross section or that it has been removed during preparation.

The experiments in graphite crucible are done in an stationary environment. The industrial SAF has movement of the charge and large amounts of gas being formed. The contact between metal or slag and the coke particles is therefore not maintained in the same manner as for the crucible. The use of industrial slags and alloys contributes to make the results obtained more representable. All the minor elements and oxides present in the industrial system is included, which includes their affect on the system.

5.2 SiC structure in the SiMn process

The XRD results showed that β-SiC is the dominant phase in the SiMn system and was found both in the metal from the HC FeMn & Si sample, and the slag samples from the industrial furnace.

β-SiC is the believed to be the stable phase below 1700 °C. The results from the HC FeMn & Si experiment supports this. The SiC formed from carbon dissolved in the metal at 1600 °C was determined to be β-SiC.

6H α-SiC was detected in sample B5-61. The sample was taken directly beneath an electrode, believed to be the hottest place in the furnace. In the Theory it was established that temperature was the main factor deciding whether α- or β-SiC was formed. The presence of α-SiC is an indication that the temperatures has reached above 1700 °C in this area of the furnace.

This is in contradiction to what is reported by several authors (Ding & Olsen, 1996b; Hoel, 1998; Olsen et al., 2007). The claim that β-SiC is the only SiC phase present in the furnace is likely to be based on equilibrium data the stability of the phases, rather than experimental data.

5.3 Wettability testing

The wetting between slag and SiC was found to be slightly better than the wetting between metal and SiC, though they were both non wetting. The slag on graphite substrate showed low wettability. Slag 1 on graphite substrate was the only sample that changed angles with increasing temperature. The lowest angle was measured to $89° \pm 1°$, which can be considered barely wetting.

Wetting toward SiC

Both slag samples were non wetting toward the SiC substrate. Slag 2 wet the SiC substrate better than Slag 1. Slag 2 had 21° difference between the left and right angle. Both these angles were smaller than the angles for the Slag 1, which indicates that the wetting was better even with the error considered.

The initial basicity for Slag 2 was 0.66, against 0.68 for the Slag 1. As MnO was reduced during the testing, the basicity changed. For the slag analyzed by EPMA, the basicity had changed to 0.59 and 0.50 for Slag 2 and 1, respectively.

Slag 1 had a decrease in MnO content of c. 9 wt.%, and changed from most basic to most acidic of the two slags. The angles did not change significantly with temperature for the two slag samples, shown in Figure 5.2. This means that the the MnO is either reduced as soon as the slag is liquid, or that the decrease in MnO content does not affect the wetting properties. Safarian & Tangstad (2009) and Park et al. (2010a) showed that the wetting increased with basicity. If this is correct, it is likely that the MnO is reduced out in the slags, giving the Slag 2 the highest basicity and the lowest wetting angle.

Wetting can also change with increasing temperature. However, none of the samples showed any change as the temperature increased.

The metal did not wet the SiC substrate. The metal samples were investigated twice as Metal 2 would not melt the first time. For Metal 1 this resulted in two angles that differed with c. 50°. This might be caused by a combination of error in the temperature measurements and difference in composition in the samples. Before the second Metal 1 sample had stabilized, the observed angle was close to that measured for the first Metal 1 sample. The angle increased as soon as the metal was completely liquid. The difference shows that there is a large uncertainty in the experiments. The final conclusion is therefore that the metal sample was non wetting toward the SiC substrate.

Metal 2 did not melt completely and the angles were not measured. The trend observed from the pictures were an angle similar to that of the second Metal 1 sample, which was $150° \pm 1°$, i.e. non wetting.

Ciftja (2009) showed good wetting between pure Si metal and SiC. The effect of increasing Si content for the metal is questionable, as the Metal 2

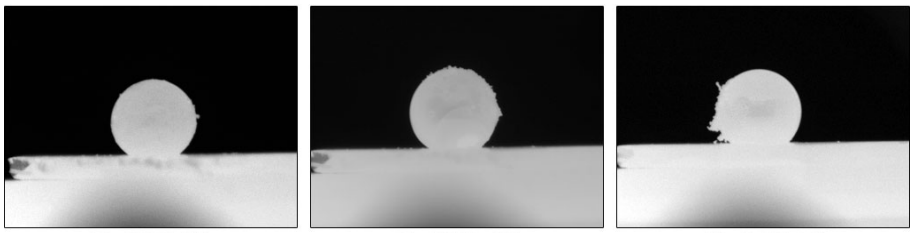

7) 1338 °C 8) 1574 °C 9) 1729 °C

(a) Slag 1

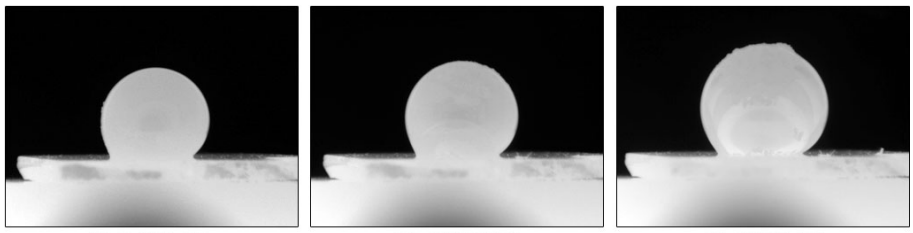

7) 1466 °C 8) 1525 °C 9) 1593 °C

(b) Slag 2

Figure 5.2: Slag 1 and Slag 2 on SiC substrate and their behavior with increasing temperature. The solid particles on the surface are SiC. The change in size for Slag 2 is due to gas formation.

sample with c. 10 wt.% more Si, did not show any tendency towards better wetting. It is, however, dificult to compare this because of the uncertanties in the measurements.

The EPMA showed that the metal eroded the substrate, which in theory could affect the wetting angle. The angles were observed to be stable for the whole temperature range after the samples were fully melted, showing the effect to be insignificant.

Wetting toward graphite

The Slag 2 was non wetting toward the graphite substrate. The angle was measured to $145° \pm 1°$, and was stable with increasing temperature. The tube furnace experiment with the same slag showed good wetting toward the crucible walls, Figure 5.3(b). This might be cause by a rougher surface on the crucible than the substrate the slag was tested on.

Slag 1 on graphite substrate was the only sample where the wetting angle

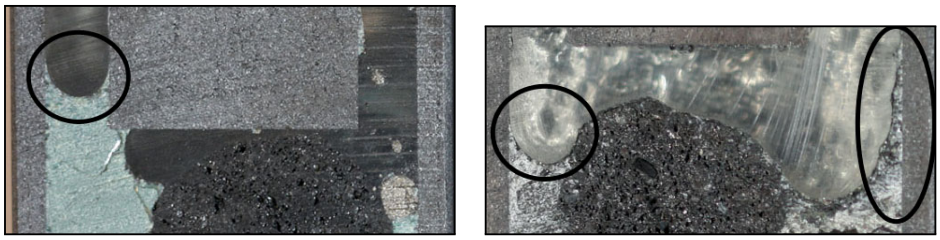

(a) Slag 1, 1600 °C (b) Slag 2, 1600 °C

Figure 5.3: Wetting toward the crucible for Slag 1 and 2.

changed with increasing temperature. The initial wetting angle, measured right after the sample was melted, showed an angle of $150° \pm 1°$. The angle decreased to $89° \pm 1°$, before it increased to c. $158° \pm 1°$.

The lowest angles were observed in the range of 1600 - 1650 °C. This fits with observations from the tube furnace, were the slag wet the crucible walls, shown in Figure 5.3(a).

There might be several reasons for the angle changing during the experiment: wetting is known to change with temperature or a reaction product might have formed between the slag and substrate. The slag is likely to be reduced by the substrate, and an increase in roughness may have affected the angle as the drop moved on the substrate.

Before gas formation, the wetting angle in the slag decreased. As gas evolution was observed, and the reduction of the slag presumably started, the particle moved on the substrate while the angle continued to decrease. The initial decrease is likely to be caused by increasing temperature.

The continuing decrease after the particle had started to move might have had more contributing factors than temperature. Ciftja (2009) showed the wetting properties of Si on graphite to change with the roughness of the substrate, decreasing with increasing roughness. A rougher surface may have caused the increased wettability as Slag 1 moved on the graphite substrate. In addition to this, the analysis on SiC substrate showed that MnO was reduced from the slag. A change in composition is likely to affect the wetting properties.

Mailliart et al. (2009) found the wetting angle to vary with temperature. The angle decreased with increasing temperatures down to a minimum, before increasing with further temperature increase. However, this was only

a small decrease and not alone enough to explain the rapid change from 89° to 158°.

As the slag reached the lowest angle at 1612 °C, the reduction of MnO in the slag is likely to occur. This can cause a metal layer to form on the graphite surface. A low MnO content will also cause an increase in silica activity, which again will promote SiC formation. Visual observations confirmed the presence of a product layer at the substrate. The decreased wetting may therefore be a result of SiC or metal forming on the slag/graphite interface.

Reliability and industrial comparability

As shown for Metal 1, the reproducibility of the experiments was low with a difference of c. 50°. The composition of the samples may be one of the main reasons for this. Both the metal and slag will solidify into separate phases during solidification, and macro segregation may also occur for the metal. The amount picked out for the sessile drop testing is c. 0.01 g. There is therefore a chance of the samples having different composition, giving different angles when tested. The general result, i.e. that the system is non wetting, should therefore be considered rather than the exact numbers.

Heating in the sessile drop furnace is done by a graphite element. For the industrial furnace heat is created from resistance as an electrical current is applied to the charge. Kazakov et al. (1993) and Mills (2011) showed that the wettability of slags decreased as a negative potential was introduced. A 40 MVA furnace will have a voltage of c. 115 V (Olsen et al., 2007). A positive potential this large may affect the wetting properties of the slag and metal. It is plausible that a potential of 115 V will affect the wettability toward SiC in an industrial furnace.

The wettability testing was carried out on a crystalline α-SiC substrate. The XRD analysis determined β-SiC to be the dominant SiC phase. The α-SiC mostly consisted of a hexagonal configuration, while β-SiC is cubic. The different crystal structures may have different wetting properties toward the slag and metal. This will cause the measured results to differ from the industrial system.

5.4 Additional observations

This section includes observations from the results that are of minor importance for the formation of SiC, but still of interest.

5.4.1 Placement of SiC in the SiMn system

Previous work by the author (Davidsen, 2010) reported that SiC was only found in the slag phase. If the densities are regarded, SiC would be expected to rise in the metal and slowly sink in the slag, illustrated in Figure 5.4. The SiC particles from the HC FeMn & Si sample had a size of c. 80 μm. This will for Metal and Slag 1 result in a rise of c. 250 $\mu m/s$ in the metal and fall of c. 1.5 $\mu m/s$ in the slag.

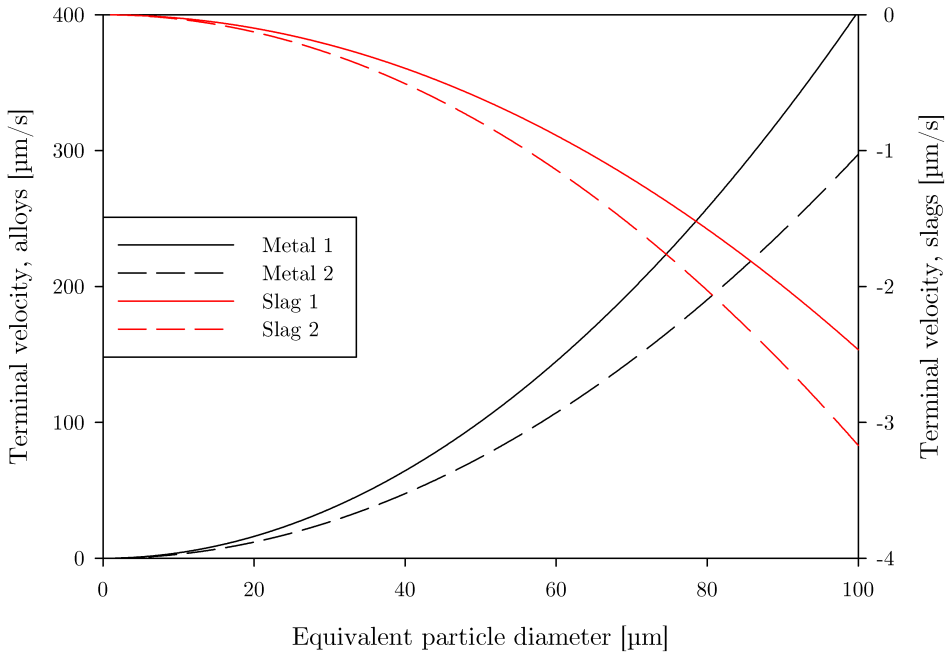

Figure 5.4: The calculated terminal velocity at 1600 °C for a SiC particle in the metal (left y-axis) and the slag (right y-axis) as a function of increasing particle diameter. The slag speed is negative as the particle is sinking instead of rising in the liquid. The calculations are based on the equations and data given in Section 2.7.

The fact that SiC is only found in the slag may be caused by the SiC in the metal rising up in the metal phase. As the metal drains down, the SiC will enter the slag. As seen in Figure 5.4, the calculated rising speed of SiC in the metal is in the order of 10^2 larger than the sinking speed in the slag. The slag wet SiC slightly better than the metal, making it preferable for SiC to enter this phase.

For the HC FeMn & Si sample SiC particles were found in the metal phase. The same is observed in the metal from the Slag 1, 1650 °C sample, Figure 5.5. This indicates that the buoyancy might be smaller than what is calculated. The slag samples indicate that the SiC is transported into the slag phase after it is formed, where it is likely to stay as the density difference is small.

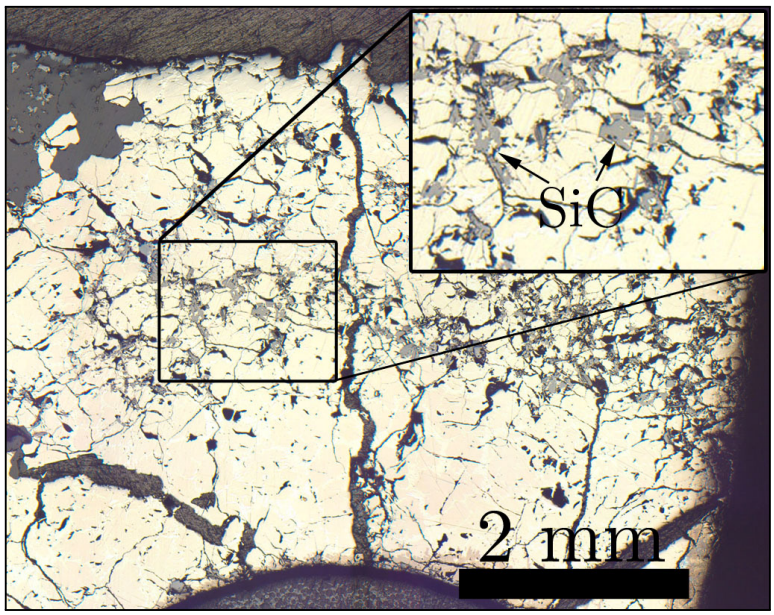

Figure 5.5: The metal phase from the Slag 1, 1650 °C. The metal is yellow and SiC is gray. A close up of the SiC is shown to the upper right.

In the industrial system the metal drains down to the bottom of the furnace, creating a separate metal layer (Olsen et al., 2007). The SiC formed in the metal may therefore drain out of the system, leaving only SiC produced from the slag in the slag phase when it solidifies. This is supported by the fact that a carbide layer is often observed on the top of solidified SiMn alloys (Hoel, 1998). No SiC was found in the metal phase in the samples

from Furnace 2, ENK. These samples were cooled very slowly, giving the SiC good time to settle and transport into the slag phase.

5.4.2 Cavity formation in the metal samples

All metal samples from the tube furnace had a cavity in the middle of the crucible, more pronounced for Metal 2 than Metal 1. The cavities may have been formed by one of the following:

- Gas formation
- Metal shrinkage during solidification
- Wetting toward the graphite crucible

The partial pressures of Mn(g) and SiO(g) over the alloys are low under 1650 °C, as seen from Figure 5.6. The figure show the partial pressures over the alloys, calculated using the activities from Section 2.2.2. The combined partial pressure of Mn(g) and SiO(g) are c. 0.02 atm over Metal 1 and 0.03 atm over Metal 2 at 1650 °C. Gas formation is therefore unlikely to create a gas channel. The cavities in the Metal 1 samples does not not have an opening to the surface. This would have been likely to be created from escaping gas if the partial pressures were high.

The metal did shrink during solidification, creating cracks in the metal and a gap between the coke particle and metal. The shrinkage itself is small and does not seem sufficient to form the cavity, it is more likely to be a contribution factor.

The wetting between the metal and crucible wall was presumably good in the tube furnace experiments, as the metal was pulled up along the graphite. The metal/graphite interface is shown in Figure 5.7 for Metal 1 and 2. It can be seen that Metal 2 crept higher up than Metal 1. The metal is pulled up the crucible wall, creating a gap in the middle, which may contribute to the cavity being formed. Better wetting toward the graphite walls may explain why Metal 2 had a larger cavity than Metal 1.

The wettability testing showed the metal to be non wetting toward the SiC substrate. As SiC is the stable carbon phase for both alloys, a SiC layer is expected to form between the metal and graphite. If SiC was formed on the graphite, then the good wetting is directly contradicting to what was observed in the wettability testing. Different wetting properties toward α- or β-SiC may be one of the reasons for this.

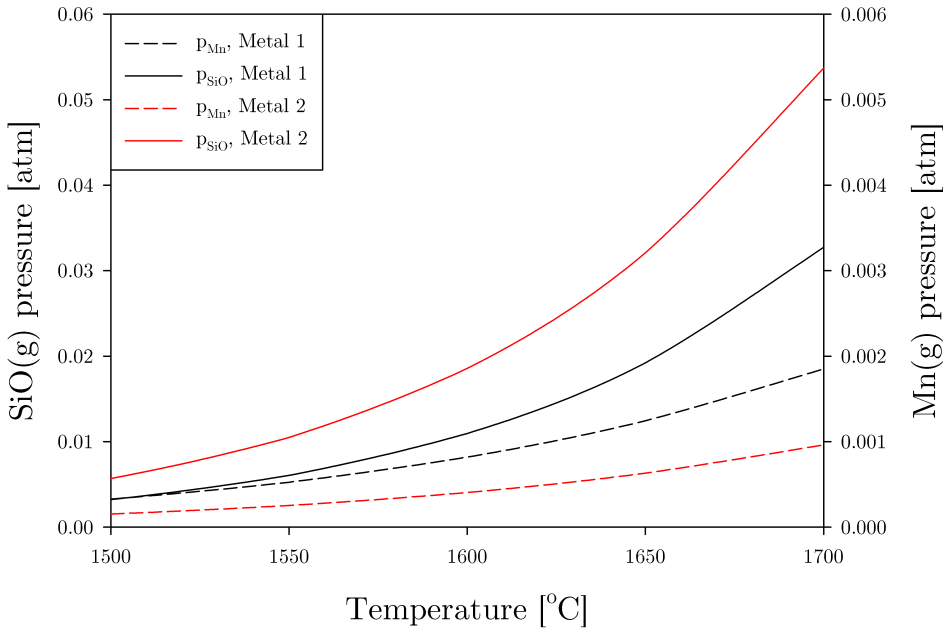

Figure 5.6: Calculated partial pressures of and SiO(g) (left axis) and Mn(g) (right axis). Metal 1 is shown in black and Metal 2 in red.

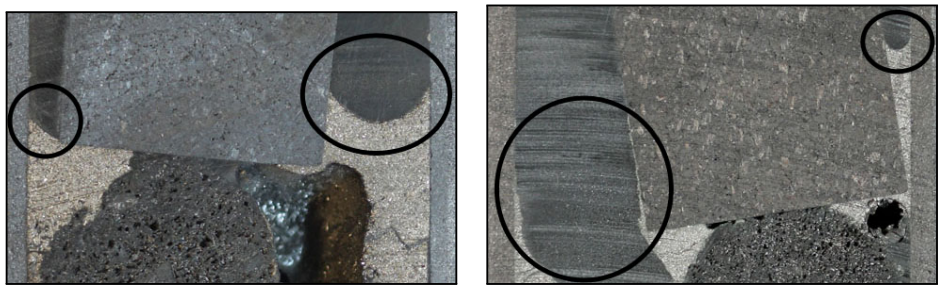

(a) Metal 1, 1650 °C

(b) Metal 2, 1650 °C

Figure 5.7: Wetting toward the crucible for Metal 1 and 2.

The gas phase may affect the wetting, as was shown by Safarian & Tangstad (2009). The wetting angle of a CaO-SiO_2 slag was found to change considerably when the atmosphere was changed from Ar(g) to CO(g). Changing atmosphere is likely to also affect the wetting properties of the metal. As the wettability testing was carried out in CO(g), and the tube furnace was run in Ar(g), this may be a contribution factor affecting the wetting in the tube furnace experiments.

5.4.3 Metal droplets and discharging of Slag 1

The Slag 1, 1600 °C sample had several metal droplets located around the coke particle. The analysis of the metal droplets showed that the metal had about the same composition as the metal further down in the crucible. The original slag only had 0.65 wt.% FeO, which is too low to produce an alloy with c. 8.5 wt.% Fe. The metal droplets are therefore likely to origin from the metal that was charged into the crucible.

The vapor pressure over the slag is assumed to be low, and Fe will have a lower vapor pressure than Mn (Rosenqvist, 2004). This rules out the possibility of large amounts of iron vaporizing and condensing higher up in the crucible.

The metal is heavier than the slag, and expected to sink. It was charged into the crucible before the slag, and should not be found high up. The slag will, as shown in the wetting experiments, melt before the metal. The metal was crushed, partly to a powder, which may float on the liquid slag. Adhesion toward the graphite may prevent the droplets from sinking down to the bottom of the crucible.

Slag 1 crept out of the crucible during the experiment at 1650 °C. This may have been caused by a combination of wetting and decreased viscosity as the temperature increased, or boiling of the slag.

The wetting between graphite and Slag 1 was found to be better between 1600 and 1650 °C. The lowest angle for the sessile drop experiments was at $89° \pm 1°$. This is a high angle, but the indication was that the wetting was at the best. The wetting of the slag toward the crucible walls at 1600 °C was found to be good, illustrated by Figure 5.3.

The viscosity of the slag will decrease with increasing temperature, changing from 0.28 to 0.22 $\mathrm{Pa \cdot s}$ in this temperature range. The decreased viscosity combined with the wetting may be the reason for the slag escaping when the temperature increased. Even though the wetting was better above 1600 °C, this does not explain how almost all the slag got out of the crucible.

Separation of the slag may be a sign of boiling. This can explain the reason for slag leaving the crucible. The viscosity of the slag causes it to form a thick foam when boiling. This foam will rise in the crucible, explaining how the slag exited from the holes in the top. Boiling may also explain why a thin layer of slag that was observed covering the inside of the crucible.

The analysis from the slag showed three different phases, where all of them

had less than 34 wt.% SiO_2. That is at least 10 wt.% less than the charged slag. The Si content in the metal had not increased significantly, indicating that the SiO_2 had not been reduced out. All the EPMA samples were analyzed at the same time, and the results were consistent. The low SiO_2 content is therefore unlikely to be caused by error in the analysis.

If the slag boiled, this will have increased the amount of gas formed from the slag. The gas phase may favor SiO_2 and MnO, resulting in the lowered values when the slag was analyzed. The loss of SiO_2 is a peculiar incident, but the reason is outside the current knowledge of the author. The matter will therefore not be discussed further.

5.4.4 Reduction of MnO during wetting experiments

Both slags had a large drop in MnO content, from 9.1 wt.% to 0.54 wt.% in Slag 1 and 3.9 wt.% to 0.69 wt.% in Slag 2. K_2O and FeO seems to be almost completely removed from the slag, too. There was not found any metal in the samples.

The oxides in the slag can be reduced either by CO(g) or the SiC substrate. The reduction of MnO with CO(g) has been showed possible by Safarian et al. (2008). This was for a HC FeMn slag with c. 45 wt.% MnO, giving a much higher MnO activity than for the slags used in the experiments. The activity of MnO in Slag 1, which had 9.1 wt.% MnO is only c. 0.03 at 1600 °C. The activities for FeO and K_2O can be assumed lower.

This leaves the reduction with the SiC substrate as reducing agent. At 1600 °C the activity of SiO_2 would be between 0.30 and 0.31 for both Slag 1 and 2. MnO may be reduced by SiC according to Equation (5.7), forming Mn and Si. The reduction of silica is also possible according to Equation (2.2), and MnO can then be reduced according to Equation (5.8). The activity of Mn in the alloy might be high enough for the metal to evaporate, Equation (2.6). Bubbling in the slag droplets were observed for both the slag samples, confirming that gas was evolved.

$$(MnO) + SiC(s) = \underline{Mn} + \underline{Si} + CO(g) \tag{5.7}$$

$$(SiO_2) + 2SiC(s) = 3\underline{Si} + CO(g) \tag{2.2}$$

$$\underline{Si} + 2(MnO) = (SiO_2) + 2\underline{Mn} \tag{5.8}$$

$$\underline{Mn} = Mn(g) \tag{2.6}$$

The constant change of the gas ensures that there will never build up a

significant partial pressure of Mn(g). As the reaction product is constantly removed, Equation (2.6) will be driven to the right resulting in the low MnO content. K_2O can be removed in a similar way.

5.4.5 Solids on the samples during the wetting experiments

The slag/SiC interface, shown in Figure 4.17(b), showed no sign of the slag eroding the substrate. For both Slag 1 and 2, particles were observed moving on the slag droplet surface during heating. One particle were confirmed to be a SiC particle, found close to the top of the Slag 2 sample. These particles are likely to have been present in the slag before the experiment started. The surface tension of the slag droplet may force SiC to the surface, even though it is denser than the slag.

The metal phase eroded the SiC substrate. Some SiC can be observed at the very top of the metal droplet. It is not possible to determine if this SiC was present in the metal at the start of the experiment. As shown in Figure 5.4, a particle with the a diameter of 80 μm would have a rising speed of c. 250 $\mu m/s$ in Metal 1. It is therefore perfectly plausible for the SiC particle to rise to the surface of the droplet during the experiment. The raw material for Metal 1 and 2 were investigated in light microscope. Only a few small SiC particles were observed. This supports the statement that the SiC in the metal droplet origins from the substrate.

5.5 Industrial SiC formation

The results obtained in this report, together with the work done during the autumn of 2010 (Davidsen, 2010), give an insight in the formation of SiC in the SiMn process. The lab scale experiments give good indications on where and how SiC is formed.

The results indicate that SiC is formed on the surface of the coke particles, and that the SiC layer grow outwards. Samples from the excavation of Furnace 2, ENK showed coke particles all the way down to the metal bath. This confirms that the coke particles are not converted into SiC as the silicon content increases.

SiC is formed through both metal and slag. The formation is faster for the metal, but the results indicate that the settling of SiC in the metal is

relatively slow. Much of the SiC formed through the metal is therefore likely to be tapped together with the metal.

In the industrial furnace, metal will drain down to the metal layer as it is formed. The time of contact between metal high in silicon and coke may therefore be limited. This will again restrict the total amount of SiC formed on the coke particles through the metal phase.

The slag will, in contrast to the metal, be in contact with the coke particles from the time it enters the high temperature zone. Tapping is done in the order of every second hour (Olsen et al., 2007), giving the slag and coke time to react. The results from Davidsen (2010) showed the majority of the reduction to happen at the top of the coke bed zone. At the time the slag passes through the topmost layer of the coke bed, most of the metal will be reduced out and SiC is the stable carbon phase. The metal will drain down, leaving the slag and coke to react.

This makes feasible for a good amount of SiC to form through the slag. The presence of α-SiC in one of the samples from the industrial furnace indicate that the temperature has exceeded 1700 °C. A higher temperature may enhance the amount of SiC formed.

SiC formed through the slag in the tube furnace experiments was transported away from the coke particle. Due to the similar densities SiC is likely to stay in the slag. As SiC is a solid, large amounts can affect the viscosity of the slag. If slag containing SiC is present in one of the inactive zones of the furnace, a small buildup of SiC-enriched slag may form. This might be the case for the excavation of Furnace 2, ENK, where a small deposit of SiC was observed between two of the electrodes.

Chapter 6

Conclusions

This thesis covers a study of the formation of silicon carbide in the SiMn process. The goal has been to determine where and how SiC is formed. The wettability of slags and alloys, and which SiC phase that is present in the process has also been investigated. The conclusions drawn are as follows.

SiC can form on a coke particle through both the metal and slag phase, and formation through the metal phase is fastest. More SiC was formed as the Si content increased. Metal 2, with c. 10 wt.% more Si, had substantially more SiC on the coke/metal boundary than Metal 1. The total degree of the coke particle turned into SiC was low as the thickest layer measuring c. 400 μm.

The effect of temperature was evident for Metal 1 with lowest Si content, resulting in a decreasing amount of SiC. This was likely to be caused by the driving force for formation, which will decrease with increasing temperature. Metal 2 yielded more SiC with increasing temperature as the high Si content makes the relative decrease in driving force smaller. The effect of temperature on SiC formation from the slag phase was small.

Silicon carbide was mainly formed as a separate layer on the outside of the coke particles, and was transported into the slag and metal. There were no signs of the SiC preferring the slag phase over the metal phase.

SiC on the coke particle is likely to be formed from Si dissolved in the metal reacting with carbon from the coke particle. For the slag, silica is presumably reduced by carbon to Si before reacting to form SiC.

β-SiC is the dominant phase in the SiMn system, but α-SiC was also found

to be present. The phase formed from carbon dissolved in the metal phase at 1600 °C was determined to be β-SiC.

Metal 1 and 2 showed non wetting properties toward the SiC substrate, the angle was constant with increasing temperature.

Slag 1 and 2 were both non wetting toward the SiC substrate and the angles were constant with increasing temperature. The slag reacted with the SiC and MnO was reduced from the slag. The lack of a metal phase and constant gas flow prevented equilibrium and resulted in a low MnO content.

Slag 2 was non wetting toward graphite and the angle was constant with temperature. Slag 1 on graphite changed wetting angle with increasing temperature. The highest and lowest angle were measured to $158^\circ \pm 1^\circ$ at 1717 °C and $89^\circ \pm 1^\circ$ at 1612 °C. The change in angle is likely to be a combined result of increased temperature, the roughness of the substrate, changes in composition caused by reduction of the slag and the formation of a reaction product on the slag/graphite interface.

Chapter 7

Further Work

To further increase the knowledge of formation of SiC in the SiMn process, several aspects are of interest:

Test the rate of formation of SiC on carbon as a function of increasing Si content. The Si content in the metal should be varied from 15 to 30 wt.%. This will show how dependent on Si the SiC formation is. The same experiments can be carried out with slags with different silica content.

Test the rate reduction for a high MnO slag with SiC as a reducing agent. This might explain why SiC is present as a separate phase and not reducing the slag.

The wettability of the metal and slag should be tested under an applied AC current to see how this affects the wetting properties. This will give a good indication if the wetting angles found in this thesis are valid for the industrial system. Testing toward a β-SiC substrate to see if this differ from α-SiC should also be carried out.

Bibliography

Aylward, G. H. & Findlay, T. J. V. (2008). *SI chemical data*. Milton: Wiley. 5th ed.

Battezzati, L. & Greer, L. (1989). The viscosity of liquid metals and alloys. *Acta Metallurgical*, 37(7), 1791–1802.

Bruker AXS (2011). D8 focus. `http://www.bruker-axs.com/d8_focus.html`. Accessed: February 10th. 2011.

Chase, M. W. (1998). *NIST-JANAF thermochemical tables*, volume no. 9 of *Journal of physical and chemical reference data, Monograph*. Washington, D.C.: American Chemical Society and the American Institute of Physics for the National Institute of Standards and Technology. 4th ed.

Ciftja, A. (2009). *Solar silicon refining: inclusions, settling, filtration, wetting*. PhD thesis, NTNU.

Ciftja, A. (2011a). *EPMA study of the escavation samples from Elkem Thamshavn*. Technical report, SINTEF. Memo.

Ciftja, A. (2011b). *XRD results from furnace excavation at Finnfjord AS*. Technical report, SINTEF. Unpublished work.

Davidsen, J. (2010). Reaction mechanisms in the silicomanganese process. Project work, NTNU.

Dhanaraj, G., Raghothamachar, B., & Dudley, M. (2010). Growth and characterization of silicon carbide crystals. In *Springer Handbook of Crystal Growth* (pp. 797–820). Springer Books.

Ding, W. (1993). *Equilibrium relations in the production of manganese alloys*. PhD thesis, NTH.

Ding, W. & Olsen, S. E. (1996a). Reaction equilibria in the production of

manganese ferroalloys. *Metallurgical and materials transactions, B*, 27, 5–17.

Ding, W. & Olsen, S. E. (1996b). Reactions between multicomponent slags and Mn-Fe-Si-C alloys: equilibrium and stoichiometry. *Scandinavian Journal of Metallurgy*, 25, 232–243.

Eidem, P. A. (2011). SiC in samples from excavation of Furnace 2, Eramet Norway Kvinesdal. Eramet Norway AS. Personal communication. Trondheim, May 27.

Ghosh, A. (2001). *Secondary Steelmaking*, chapter 4. CRC Press: Kanpur.

Goodge, J. (2009). Electron probe micro-analyzer (EPMA) . `http://serc.carleton.edu/research_education/geochemsheets/techniques/EPMA.html`. Accessed: November 28th. 2010.

Gupta, G., Kumar, P. V., Rudolph, V. R., & Gupta, M. (2001). Heat-transfer model for the Acheson process. *Metallurgical and Materials Transactions B*, 32(A), 1301–1308.

Harris, G. L. (1995). *Properties of silicon carbide*, chapter 2. IEE: London.

Hoel, E. G. (1998). *Structures and phase relations in silicomanganese alloys*. PhD thesis, NTH, Trondheim.

Hon, M. H. & Davis, R. F. (1980). Self-diffusion of ^{30}Si in polycrystalline β-SiC. *Journal of Materials Science*, 15, 2073–2080.

Ivantsov, V. & Dmitriev, V. (1998). Dissolution and growth of silicon carbide crystals in melt-solutions. *Materials Science Forum*, Silicon Carbide, III-Nitrides and Related Materials(73), 264.268.

JEOL AB (2008). Jeol JXA-8500F electron probe micro analyzer (EPMA). Datasheet.

Kazakov, A. A., Matveev, Y. V., Arykova, L. A., & Ryabov, V. V. (1993). Effect of electrical potential on slag impregnation of porous refractories. *Russian Metallurgy (Metally)*, 4, 94–96.

Kordina, O. (1994). *Growth and characterisation of silicon carbide power device material*. PhD thesis, Universitetet i Linköping.

Krishnarao, R. V. & Subrahmanyam, J. (1995). Formation of SiC from rice husk silica-carbon black mixture: Effect of rapid heating. *Ceramics International*, 22, 489–492.

Li, C., Huang, J., Cao, L., & Lu, J. (2009). Synthesis of SiC nanowires from gaseous SiO and pyrolyzed bamboo slices. In *Journal of Physics: Conference Series*, volume 152.

Lindstad, L. H. (2002). *Recrystallization of silicon carbide*. PhD thesis, NTH, Trondheim.

Mailliart, O., Chaumat, V., & Hodaj, F. (2009). Wetting and interfacial interactions in the CaO-Al_2O_3-SiO_2/silicon carbide system. *Journal of Materials Science*, 45, 2126–2132.

Mills, K. (2011). The estimation of slag properties. In *Southern African Pyrometallurgy 2011 International Conference*, volume 1 (pp. 391–443). Johannesburgh, SA.

Moe, M. A. (2011). SiC structure from the Acheson process at Washington Mills. E-mail correspondence 26.01.2011, Washington Mills AS, Orkanger.

Neerland, I. M. (1986). *Silicon Carbide Production by the Acheson Process. A Critical Literature Review*. Technical report, SINTEF.

Nelson, W. E., Halden, F. A., & Rosengreen, A. (1966). Growth and properties of β-SiC single crystals. *Journal of Applied Physics*, 37(1), 333–336.

Olsen, S. E. (2001). *Fundamental principles of silicomanganese production*. Technical report, SINTEF, Materials Technology.

Olsen, S. E., Tangstad, M., & Lindstad, T. (2007). *Production of manganese ferroalloys*. Trondheim: Tapir Akademiske Forlag.

PANalytical B.V (2010). X-ray diffraction. `http://www.panalytical.com/index.cfm`. Accessed: February 10th, 2011.

Park, J. H., Park, G. H., & Lee, Y. E. (2010a). Carbide capacity of CaO-SiO_2-MnO slag for the production of manganese alloys. *ISIJ International*, 50(8), 1078–1083.

Park, J. H., Park, J. G., Min, D. J., Lee, Y. E., & Kang, Y.-B. (2010b). In situ observation of the dissolution phenomena of SiC particle in CaO-SiO_2-MnO slag. *Journal of the European Ceramic Society*, 30(15), 3181–3186.

Raanes, M. (2011). Error in carbon measurement from the EPMA. NTNU. Personal communication. Trondheim, May 30.

Roina, A. (2002). HSC chemistry 5.11. Outokumpu.

Rosenqvist, T. (2004). *Principles of Extractive Metallurgy*, chapter 10. Tapir Forlag: Trondheim.

Safarian, J. (2007). *Kinetics and mechanisms of reduction of MnO-containing silicate slags by selected forms of carbonaceous materials*. PhD thesis, Norges teknisk-naturvitenskapelige universitet, Trondheim.

Safarian, J. & Tangstad, M. (2009). Wettability of silicon carbide by CaO-SiO_2 slags. *Metallurgical and Materials Transactions B*, 40B(December), 920–928.

Safarian, J., Tranell, G., Kolbeinsen, L., Tangstad, M., Gaal, S., & Kaczorowski, J. (2008). Reduction kinetics of MnO from high-carbon ferromanganese salgs by carbonaceous materials in Ar and CO atmospheres. *Metallurgical and materials transactions, B, Process metallurgy and materials processing science*, 39(B), 702–712.

Sandvik, K. L., Digre, M., & Malvik, T. (1999). *Oppredning av primære og sekundære råstoffer*. Trondheim: Tapir.

Schei, A., Tuset, J. K., & Tveit, H. (1998). *Production of high silicon alloys*, chapter 1. Tapir: Trondheim.

Seetharaman, S. (2005). *Fundamentals of metallurgy*, chapter 4. CRC Press: Boca Raton.

Sørensen, B. E. (2011). Interpretation of XRD patterns. NTNU. Personal communication. Trondheim, June 1.

Swinbourne, D. R., Rankin, W. J., & Eric, R. H. (1993). The effect of alumina in slag on manganese and silicon distributions in silicomanganese smelting. *Metallurgical and materials transactions, B*, 26, 59–65.

Tang, K. (2011). Viscosities of SiMn alloys and slags. SINTEF. Personal communication. Trondheim, May 24.

Tangstad, M. (2011). Gas pressures in SiMn and silicon production. NTNU. Personal communication. Trondheim, March 21.

Tranell, G., Gaal, S., D, L., Tangstad, M., & Safarian, J. (2007). Reduction kinetics of manganese oxide from HC FeMn slags. In *INFACON XI* (pp. 231–240). New Dehli, India.

von Bahr, M. (2003). *Wetting and Capillary Flow of Surfactant Solutions and Inks*. PhD thesis, Lund university.

Washington Mills (2010). Carborex. http://www.washingtonmills.no. Datasheet no.1, Accessed: January 10th, 2010.

Yara Praxair (2011). Beskyttelsesgasser. http://www.yarapraxair.no/Gass/Beskyttelsesgasser/. Accessed: May 28th, 2011.

Zhou, H. & Singh, R. N. (1995). Kinetics model for the growth of silicon carbide by the reaction of liquid silicon with carbon. *Journal of the American Ceramic Society*, 78(9), 2456–2462.

Appendix A

Light microscope pictures

This appendix shows the light microscope pictures taken from the tube furnace samples. These pictures gives an overview of the coke/slag and coke/metal boundary for the whole area of interest. The figures are summarized in Table A.1. All pictures are taken at 2.5x magnification.

Table A.1: Summary of the wetting pictures.

#	Sample	Figure
1	Metal 1, 1600 °C	A.1
2	Metal 1, 1650 °C	A.2
3	Metal 2, 1600 °C	A.3
4	Metal 2, 1650 °C	A.4
5	Slag 1, 1600 °C	A.5
6	Slag 1, 1650 °C	A.6
7	Slag 2, 1600 °C	A.7

Figure A.1: Overview of the Metal 1, 1600 °C sample. The coke particle is shown in brown at the top, and the metal at the bottom and to the right (light yellow). The gray phase along the edge of the coke particle is SiC, the gap in between is epoxy.

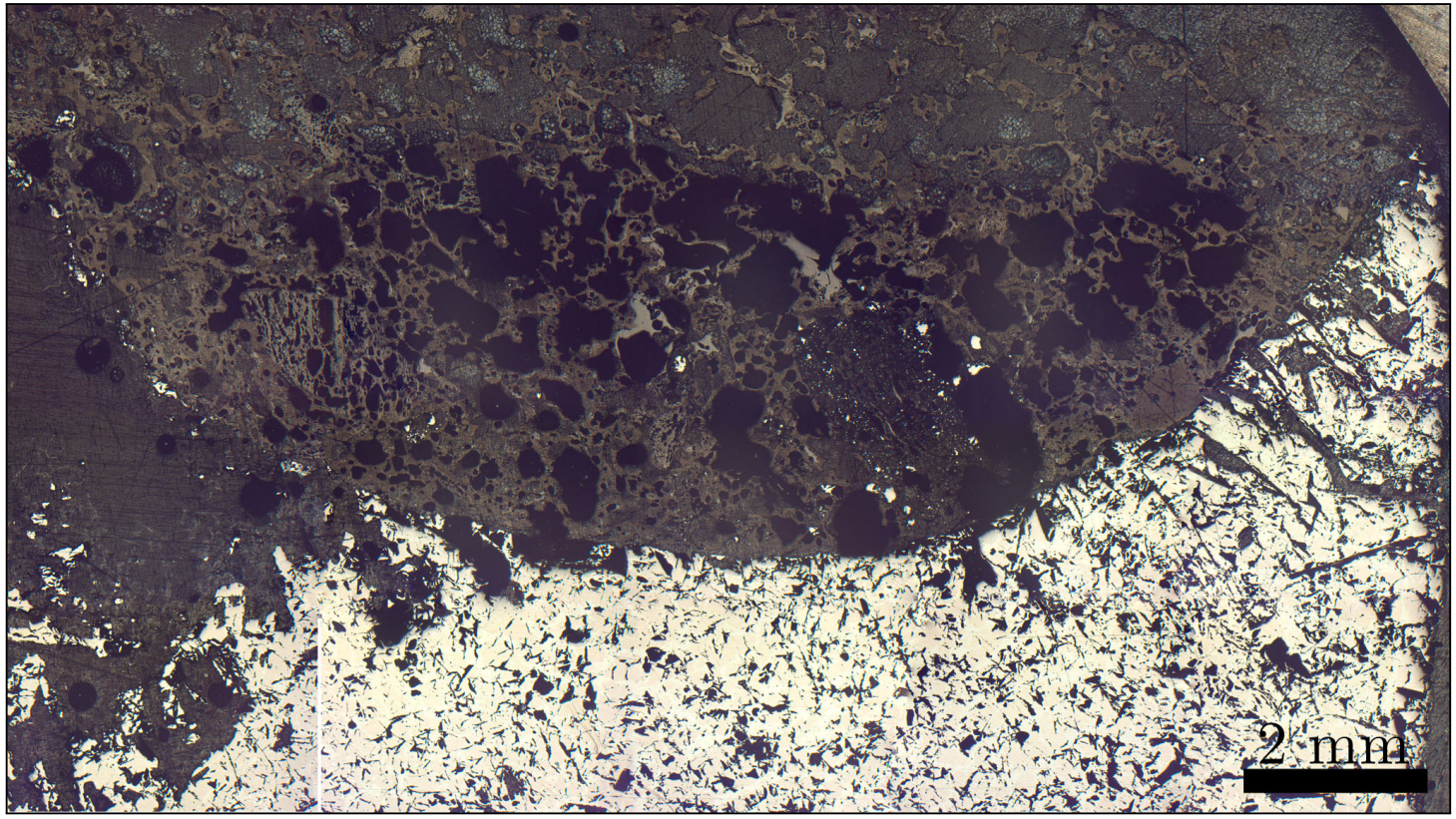

Figure A.2: Overview of the Metal 1, 1650 °C sample. Coke particle (brown) at the top and metal (light yellow) at the bottom.

Figure A.3: Overview of the Metal 2, 1600 °C sample. Coke particle (brown) and metal (yellow) beneath. SiC (gray) is found along the whole coke/metal boundary and in the metal.

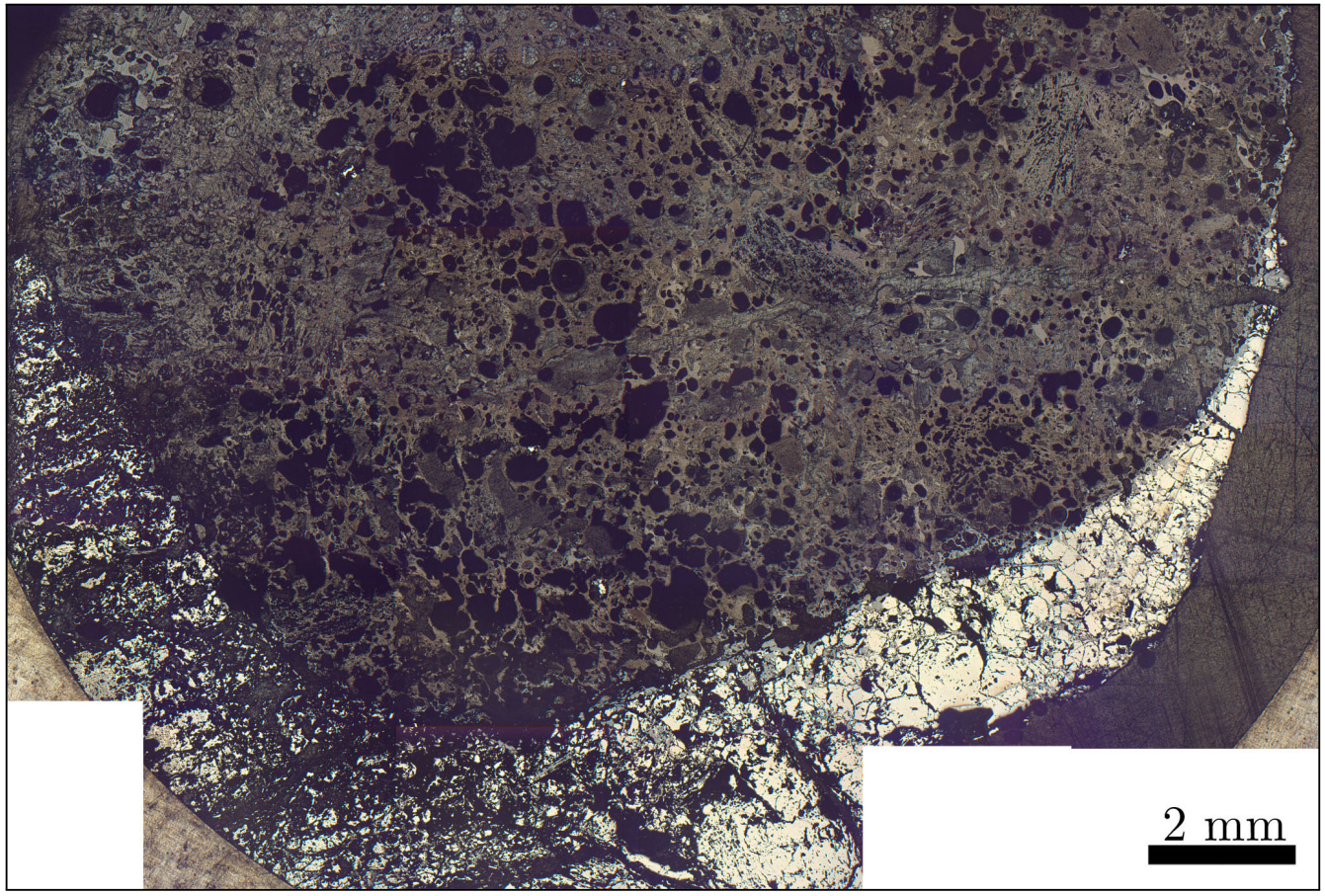

Figure A.4: The Metal 2, 1650 °C sample. Coke particle (brown) with metal (yellow) beneath. SiC (gray) is found along the whole coke/metal boundary.

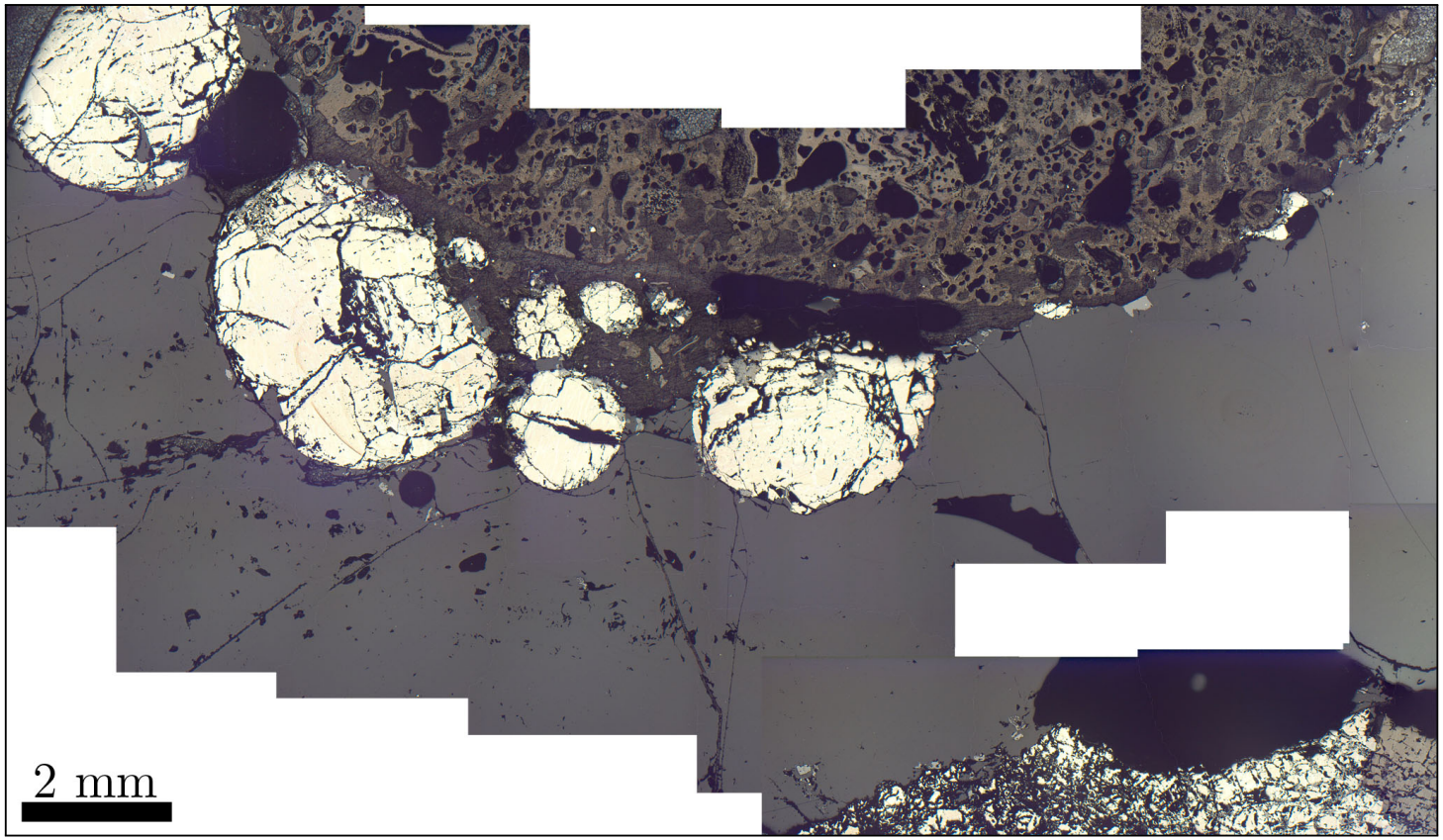

Figure A.5: The Slag 1, 1600 °C sample. Coke particle (brown) at the top with the metal droplets (yellow) beneath, surrounded by slag (dark gray). The original metal from the bottom of the crucible is shown at the bottom right. SiC (gray) is found at the edge of the coke particle and in the metal droplets.

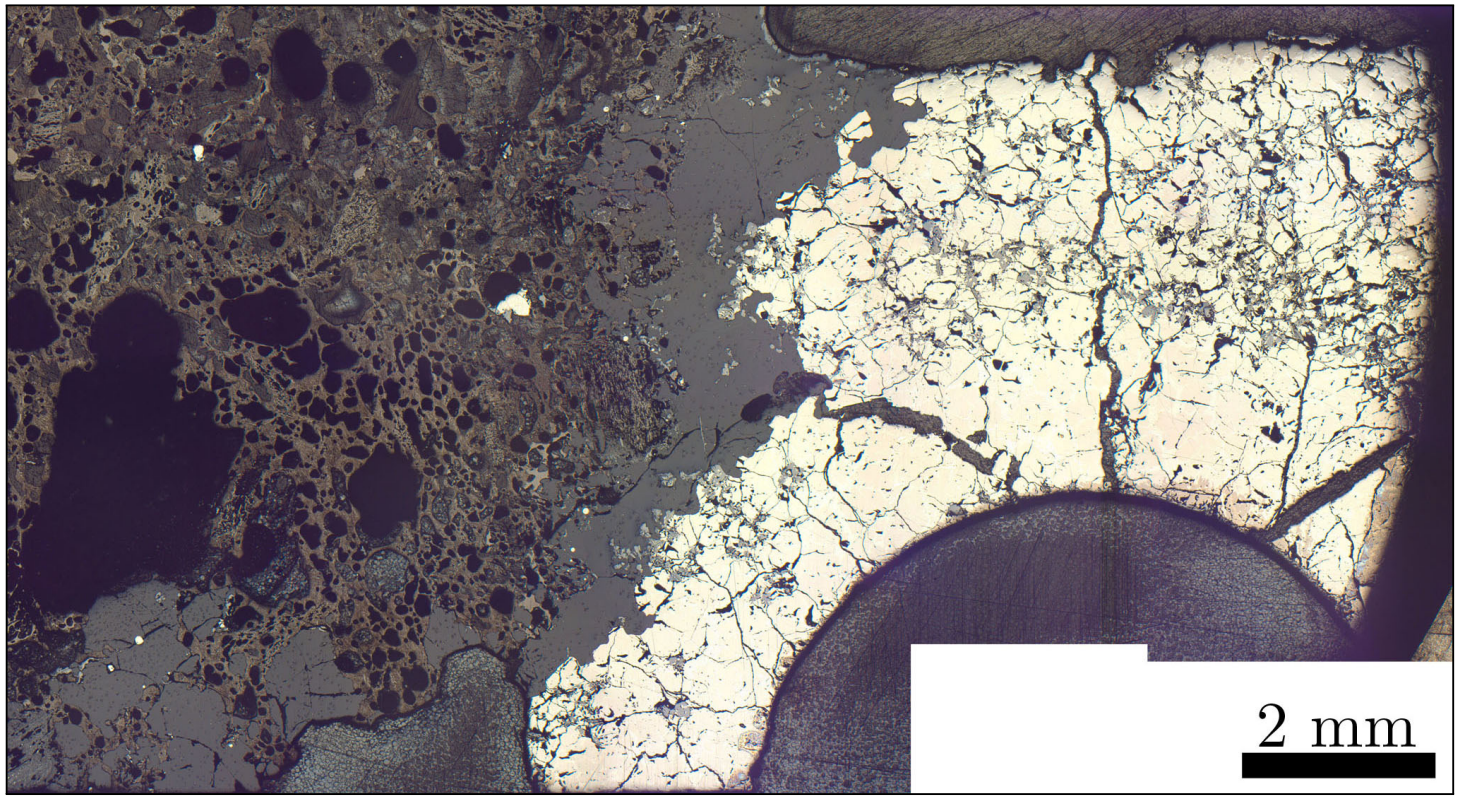

Figure A.6: The Slag 1, 1650 °C sample. Coke particle (brown) to the left, slag (dark gray) in the middle and metal (yellow) to the right. SiC (gray) is mostly found in the slag and metal phase.

Figure A.7: The Slag 2, 1600 °C sample. Coke particle (brown) at the top, slag (dark gray) in the middle and metal (yellow) at the bottom. The gray phase at the sides of the metal are residue of the carbon layer which was added for EPMA, no SiC is visible.

Appendix B

Wetting results

This appendix show the progress for the wetting samples with increasing temperature. The figures are summarized in Table B.1.

Table B.1: Summary of the wetting pictures.

Sample	Figure
Metal 1 on SiC (1)	B.1
Metal 1 on SiC (2)	B.2
Metal 2 on SiC	B.3
Slag 1 on graphite	B.4
Slag 2 on SiC	B.5
Slag 2 on graphite	B.6

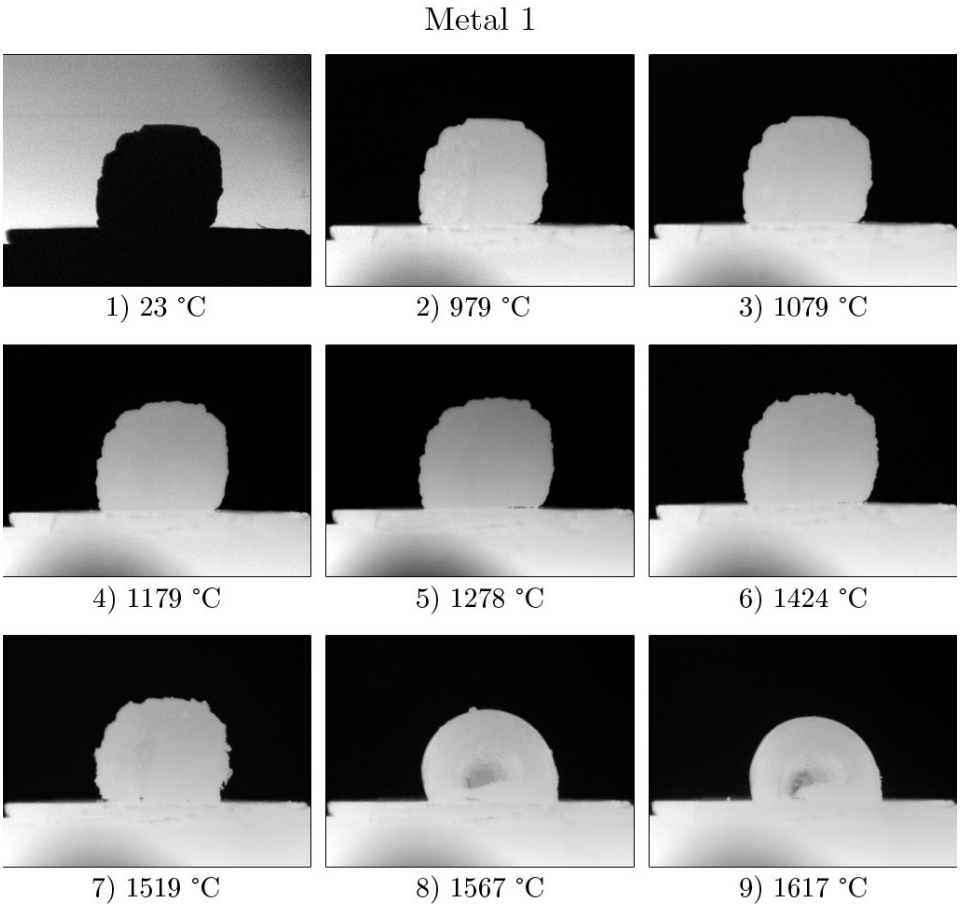

Figure B.1: The changes in the first Metal 1 sample with increasing temperature.

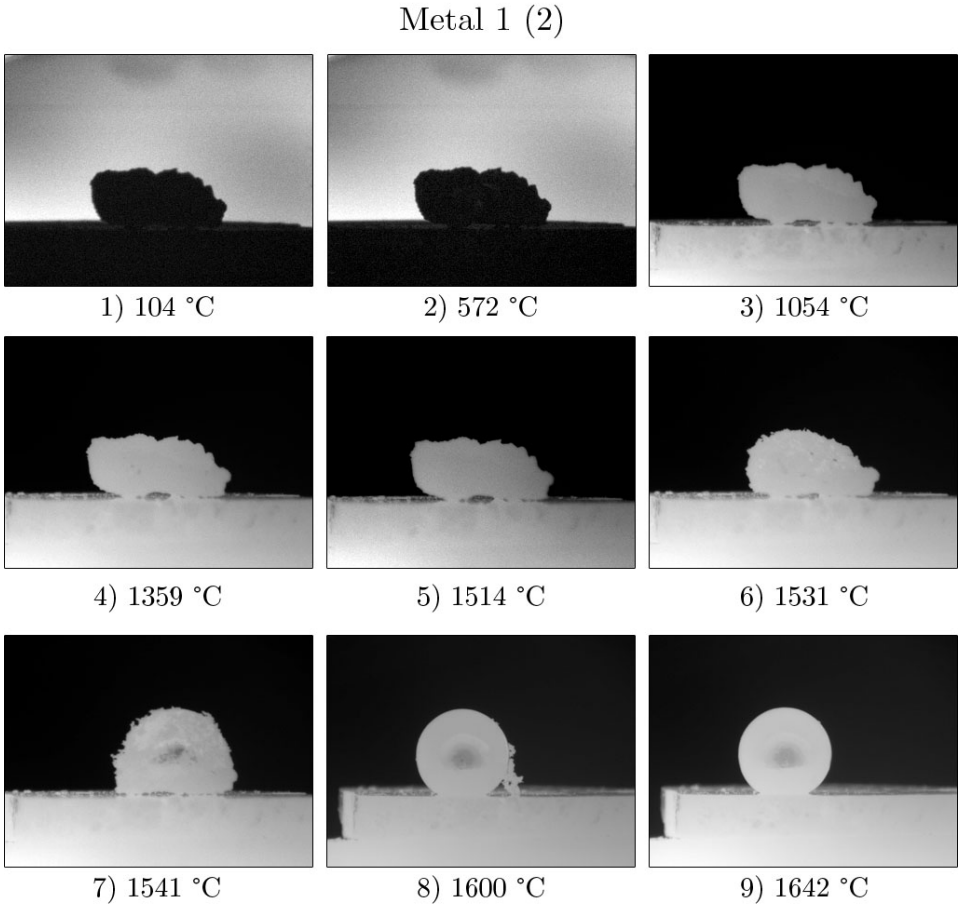

Figure B.2: The changes in the second Metal 1 sample with increasing temperature. Sample starts to melt at c. 1531 °C, Picture 6), and is fully melted at c. 1600 degree C.

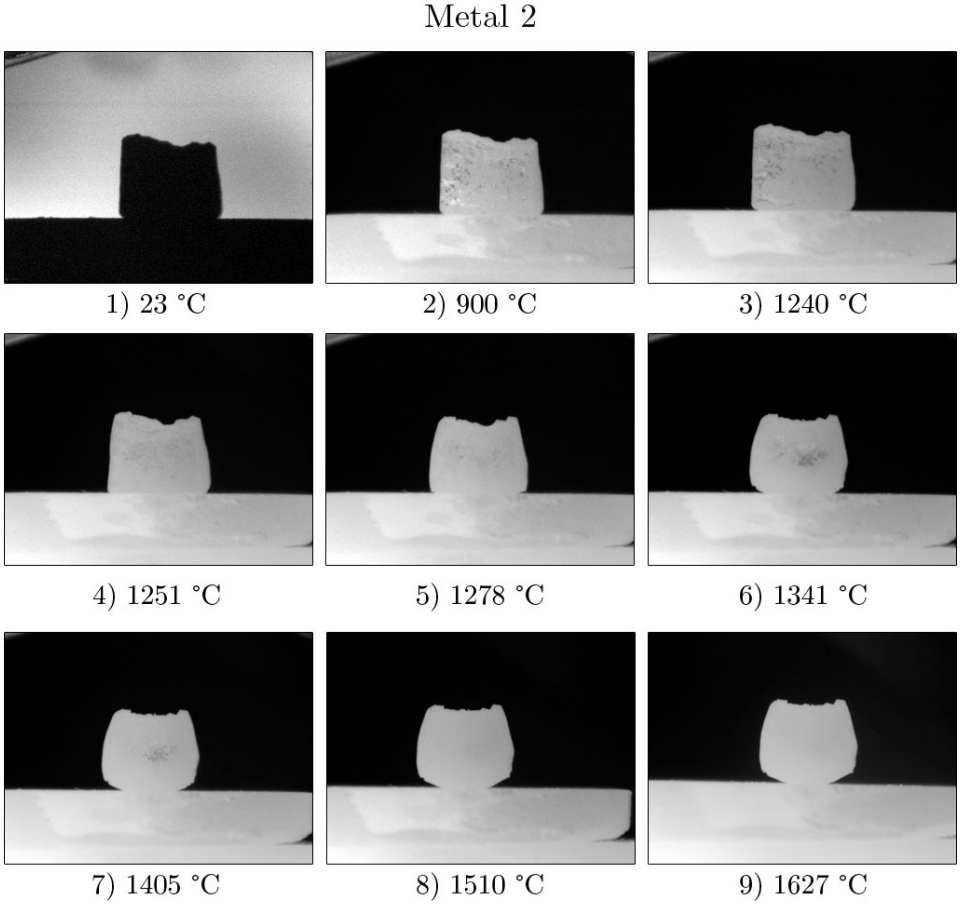

Figure B.3: The changes in the Metal 2 sample with increasing temperature. The sample softened at c. 1240 °C, and melting started at c. 1341 °C.

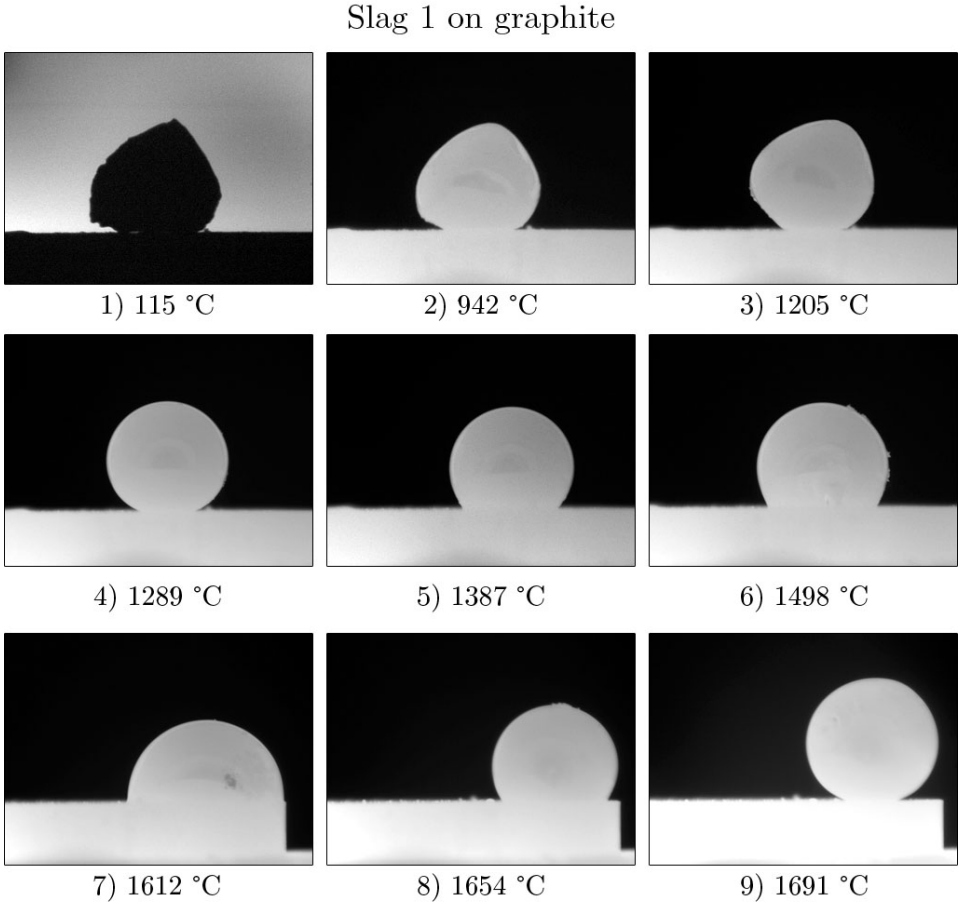

Figure B.4: The changes in the Slag 1 on graphite substrate.

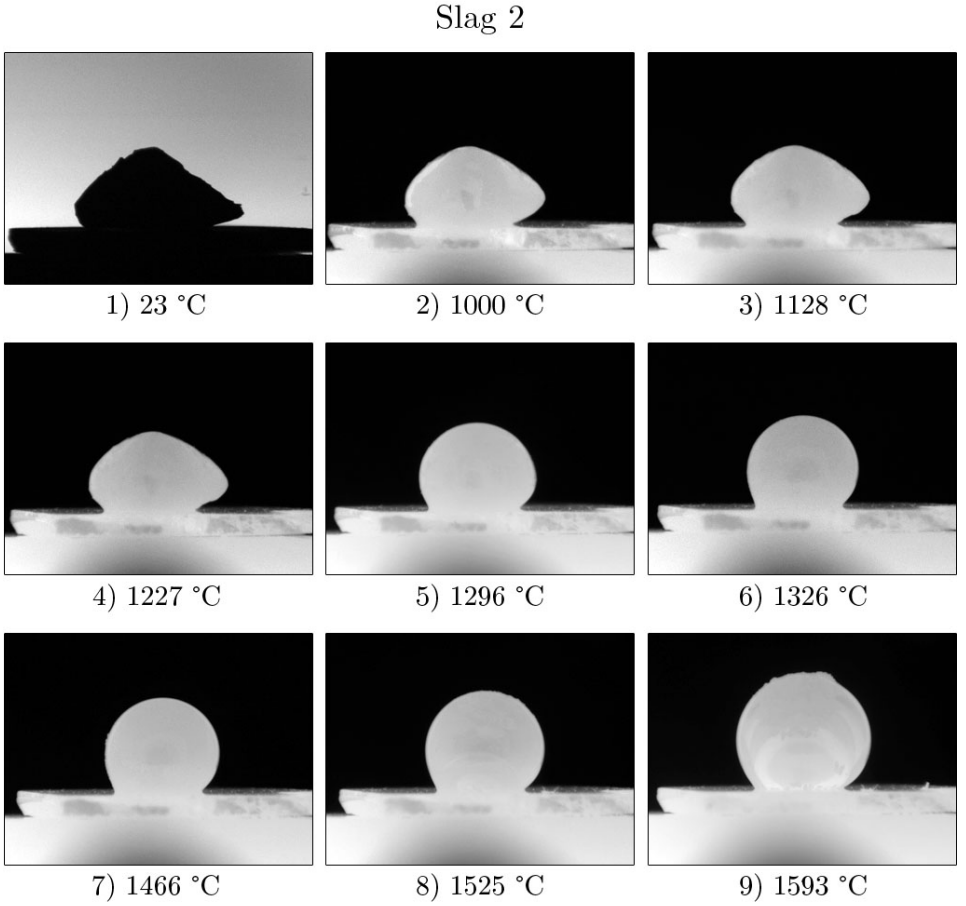

Figure B.5: The changes in the Metal 2 sample with increasing temperature. The sample melted relatively early. Gas evolution is observed towards the end of the experiment, shown in Picture 8) and 9).

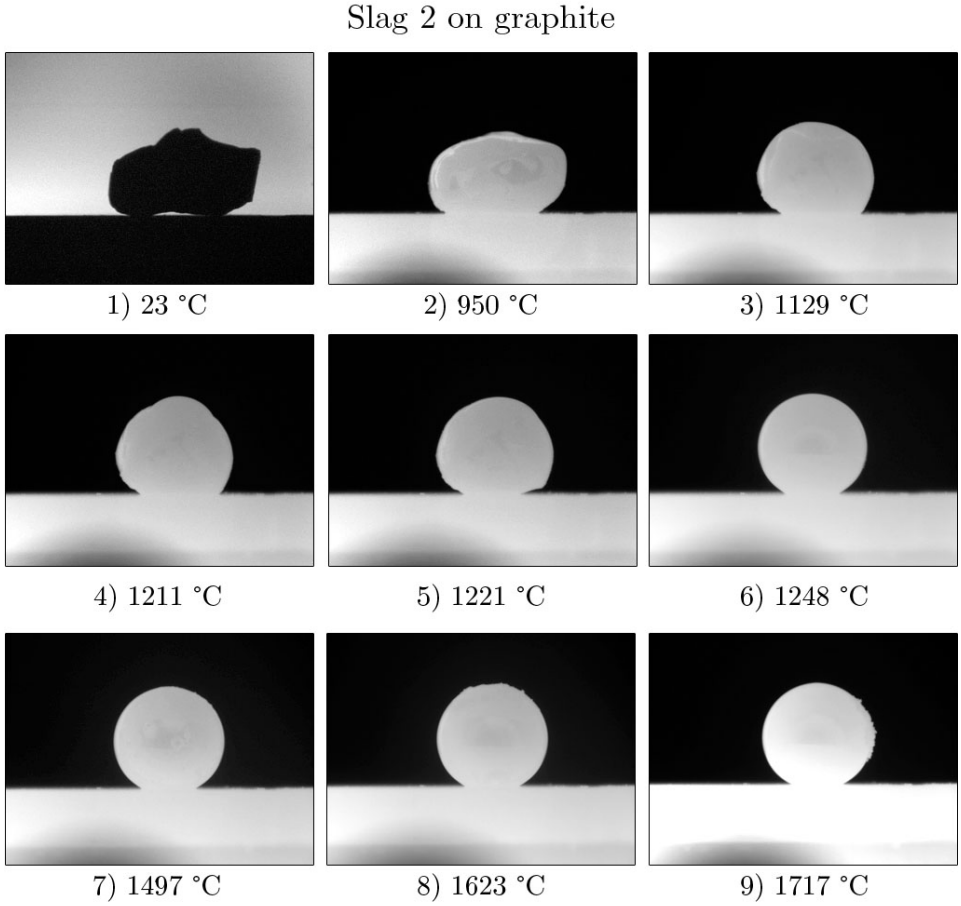

Figure B.6: The changes in the Slag 2 on graphite substrate.

Appendix C

XRD patterns

The full XRD patterns for the slag and metal analysis are shown in this appendix. The scans are summarized in Table C.1.

Table C.1: The XRD scans

Sample	Figure
HC FeMn & Si	C.1
B5-61	C.2
V1 4500	C.3
V4 4850	C.4

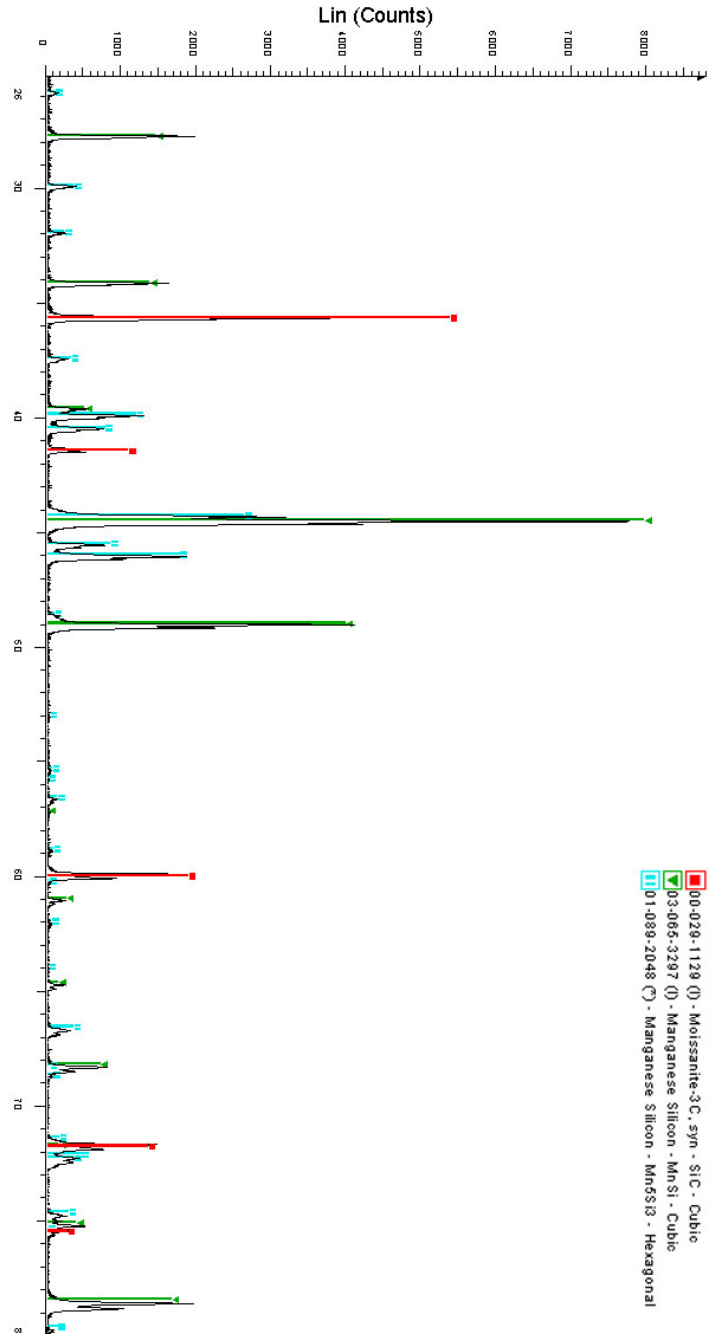

Figure C.1: XRD scan of the HC FeMn & Si sample.

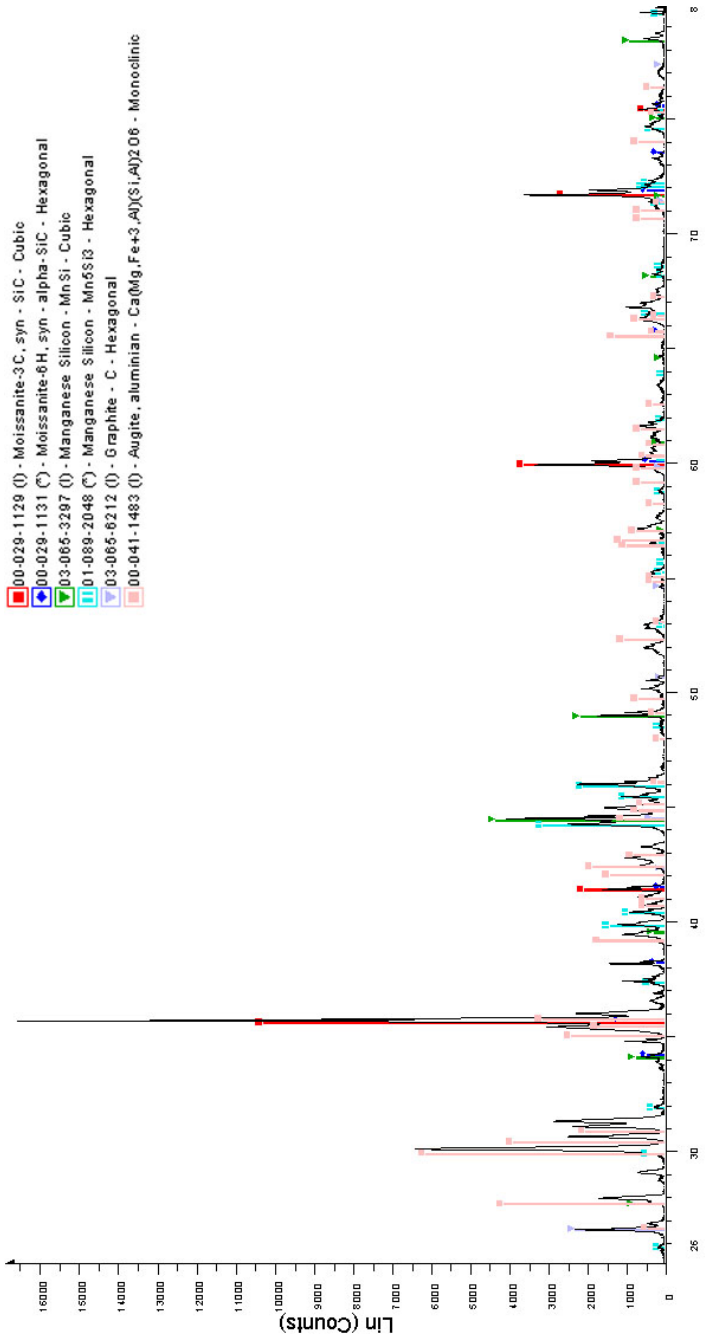

Figure C.2: XRD scan of the B5-61 sample.

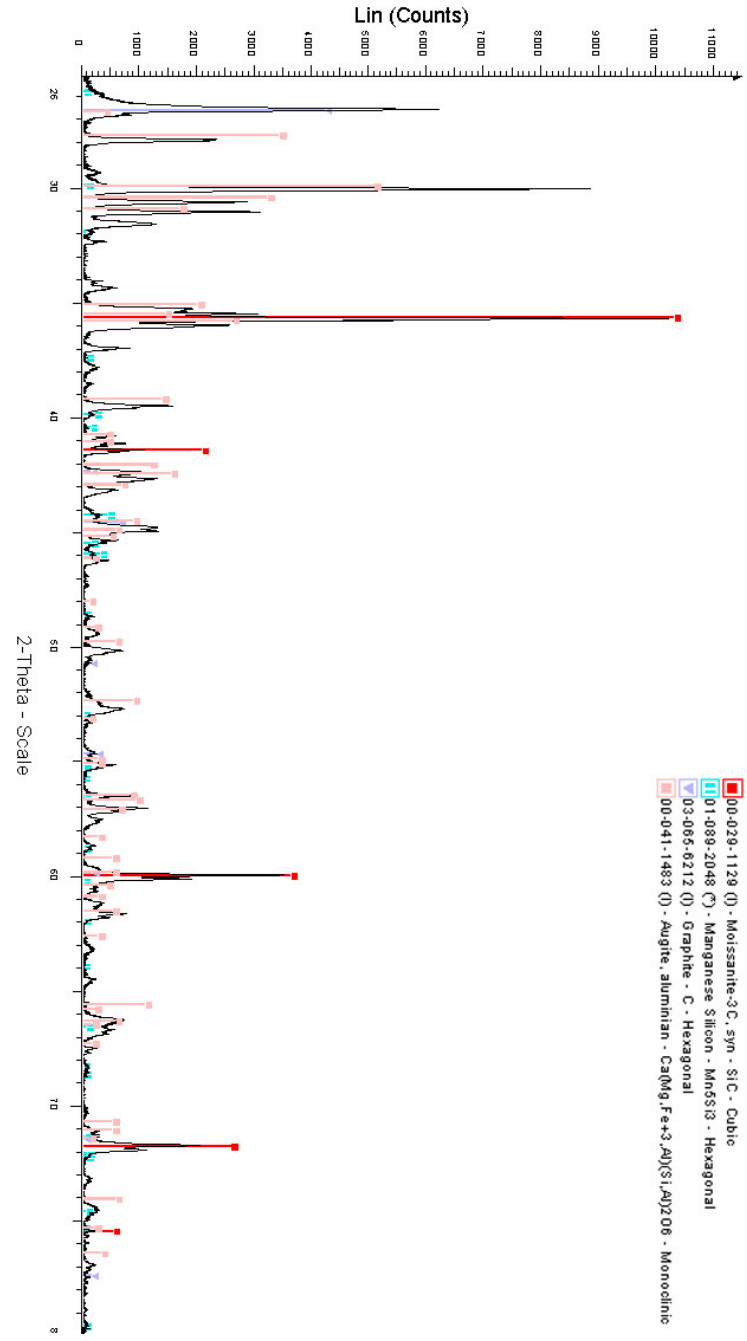

Figure C.3: XRD scan of the V1 4500 sample.

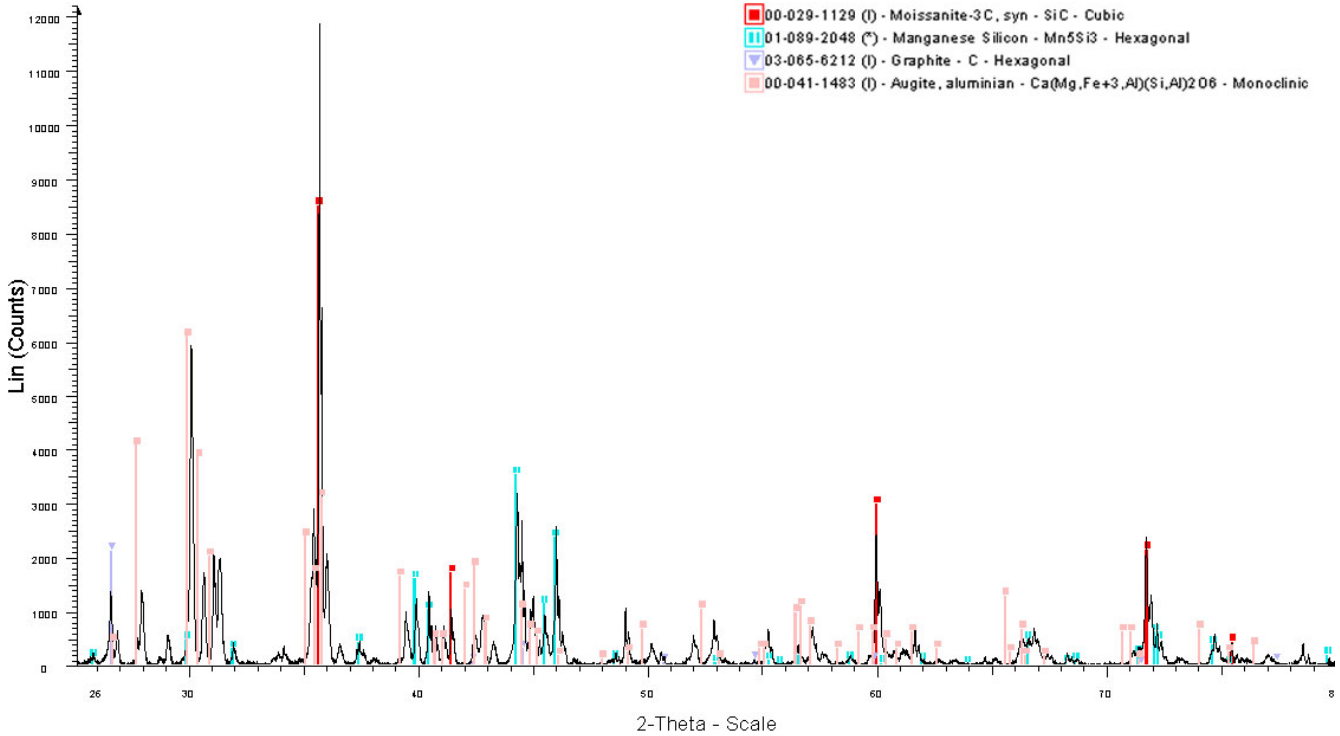

Figure C.4: XRD scan of the V4 4850 sample.

Appendix D

Tube furnace operation parameters

The furnace was run according to the following procedures. The letters in the text refers to Figure D.1.

1. Before the sample holder is removed, checked that the pressure is c. 1 atm
2. Unscrew the nut (m) securing the sample holder, lower it to bottom position and secure the nut
3. Remove the lock ring (l)
4. Carefully pull out the the sample holder
5. Check that sample holder is clean/ free of soot and dirt
6. Put the crucible into the sample holder
7. Insert the holder, mount the lock ring (l) and secure it
8. Unlock the nut and slide the sample to top position. Lock the ring so the sample is secured in top position
9. Unscrew the nut and slide the top thermocouple (a) down until it touches the lid of the crucible. Move it c. 10 mm up and tighten the nut
10. Make sure the vacuum valve (h) is closed, turn on the vacuum pump

11. Open the vacuum valve, first carefully, then gradually more as the pressure decreases
12. As the air is pumped out, set the furnace program. Buttons are explained in Figure D.2.
    (a) Press "page" button until "Pid" shows in the display, press the "scroll" button to select
    (b) Set "Pid 1" and "Pid 2" to right values, see Table D.1, make sure the manual effect knob is set to "max"
    (c) Press the "page" button until the display shows "Prog list", press "scroll" until "Seg.n 1" is displayed
    (d) Set the program according to heating program, see Table D.1 and D.2
13. Wait until the target pressure, c. $2 \cdot 10^{-1}$ mbar, is reached
14. Turn on the cooling water, turn the two black handles to vertical position. Check that the water is flowing!
15. Turn on the main valve on the argon bottle, adjust the black valve until the pressure out is c. 2 bar
16. Open the inlet gas valve to the furnace, turn it carefully toward the green tube. When the pressure in the furnace is increasing with c. 1 mbar/sec, close the vacuum valve
17. Fill the furnace to c. 1 atm Ar(g), slowly at first, then faster as the pressure increase
18. As the PZD display shows a value of c. 2+0, turn the valve over toward the blue tube (regulated)
19. Open the outlet valve carefully, adjust until the bubble rate is c. 1 bubble/sec
20. Turn on the white power switch
21. Press the "run" button on the controller
22. Check that the temperature is rising and that the furnace is operating smoothly
23. As the program stops, turn of the power switch. Program can be stopped manually by holding in the "run" button

24. Close the output valve to prevent suction
25. Close the gas inlet valve and main valve to the gas bottle
26. Let the water flow until the furnace is cooled to about room temperature and then turn it off
27. When extracting the sample, first turn on the gas and then turn the gas inlet valve slightly toward the green tube
28. Open the gas outlet valve to flush out some of the gas inside the furnace
29. Close both gas valves and main valve to gas bottle
30. Adjust the pressure to 1 atm before taking out the sample

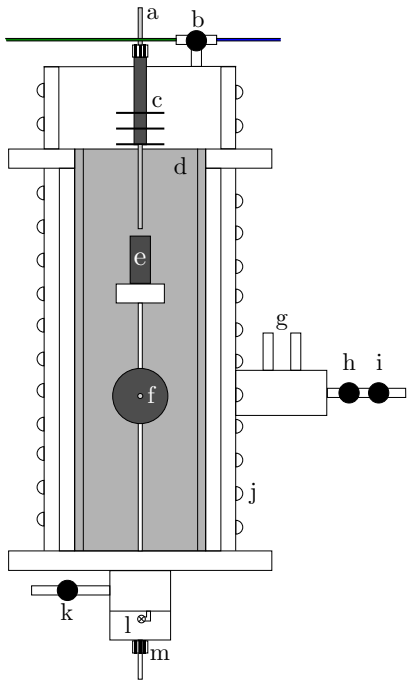

a - Thermocouple with alumina tube, top
b - Gas inlet valve
c - Heat shield
d - Graphite heating element
e - Crucuble with sample
f - Thermocouple with alumina tube, side
g - Pressure probes
h - Vacuum valve
i - Air inlet valve
j - Water cooling tubes
k - Gas outlet valve
l - Lock ring for sample holder
m - Nut for securing sample holder

Figure D.1: Illustrative cross-sectional sketch of the vertical tube furnace.

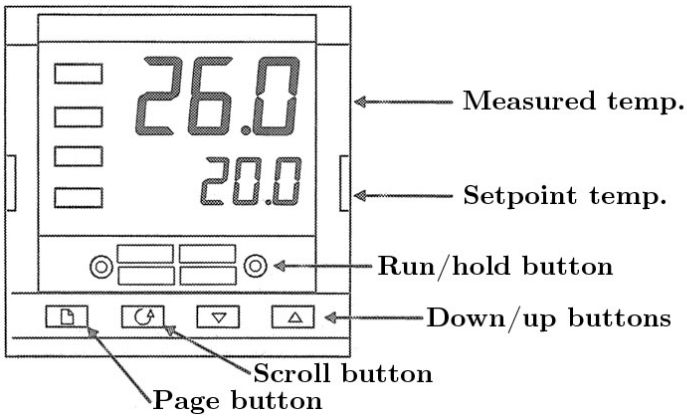

Figure D.2: Sketch of the control display.

Table D.1: The Pid and global program settings.

Pid settings		Global program settings	
G.SP	600	Hb	OFF
Pb	360	HbU	0
ti	825	rmP.U	min
td	137	dwl.U	min
rES	0.0		
Hcb	Auto		
Lcb	Auto		
Pb2	26		
ti2	43		
td2	7		
rES2	0.0		
Hcb2	Auto		
Lcb2	Auto		

Table D.2: Heating program used for the tube furnace. The secondary temperatures are for the high temperature experiments. The heating rate is calculated from the target temperature and duration, and not present as a setting in the controller.

Step (Seg.n)	Type	T_{target} (tGt) [°C]	Duration [min]	Heating rate [°C/min]
1	rmPt	600	30	20
2	rmPt	1550	30	32
3	rmPt	1600/1650	10	5/10
4	dwell	1600/1650	60	-
5	end		reset (stop)	-